Simulation of Thermal Energy Transport in a Fully-Integrated Surface/Subsurface Framework

by

Andrea Elizabeth Brookfield

A thesis
presented to the University of Waterloo
in fulfillment of the
thesis requirement for the degree of
Doctor of Philosophy
in
Earth Sciences

Waterloo, Ontario, Canada, 2009

AUTHOR'S DECLARATION

I hereby declare that I am the sole author of this thesis. This is a true copy of the thesis, including any required final revisions, as accepted by my examiners.

I understand that my thesis may be made electronically available to the public.

Abstract

Thermal stream loadings from both natural and anthropogenic sources have significant relevance with respect to ecosystem health and water resources management, particularly in the context of future climate change. In recent years, there has been an increase in field-based research directed towards characterizing thermal energy transport exchange processes that occur at the surface water/groundwater interface of streams. In spite of this effort, relatively little work has been performed to simulate these exchanges and elucidate their roles in mediating surface water temperatures and to simultaneously take into account all the pertinent hydrological, meteorological and surface/variably-saturated subsurface processes. To address this issue, HydroGeoSphere, a fully-integrated surface/subsurface flow and transport model, was enhanced to include fully-integrated thermal energy transport. HydroGeoSphere can simulate water flow, evapotranspiration, and advective-dispersive heat and solute transport over the 2D land surface and water flow and heat and solute transport in 3D subsurface variably-saturated conditions.

In this work, the new thermal capabilities of HydroGeoSphere are tested and verified by comparing HydroGeoSphere simulation results to those from a previous subsurface thermal groundwater injection study, and also by simulating an example of atmospheric thermal energy exchange. A proof of concept simulation is also presented which illustrates the ability of HydroGeoSphere to simulate fully-integrated surface/subsurface thermal energy transport. High-resolution 3D numerical simulations of a well-characterized reach of the Pine River in Ontario, Canada are also presented to demonstrate steady-state thermal energy transport in an atmosphere-groundwater-surface water system. The HydroGeoSphere simulation successfully matched the spatial variations in the thermal patterns observed in the river bed, the surface water and the groundwater.

Transient simulations of the high-resolution Pine River domain are also presented. Diurnal atmospheric conditions were incorporated to illustrate the importance of fluctuations in atmospheric parameters on the entire hydrologic regime. The diurnal atmospheric input fluxes were found to not only change the temperatures of the surface and subsurface throughout the cycle, but also the magnitude and direction of the transfer of thermal energy between the surface and subsurface.

Precipitation events were also simulated for the Pine River domain using three different rainfall rates. The surface temperatures responded quickly to the rainfall events, whereas the subsurface temperatures were slower to respond in regions where infiltration was not significant. A thermal

energy signal from the precipitation event was evident in the subsurface, and dissipated once the rainfall ceased. This indicates that temperature can potentially be used as a tracer for hydrograph separation.

The potential of a thermal energy tracer for hydrograph separation was investigated using HydroGeoSphere simulations of the Borden rainfall-runoff experiment. These results matched both measured and previous simulation results using a bromide tracer. The hydrograph separation results from the thermal energy tracer were sensitive to temperature conditions in the subsurface, although this sensitivity reduced considerably when the precipitation event and subsurface temperatures were significantly different.

The contribution of each atmospheric component to thermal energy transport was investigated using the Pine River and Borden examples. Each atmospheric component was individually neglected from the simulation of both sites to investigate their impact on thermal energy transport. The results show that longwave radiation dominates the atmospheric inputs for the Borden example, whereas shortwave radiation dominates in the Pine River example. This indicates that the atmospheric contributions to the thermal energy distribution are site-specific and cannot be generalized. In addition, these results indicate that the atmospheric contributions should not be ignored; measuring atmospheric data in the field is an important component in developing an accurate thermal energy transport model.

The addition of thermal energy transport to HydroGeoSphere provides a valuable tool for investigating the impact of anthropogenic and non-anthropogenic changes to the atmospheric and hydrological thermal energy system. This computational framework can be used to provide quantitative guidance towards establishing the conditions needed to maintain a healthy ecosystem.

Acknowledgements

I would like to extend my appreciation to my supervisor Dr. Ed Sudicky for his advice and guidance through all aspects of this project. I would also like to thank the members of my committee; Drs. Bill Annable, David Blowes and Jon Sykes, for all the input they have provided throughout the course of this study.

I would also like to thank the members of our research group who were always there to help me through any modelling or coding related crisis, specifically Rob McLaren and Young-Jin Park.

Finally, I would like to thank all my friends and family who have supported me throughout my prolonged university career. Most notably, I would like to thank my husband Randy for his encouragement and patience, my parents for their endless support and blind faith that I'll eventually finish school, and to my extended family who have long-since stopped asking when I'll be finished and when I'll get a job.

Table of Contents

List of Figures

List of Tables

Chapter 1

Introduction

Hydrological thermal conditions are an integral part of ecosystem health. Many aquatic species are temperature-sensitive and even small changes in the thermal conditions of their habitat can be detrimental. For example, the brook trout (*Salvelinus fontinaulis*) has an optimum spawning and incubation temperature range of 6°C to 9°C, and a 50% mortality rate at 11.7°C (Hokanson *et al.,* 1973). Natural and anthropogenic stressors, including land use changes, effluent discharge, and climate change, can impact the thermal conditions of an ecosystem. These impacts not only affect aquatic species, but can also influence the global hydrological system. As Wagener and Franks (2005) state: "Climate change threatens global water resource availability and often has a significant impact on components of the hydrological cycle. It affects the availability of freshwater for domestic use, food production, industrial usage and hydro-power generation. Climate change also affects the safety and quality of the human and natural environment through an increase in floods, droughts and erosion, and a decrease in water quality and ecosystem diversity." In order to evaluate the impacts of thermal changes on the eco-hydrologic environment, it is critical to appropriately account for the hydrologic and thermal interactions between the atmospheric and hydrologic systems. Due to the complexity of these interactions between the various sub-systems, numerical modelling is a suitable mechanism for evaluating impacts of climate change on water resources.

1.1 Previous Research

There are several modelling packages available that are capable of simulating either surface or subsurface thermal energy transport. The subsurface thermal transport models, such as VS2DI (Hsieh *et al*., 2000) and SUTRA (Voss, 1984), can simulate variably-saturated thermal transport in two or three dimensions; however, these models treat the surface as a boundary condition and cannot properly simulate the thermal or water flow exchange between the two domains. While these models are appropriate for simulating subsurface regimes with little to no surface interaction, they cannot capture the thermal energy transport throughout the entire hydrological system. There are also several models available for simulating stream/river temperature regimes, as summarized by Caissie (2006). These models, however, either ignore or simplify the groundwater contributions to the stream/river thermal conditions. The existing land surface thermal energy transport packages have similar problems, in that they can adequately represent the land surface thermal energy transport, but have serious limitations when addressing thermal energy in the

subsurface. However, there has been significant research aimed towards evaluating the effects of atmospheric changes on the hydrological system using some of the existing land surface models. The research in this area stems from the further development of land surface schemes (LSSs) and the coupling of atmospheric models to hydrological models using LSSs as the interface.

1.1.1 Land Surface Schemes (LSSs)

Most land surface schemes include only a simplistic treatment of the subsurface, if it is accounted for at all. However, with increased attention on how the location of the water table and the soil moisture profile impacts both the surface hydrological system, and the atmospheric regime, these land surface schemes have begun to incorporate increasingly robust and physically representative subsurface models.

There are numerous land surface schemes available, varying in complexity and emphasis. Some focus on the canopy processes and have a very simple treatment of the soil and groundwater, whereas others focus on the soil system and maintain a very rudimentary method of dealing with canopy interaction. In Canada, one of the most prevalent land surface schemes is CLASS, the Canadian LAnd Surface Scheme (Verseghy, 1991). CLASS incorporates three soil layers and a physically-based treatment of energy and moisture fluxes at the surface and across the boundary layers, including the canopy. Lateral heat and moisture flow is neglected in all soil layers, and the heat and moisture transfer between layers is gradient based. Energy and moisture exchange also occurs between the surface and the atmosphere. The surface temperature in CLASS is evaluated using the surface energy balance equation, which is a non-linear function of the surface temperature. CLASS also includes a physically-based treatment of energy and moisture fluxes from the canopy, in addition to the radiation and the precipitation that cascades through it. These canopy parameters are averaged based on all the different vegetation types present in the grid area (Verseghy, 1991).

Other land surface schemes include SWAP (Soil Water-Atmosphere-Plants), a physically-based model that simulates the interaction between the land surface and the atmosphere throughout the year, and is formulated to be used with atmospheric forcings from the lowest layer of a GCM. SWAP primarily uses analytical methods to solve the systems of equations, minimizing computational burden (Gusev and Nasanova, 2002). The model Simple Biosphere (SiB) takes a different approach in evaluating the transfer of energy, mass and momentum between the atmosphere and the vegetated surface. The approach is to model the vegetation itself, and to let the vegetation determine the interaction between the atmosphere and the land surface. "The morphological and physiological characteristics of the vegetation community in a grid area are used to derive coefficients and resistances that govern the momentum, radiation, and sensible

and latent heat (water vapor) fluxes between the surface and atmosphere." (Sellers *et al*., 1986). Additionally, SEWAB (Surface Energy and Water Balance) is a one-dimensional (vertical) land surface model, designed to couple to both atmospheric and hydrological models by semi-implicitly solving the diffusion equations for heat and moisture, and calculating surface runoff and baseflow as saturation excess runoff (Mengelkamp *et al*., 1999).

1.1.2 Linked Atmospheric and Hydrological Models

The 'coupling' of hydrological and atmospheric models has often been linked and not coupled, by forcing the output from the atmospheric model into the hydrological model. Heat and moisture transfer are often considered only in the vertical direction for the soil, atmosphere and vegetation. In addition, the resolution of most linked atmospheric and hydrological models remains at the sub-basin scale which is far too coarse for detailed hydrological evaluations.

An example of a coupled atmospheric and land surface scheme (LSS) model is WATCLASS, a coupled stream-routing/land surface scheme created by coupling CLASS and WATFLOOD. The coupling of WATFLOOD to CLASS allow for the simulation of the surface flow using the lateral flow generation in WATFLOOD, and the land surface energy fluxes from CLASS. The subsurface within WATFLOOD is limited to interflow from the near-surface soil layer using a parameterization of Richards' equation and base flow produced by Darcian flow from the bottom of the third layer based upon the surface topography gradients (Snelgrove, 2002).

Other couplings include the land surface model Common Land Model (CLM) and the variably-saturated groundwater model ParFlow, coupled as a single-column model. The subsurface in this model solves the variably-saturated Richards' equation, which is linked to the surface through water balance equations. Results have been presented in one dimension (Maxwell and Miller, 2005), and in three dimensions (Maxwell *et al*., 2007). However, the subsurface temperatures and thermal interaction between the surface and subsurface are simplified and there only exists a surface soil temperature, and a deep soil temperature. CLASP (Coupled Land-Atmosphere Simulation Program) is another model that couples the land surface with the atmosphere. It emulates a single column of an atmospheric GCM (AGCM), but with spatially-distributed land surface processes. Land-atmosphere feedbacks are considered in the AGCM, the simulation is nested in a larger-scale atmospheric model, and it includes sub-basin-scale resolution of watershed hydrology (Gutowski *et al*., 2002). While WATCLASS, CLASP and the coupling of CLM and ParFlow are excellent advances in the analysis of thermal atmospheric impacts on the hydrological system, the

3

treatment of the subsurface thermal regime remains simplistic and the resolution is too course for detailed evaluation, being on the order of kilometers for each grid block.

As Varis *et al.,* (2004) state: "To meet the challenges focused on water resources management, the quantification of climate change impact on basin scale hydrology is essential." The evaluation of thermal variations on basin-scale hydrology requires a capable, robust, hydrological model. In addition, recent research indicates that groundwater storage and lateral subsurface flow should not be ignored in climate-change simulations as these processes can determine the relative susceptibility of regions to the subsequent changes in precipitation and temperature (Maxwell and Kollet, 2008). Physically-based, fully-integrated surface/subsurface models have significant potential for assessing all of these impacts in a holistic manner through the elimination of the artificial boundary between the surface and subsurface that exists in the externally or iteratively-coupled models. One such model is HydroGeoSphere, a fully-integrated three-dimensional surface/subsurface flow and transport model. Previous work incorporated saturated-zone heat transport into HydroGeoSphere (Graf, 2005), but did not include transport in the surface water regime and atmospheric/land surface thermal interactions.

1.2 Objectives

This research was designed to develop and demonstrate the fully-integrated thermal energy transport capabilities of HydroGeoSphere. The goal was to create a robust model that can provide quantitative guidance to evaluate the conditions necessary to maintain a balance between a healthy ecosystem and consumptive water use.

Specific objectives of this research include:

- To further develop HydroGeoSphere to include thermal transport in all regimes. Previous work by Graf (2005) included thermal transport in the saturated subsurface media alone. The current research will build upon Graf's work to include thermal transport in the unsaturated zone and the surface, with coupling between the two regimes. The equations used for both the variably-saturated subsurface and surface heat transport were variations of the contaminant transport equation, altered to represent a flux of thermal energy.
- Atmospheric inputs to the land surface will be included to properly simulate the thermal conditions in both the surface water and in the subsurface. These atmospheric inputs include shortwave and longwave radiation and sensible and latent heat fluxes.

- Results will be presented verifying the new thermal transport capabilities in HydroGeoSphere. As there are no benchmarks available for a fully-coupled thermal transport simulation, verifying the thermal regime involves many steps. Firstly, each individual component must be separately verified by comparing the results of the variably-saturated subsurface thermal transport portion of HydroGeoSphere to results from another groundwater thermal transport model (Molson *et al.,* 1992). The surface water component, including the atmospheric inputs, will be verified using CLASS (Verseghy, 1991). Once each component is verified, a fully-coupled thermal transport domain will be simulated as proof of concept.

- To further demonstrate the thermal energy transport capabilities of HydroGeoSphere, a field site with adequate hydrological and thermal data will be used for comparison to HydroGeoSphere simulation results for the site. A section of Pine River, located in Angus, Ontario, was characterized and monitored by Conant (2001) for both hydrological parameters and thermal conditions. This site is ideal for demonstrating the abilities of HydroGeoSphere.

- Diurnal atmospheric input fluctuations will be simulated for the Pine River example to investigate the impacts of temporal atmospheric changes on the surface/subsurface temperatures. Discrete precipitation events are also simulated to demonstrate the impacts of different rainfall rates on the thermal energy system.

- To investigate, and illustrate the potential for a thermal energy tracer to be used in hydrograph separation.

- The final objective is to investigate the sensitivity of the temperature regime to each of the atmospheric conditions. Each atmospheric input will be neglected individually in the Pine River example. These simulations will illustrate the impact of each atmospheric thermal input and determine if any one of the atmospheric contributions is dominant.

Overall, this research provides a tool capable of simulating and evaluating the impacts of anthropogenic and non-anthropogenic impacts on the hydrological thermal regime. These can include a variety of sources such as increased stream temperature from waste water discharge, land use change, or climate change. HydroGeoSphere is capable of evaluating and simulating these impacts at on a large scale, with greater resolution than previously available from current hydrological models or land surface schemes.

1.3 Thesis Organization

Chapter 2 provides an introduction to thermal energy transport, and the specific equations implemented in HydroGeoSphere for variably-saturated subsurface and surface thermal energy transport, in addition to the equations used to couple the thermal energy transport between regimes. The approach and equations used to account for atmospheric thermal inputs are also given. Chapter 3 outlines the verification simulations for thermal energy transport in HydroGeoSphere. The individual subsurface and surface/atmosphere verification, in addition to fully-coupled proof of concept simulations, are outlined and results are presented. Chapter 4 provides a description of the Pine River field site, and the associated conceptual model. Simulation results are then compared to available field data to demonstrate the ability of HydroGeoSphere to represent the processes and thermal energy conditions in the field. Chapter 5 provides results from transient thermal energy simulations of the Pine River field site, for both diurnal fluctuations in atmospheric inputs, and discrete rainfall events. Chapter 6 investigates the potential for the use of thermal energy as a tracer for hydrograph separation. Chapter 7 outlines the importance of select atmospheric input parameters in determining the thermal conditions within the surface/subsurface hydrologic regime. Several simulations are used to show the impacts of these parameters on the entire hydrologic system, specifically the thermal energy exchange between the surface and subsurface. Chapter 8 provides an overall summary and conclusions from this research.

Chapter 2

Development of Thermal Energy Transport in HydroGeoSphere

2.1 Introduction

Recent research has highlighted the importance of quantifying the impacts of climate change on the hydrological and ecological regimes, prompting the need for a model capable of assessing thermal energy transport in a holistic manner. The fully-integrated framework of HydroGeoSphere made it an ideal choice for integrating the thermal energy transport system. HydroGeoSphere is a fully-integrated three-dimensional surface/subsurface flow and transport model. It is capable of two-dimensional overland/stream flow and transport and three-dimensional variably-saturated flow and transport in the subsurface including macropores, fractures and karst conduits. These media are fully-coupled and employ a simultaneous solution of the surface/subsurface flow and transport equations using a Control-Volume Finite Element method (Therrien *et al.,* 2007). Solving the surface and subsurface equations simultaneously for both flow and transport allows for a complete coupling of the interactions within and between the domains. These interactions can play a very important role in assessing the impacts of hydrological, chemical or thermal stressors. Without the integrated approach, these interactions cannot be properly quantified because some form of abstraction of the physical processes would be necessary.

Graf (2005) incorporated heat transport within the saturated-zone flow regime into HydroGeoSphere together with temperature-dependent fluid properties, such as viscosity and density. The model's capability was successfully demonstrated for the case of thermohaline flow and transport in porous and fractured porous media (Graf and Therrien, 2007). This work extends the model's capability to include thermal energy transport in the unsaturated zone and in the surface water, which is considered a key step in the linkage between the atmospheric and hydrologic systems. Surface heat fluxes from atmospheric inputs are an important source/sink of thermal energy, especially to the surface water system. As such, surface heat fluxes across the land surface were also incorporated into HydroGeoSphere. The following sections will give a brief overview of the equations used to simulate the thermal energy transport in HydroGeoSphere. A complete description of the physical processes and governing flow and solute transport equations that form the basis of HydroGeoSphere can be found in Therrien *et al*. (2007) and therefore will not be presented here.

2.2 Surface/Variably-Saturated Subsurface Heat Transport

The equation describing thermal energy transport in the unsaturated zone is similar to that for the saturated zone, with the inclusion of a saturation term in the bulk transport parameters. The general equation for variably-saturated subsurface thermal energy transport following Molson *et al.* (1992) is given by:

$$\left[\frac{\partial \rho_b c_b T}{\partial t}\right] = -\nabla[\mathbf{q}\rho_w c_w T - (k_b + c_b \rho_b \mathbf{D})\nabla T] \pm Q_T + \Omega_o \quad (1)$$

where ρ is the density, c is the heat capacity, T is the temperature of the bulk subsurface, t is time, $\mathbf{q}$ is the Darcy flux in the subsurface, k is the thermal conductivity term, $\mathbf{D}$ is the thermal dispersion term, Q_T is a thermal source/sink and Ω_o is the thermal surface/subsurface interaction term, which will be discussed in a following section. The subscript b denotes a bulk term, whereas w represents the aqueous phase.

In equation 1 the Darcy flux ($\mathbf{q}$) in the subsurface is calculated from a numerical solution of the mixed form of Richards' equation, which is valid both above and below the water table, and the water saturation term is included in each of the bulk property terms.

The thermal dispersion term ($\mathbf{D}$) is calculated for each flow direction, and for cross-terms to account for anisotropic systems, following (Burnett and Frind, 1987):

$$D_{xx} = \alpha_l \frac{q_x^2}{|q|} + \alpha_{th} \frac{q_y^2}{|q|} + \alpha_{tv} \frac{q_z^2}{|q|} + D^* \quad (2a)$$

$$D_{yy} = \alpha_{th} \frac{q_x^2}{|q|} + \alpha_l \frac{q_y^2}{|q|} + \alpha_{tv} \frac{q_z^2}{|q|} + D^* \quad (2b)$$

$$D_{zz} = \alpha_{tv} \frac{q_x^2}{|q|} + \alpha_{tv} \frac{q_y^2}{|q|} + \alpha_l \frac{q_z^2}{|q|} + D^* \quad (2c)$$

$$D_{xy} = D_{yx} = (\alpha_l - \alpha_{th}) \frac{q_x q_y}{|q|} \quad (2d)$$

$$D_{xz} = D_{zx} = (\alpha_l - \alpha_{tv}) \frac{q_x q_z}{|q|} \quad (2e)$$

$$D_{yz} = D_{zy} = (\alpha_l - \alpha_{tv}) \frac{q_y q_z}{|q|} \quad (2f)$$

where α_l, α_{th}, and α_{tv} are the longitudinal, horizontal transverse and vertical transverse dispersivities, $|\boldsymbol{q}|$ is the magnitude of the Darcy flux, and D^* is the effective molecular diffusion coefficient. The bulk parameters, with the exception of thermal conductivity, are calculated by a volumetric average approximation; for example:

$$\rho_b = (1 - \theta)\rho_s + S_w\theta\rho_w + (1 - S_w)\theta\rho_a \quad (3)$$

where θ is porosity, S_w represents the water saturation and the subscripts s and a represent the matrix solids and the air phase, respectively.

The bulk thermal conductivity term (k_b) can either be specified, or calculated. It represents the thermal conductivity of the entire cell, which can include the matrix solids, the aqueous phase and air. Specifying a bulk thermal conductivity may be appropriate for saturated flow conditions, when the phase composition of the subsurface does not vary with space or time; however under variably-saturated flow conditions, the saturations of air and water in the subsurface may change with time, and thus the thermal conductivity may also change. Calculating a three-phase thermal conductivity is not straightforward; several approaches have been presented, and no one method has proven to consistently provide more representative solutions than others (Chaudhary and Bhandari, 1968, Markle *et al.*, 2006). Two methods of calculating the bulk thermal conductivity are available in HydroGeoSphere, allowing the user to determine which method is appropriate for their simulations. The first method uses a volumetric average approximation similar to that employed in SUTRA (Voss, 1984):

$$k_b = (1 - \theta)k_s + S_w\theta k_w + (1 - S_w)\theta k_a \quad (4)$$

The second approximation extends the accepted two-phase thermal conductivity calculation provided by Sass *et al.*, (1977) by calculating both a dry and saturated thermal conductivity (k_{dry} and k_{sat}, respectively), and then determining the bulk thermal conductivity using a linear interpolation between the dry and saturated thermal conductivities based on the degree of water saturation:

$$k_{dry} = k_s^{(1-\theta)}k_a^{\theta} \quad (5)$$

$$k_{sat} = k_s^{(1-\theta)}k_w^{\theta} \quad (6)$$

$$k_b = S_w k_{sat} + (1 - S_w)k_{dry} \quad (7)$$

The equation describing thermal energy transport in the surface water is similar to that for solute transport in the surface water. Following the solute transport equation by Therrien *et al.* (2007), it is given by:

9

$$\frac{\partial \rho_w c_w d_o T_o}{\partial t} = -\nabla[\boldsymbol{q_o}\rho_w c_w T_o - (k_w + \boldsymbol{D_o}\rho_w c_w)d_o \nabla T_o] + E_{atm} \pm Q_{T_o} - d_o \Omega_o \quad (8)$$

where d is the depth of the surface water, E_{atm} represents the atmospheric inputs to the surface thermal energy system, and the subscript o denotes overland (or stream) flow. Both solute and thermal energy transport are depth averaged in the surface domain within HydroGeoSphere.

In equation 8, the overland water flux ($\boldsymbol{q_o}$) is calculated from the numerical solution of the Diffusion-wave equation, together with Manning's equation, which is fully coupled to the Richards' equation describing subsurface flow. These derivations for thermal energy transport are hydrodynamically, and not thermodynamically based, and are not applicable to high temperature, high pressure hydrothermal conditions, but are valid for most shallow groundwater/surface water systems. In addition, the surface thermal regime is depth-averaged and cannot represent thermal stratification in surface water bodies.

2.3 Surface/Subsurface Thermal Energy Transport Coupling

The coupling of the surface and subsurface thermal continua is similar to that used for advective-dispersive contaminant transport in HydroGeoSphere. There are two methods of coupling the surface and subsurface continua, the common node and the dual node approaches. The common node approach is based on the assumption of continuity of temperature at the surface/subsurface interface. The dual node approach on the other hand uses a first-order flux relation to transfer heat from one domain to the other. The equation for the dual-node coupling of the surface and subsurface thermal equations follows Therrien *et al.* (2007) and is given by:

$$\Omega_o = \rho_w c_w T_{ups} \Gamma_o + \alpha_o \rho_{dwn} c_{dwn}(T - T_o) \quad (9)$$

where Γ_o represents the aqueous exchange flux between the surface and subsurface (the amount of water flowing between the two regimes) and α_o is an energy transfer coefficient determined by the thermal dispersivity over the depth of the surface/subsurface exchange zone. The subscript *ups* represents the "upstream" direction, and the subscript *dwn* represents the "downstream" direction (i.e. $T_{ups}=T$, $\rho_{dwn}c_{dwn}= \rho_w c_w$ when $\Gamma_o>0$ and $T_{ups}=T_o$, $\rho_{dwn}c_{dwn}= \rho_b c_b$ when $\Gamma_o<0$).

The most significant difference between the solute and the thermal transport coupling equations is the treatment of mass/energy transfer between the surface and subsurface. The downstream parameters are used to differentiate between the amount of thermal energy required to change the temperature of the surface and the subsurface domains, respectively. When the diffusive gradient is transferring thermal energy to the

subsurface, the bulk heat capacity and density parameters regulate how much the temperature of the bulk subsurface changes given the amount of thermal energy added. Conversely, when the diffusive gradient is transporting thermal energy to the surface, the aqueous heat capacity and density terms regulate how much the surface water temperature increases given the thermal energy inputs. As the bulk and aqueous heat capacity and density terms can be significantly different, the amount of energy required to change the temperature of the surface and subsurface regimes can also be different. For this formulation, the downstream location (where the energy is diffusing to) determines how much thermal energy is required to reduce the thermal gradient between regimes.

The movement of a solute between the two regimes is different from heat because a non-sorbing solute has a tendency to remain in the aqueous phase, whereas thermal energy tends to preferentially transfer into the solid phase of the porous medium, thus affecting the bulk temperature.

2.4 Atmospheric Thermal Energy Inputs

The inclusion of atmospheric thermal energy inputs is necessary to properly simulate the surface and subsurface temperature regimes. In this work, the atmospheric inputs from CLASS (Verseghy, 1991) are used to determine the surface heat fluxes in HydroGeoSphere. CLASS is a well established land surface scheme, and the atmospheric inputs incorporated into CLASS have been demonstrated to be representative (Verseghy, 1991). In addition to the reliability of the CLASS approach, the equations used for atmospheric inputs are also computationally inexpensive, relative to other atmospheric models, and thus are appropriate for implementing into HydroGeoSphere.

The atmospheric input included in HydroGeoSphere has four components, net shortwave radiation (K_*), net longwave radiation (L_*), sensible heat flux (Q_H) and latent heat flux (Q_E). The sum of these components represents the total atmospheric input to the surface thermal energy system.

$$E_{atm} = K_* + L_* + Q_H + Q_E \quad (10)$$

All of the equations used here are taken from CLASS (Verseghy, 1991) with the exception of the incoming longwave radiation calculation, which is adapted from Fassnacht *et al.* (2001). All of the atmospheric thermal inputs are calculated explicitly, and are treated as a source/sink term in the thermal energy transport equation for the surface regime. A limitation to this approach is that the model does not provide feedback to the atmosphere; however, given the scale of the atmospheric regime, it is assumed that the feedback from the smaller hydrologic domains is negligible.

2.4.1 Net Shortwave Radiation (K_*)

Shortwave radiation is the radiant energy in the visible, near-ultraviolet and near-infrared wavelengths from the atmosphere to the Earth's surface, broadly defined as between 0.1 and 5.0 micrometers. The equation used to calculate the thermal energy input to the surface from net shortwave radiation follows Verseghy (1991) and is:

$$K_* = (1 - \alpha_g) K^{\downarrow} \quad (11)$$

where α_g is the ground surface albedo, and $K^{\downarrow}$ is the incoming shortwave radiation. Ground surface albedo is dependent on the water content of the surficial soil, as formulated by Idso $et\ al.,$(1975), and is given by:

$$\alpha_g = \frac{S_w(1-\theta)(\alpha_{sat}-\alpha_{dry})}{0.20} + \alpha_{dry} \quad when\ S_w(1-\theta) < 0.20 \quad (12)$$

$$\alpha_g = \alpha_{sat} \quad\quad\quad\quad\quad when\ S_w(1-\theta) \geq 0.20 \quad (13)$$

where α_{sat} and α_{dry} are the limiting wet and dry soil albedoes.

A variation of this equation is also available in HydroGeoSphere to account for cloud and canopy cover (given by C_c):

$$K_* = (1 - C_c)(1 - \alpha_g)K^{\downarrow} \quad (14)$$

The cloud and canopy cover term (C_c) varies between 0 and 1 and represents the fraction of the sky that is blocked by either clouds or vegetation from the ground surface.

2.4.2 Net Longwave Radiation (L_*)

Longwave radiation is the infrared energy emitted by the earth and atmosphere at wavelengths between about 5 and 25 micrometers. The equation for net longwave radiation to the surface following Verseghy (1992) is:

$$L_* = L^{\downarrow} - \sigma T_g^4 \quad (15)$$

where $L^{\downarrow}$ is the incoming longwave radiation, σ is the Steffan-Boltzmann constant, and T_g is the ground surface temperature (temperature of the surface regime). In the original CLASS formulation, the incoming radiation term is specified as an input parameter. However, due to the lack of longwave radiation data (incoming longwave radiation is not routinely measured), incoming longwave radiation can also be calculated in HydroGeoSphere using the formulation given by Fassnacht $et\ al.$ (2001):

$$L^{\downarrow} = \varepsilon_{at}\sigma T_a^4 \quad (16)$$

where T_a is the air temperature, ε_{at} is the integrated emissivity of the atmosphere and canopy, calculated by:

$$\varepsilon_{at} = (0.53 + 0.2055e_a^{0.5})(1 + 0.40C_c) \quad (17)$$

where e_a is the near surface vapour pressure. Emissivity is limited so that it cannot exceed 1.0, ensuring that the incoming longwave radiation is not overestimated.

2.4.3 Sensible Heat Flux (Q$_H$)

Sensible heat flux represents the movement of energy from the Earth to the air above typically via conduction. The equation used for sensible heat flux follows Verserghy (1991) and is given by:

$$Q_H = \rho_a c_a V_a c_D [T_a - T_g] \quad (18)$$

where ρ_a is the density of the air, c_a is the specific heat of the air, V_a is the wind speed and c_D is the drag coefficient.

2.4.4 Latent Heat Flux (Q$_E$)

Latent heat flux represents the energy transfer during the evaporation/condensation process. There are three methods of accounting for evaporation in the flow solution. The quantity of water evaporated/condensed in the flow solution provides the basis for the amount of energy transferred between the atmospheric and hydrologic regimes for latent heat flux. As such, the evaporation rate used in the flow solution must be linked to the latent heat flux term used to calculate the atmospheric thermal energy inputs.

The first, and most simplistic method of accounting for evaporation, is to simply reduce the precipitation rate applied to the surface of the domain by the evaporation rate. By not explicitly specifying or calculating the evaporation rate in HydroGeoSphere, the latent heat flux must be determined independently. In this case the equation used by CLASS (Verseghy, 1991) is used, given by:

$$Q_E = L_V \rho_a V_a c_D [SH_a - SH_g] \quad (19)$$

Where L_V is the latent heat of vaporization, SH_a is the specific humidity of the air, and SH_g is the specific humidity of the ground surface. Specific humidity of the ground surface is calculated using the same formulation given by Verseghy (1991):

$$SH_g = hSH_{sat}[T_g] \quad (20)$$

Where *h* is the relative humidity of the air in the surface soils, calculated by:

$$h = exp\left[\frac{-g\psi_g}{R_w T_g}\right] \quad (21)$$

and $SH_{sat}[T_g]$ is the saturation specific humidity at T_g, given by:

$$SH_{sat}[T_g] = \frac{0.622 e_{sat}[T_g]}{p_a - 0.378 e_{sat}[T_g]} \quad (22)$$

In these equations, *g* represents the acceleration due to gravity, ψ_g is the soil-water suction at the surface, R_w is the gas constant for water vapour, $e_{sat}[T_g]$ is the saturation vapour pressure at the ground surface and p_a is the air pressure.

Evaporation can also be specified or calculated in HydroGeoSphere. When evaporation is specified, the evaporation rate is input to HydroGeoSphere and is subtracted from the incoming precipitation throughout the simulation. Internally calculating the evaporation rate is a more complex approach, based on the empirical Hargreaves equation for determining the potential evapotranspiration, and then calculating the actual evapotranspiration as a combination of plant transpiration and evaporation from the surface and the subsurface domains. The equations for this approach are given in detail by Li *et al.*, (2008). Whether the evaporation is specified or calculated, the latent heat flux is then determined from the evaporation rate used in the flow solution, ensuring continuity between the flow and thermal transport simulations. The latent heat flux equation for a specified or calculated evaporation rates is:

$$Q_E = L_V E_{flux} \rho_w \quad (23)$$

where E_{flux} is the specified or calculated evaporation rate.

2.5 Numerical Implementation

The numerical implementation of variably-saturated subsurface thermal energy transport is similar to that given by Graf (2005). The discrete form of equation 1 is given by:

$$\sum_{J=1}^{N_n} T_J^{L+1} \left\{ \sum_e \int_{V^e} \left(\frac{\rho_b c_b}{\Delta t} w_I w_J + (q_i \rho_w c_w) w_I \frac{\partial w_J}{\partial x_i} + (k_b + \rho_b c_b D_{ij}) \frac{\partial w_I}{\partial x_i} \frac{\partial w_J}{\partial x_j} \right) dV^e \right\}$$

$$= \sum_{J=1}^{N_n} T_J^L \left\{ \sum_e \int_{V^e} \left(\frac{\rho_b c_b}{\Delta t} w_I w_J \right) dV^e \right\}$$

$$+ \sum_{J=1}^{N_n} \left\{ \sum_e \oint_{\Gamma_e} \left((k_b + \rho_b c_b D_{ij}) w_I \frac{\partial T}{\partial n} \right) d\Gamma_e + \sum_e \int_{V^e} (\pm Q_T) w_I \, dV^e \right.$$

$$\left. + \sum_e \int_{\Gamma_b} \Omega_o \, w_I d\Gamma_b \right\} \qquad i,j = 1,2,3 \quad (24)$$

where N_n represents the total number of subsurface nodes, L represents the time level at which a solution is known and L+1 represents the time level for which a solution is desired, $\sum_e$ represents the sum over all porous media elements connected to node J, V^e represents the elemental volume, w_I and w_J represent the linear basis functions following the Galerkin approach, Γ_e represents the elemental boundary with n as the unit vector normal to the boundary, and Γ_b represents the elemental boundary between the surface and subsurface domains.

The numerical implementation of the surface thermal energy transport equation is similar to that for the subsurface; however, the surface equation is depth-averaged and is thus evaluated over the elemental area (A^e), not volume. In addition, the surface thermal energy transport equation includes E_{atm} representing the atmospheric inputs to the surface thermal energy system. The discrete equation for the surface regime is given by:

$$\sum_{J=1}^{N_{on}} T_{oJ}^{L+1} \left\{ \sum_{e^o} \int_{A^e} \left(\frac{\rho_w c_w d_o}{\Delta t} w_I w_J + (q_{oi} \rho_w c_w) w_I \frac{\partial w_J}{\partial x_i} + (k_w + \rho_w c_w D_{oij}) d_o \frac{\partial w_I}{\partial x_i} \frac{\partial w_J}{\partial x_j} \right) dA^e \right\}$$

$$= \sum_{J=1}^{N_{on}} T_{oJ}^{L} \left\{ \sum_{e^o} \int_{A^e} \left(\frac{\rho_w c_w d_o}{\Delta t} w_I w_J \right) dA^e \right\}$$

$$+ \sum_{J=1}^{N_{on}} \left\{ \sum_{e^o} \oint_{\Gamma_e} \left((k_w + \rho_w c_w D_{oij}) d_o w_I \frac{\partial T}{\partial n} \right) d\Gamma_e + \sum_{e^o} \int_{A^e} (E_{atm} \pm Q_T) w_I \, dA^e$$

$$+ \sum_{e^o} \int_{\Gamma_b} \Omega_o \, d_o w_I d\Gamma_b \right\} \qquad i,j = 1,2 \quad (25)$$

where N_{on} represents the number of overland flow nodes, and e^o represents overland elements.

2.6 Solution Strategies

HydroGeoSphere solves either linear equations (fully-saturated subsurface flow or solute transport) or non-linear equations (variably-saturated subsurface flow, surface flow, density-dependent flow, etc.). All of the non-linear equations, with the exception of the density-dependent flow equation, are solved using the Newton-Raphson linearization method.

Because fluid density is dependent upon both solute concentration and temperature, the governing equations for variable-density flow and solute and thermal transport are naturally coupled. The density variations cause nonlinearities in the flow solution, and are handled in HydroGeoSphere using Picard iterations, a sequential iteration approach. This method links the flow and transport solution, alternatively solving the two governing equations, until convergence is achieved at each time step.

When density is not a variable, the flow and transport solutions are decoupled. This two step approach works well for small time steps; however, if non-uniform time steps are used, the time increment may become too large and produce non-physical temperature values. HydroGeoSphere utilizes an adaptive time stepping scheme to avoid these problems and to stabilize the solution. For thermal energy transport, the selective time step size follows Therrien *et al*. (2007) and depends on the absolute change in temperature according to:

$$(\Delta t)^{L+1} = \frac{T^*}{max|T^{L+1} - T^L|} (\Delta t)^L \quad (26)$$

where T^* is the maximum absolute change in temperature allowed during a single time step. If the maximum change in temperature is greater than the allowable value, the fraction in equation 26 becomes less than unity, and the new time step is then chosen to be smaller than the previous. In this case, the previous time step is repeated using the new reduced time step without updating the material properties.

2.7 Thermal Energy Input Fluxes

Some input fluxes and boundary conditions for thermal energy transport were previously incorporated into HydroGeoSphere by Graf (2005), such as the prescribed temperature boundaries. Other thermal energy inputs were developed during this research; specifically the temperature flux input and atmospheric inputs.

2.7.1 Temperature Input Flux

The temperature input flux is incorporated into HydroGeoSphere to account for the thermal energy associated with incoming fluid flux. The temperature input flux can be used in both the surface and subsurface domains. The general equation is given as:

$$Q_{heat_i} = Q(\rho_{in} c_{in} T_{in} - \rho_i c_i T_i) \quad (27)$$

where Q_{heat_i} is the temperature flux into node i, Q is the volumetric flux of the carrier fluid, ρ is density, c is the heat capacity, T is the temperature, *in* denotes the input term, and *i* denotes a nodal term. The density and heat capacity terms vary depending on the material associated with the node or input flux (bulk or water). A temperature flux associated with surface water entering the surface domain (for example, a stream inlet) would use ρ and c terms for water for both the input condition (incoming surface water), and the surface node receiving the incoming fluid. However, the injection of heated water into the subsurface would use ρ and c terms for water for the injected fluid, but would use bulk values for the subsurface node.

2.7.2 Atmospheric Thermal Inputs

The atmospheric temperature inputs implemented into HydroGeoSphere include prescribed values (i.e. incoming shortwave radiation, air temperature, cloud cover, etc.) or values determined by a sinusoidal input function. The addition of atmospheric inputs which can vary sinusoidally with time allows for the representation of diurnal fluxes for air temperature, shortwave radiation and wind speed.

2.8 Seasonal Processes

Winter processes, including soil freeze/thaw and snow melt/accumulation, are not accounted for in any of the simulations presented in this work; however, incorporating these components into HydroGeoSphere is important for capturing the flow and thermal transport responses due to seasonal fluctuations. Work has been initiated to develop cold weather processes into HydroGeoSphere, but it is a topic of future research.

The effects of soil freeze and thaw were previously addressed in HydroGeoSphere by Lemieux (2006), Lemieux *et al*., (2008a, 2008b, 2008c) in a pragmatic way without rigorously accounting for phase changes due to soil freezing and thawing. Lemieux *et al*., (2008b) allowed hydraulic conductivity to vary between a frozen and unfrozen value, a difference that is commonly as large as six orders of magnitude. Freezing of the subsurface is not an instantaneous process; instead, the hydraulic conductivity was linearly interpolated over time by Lemieux (2006) to progressively reduce or increase the hydraulic conductivity values between the frozen and unfrozen states. When these changes were incorporated by Lemieux *et al*., (2008b), there were no internally calculated indicators of the thermal state to drive the change between a frozen and unfrozen hydraulic conductivity. Instead, the thermal state of the subsurface was determined externally by a separate computational model (Tarasov and Peltier, 2007). The thermal state of the subsurface can now be internally calculated, and therefore the potential to perform soil freeze/thaw calculations internally now exists in HydroGeoSphere, although it remains untested and is beyond the scope of this research.

Snow accumulation and melt is also an important component for both flow and thermal energy transport. There are several snow hydrology models available, such as SNTHERM (Jordan, 1991), PRMS (Leavesley *et al*., 1983) and SNAP (Albert and Krajeski, 1998), which may be coupled or incorporated into HydroGeoSphere in the future for proper representation of these winter/spring processes. This research focuses on warm weather scenarios, and therefore the lack of winter processes does not impact the simulations presented here. Future research will incorporate winter processes into HydroGeoSphere for a more complete description of flow and transport processes over all four seasons.

2.9 Summary

Because recent research highlights the importance of assessing atmospheric changes on the entire hydrological regime, the ability to simulate thermal energy transport in a fully-integrated hydrological system, including atmospheric inputs, becomes important (Maxwell and Kollet, 2008). Such a development will allow for a quantitative evaluation and analysis of, for example, climate change impacts, land use changes and river restoration designs on the overall ecosystem health.

The fully-integrated surface/subsurface model HydroGeoSphere has been adapted to simulate thermal energy transport in the fully-integrated surface/subsurface regimes. Atmospheric thermal energy inputs have also been included to account for shortwave and longwave radiation, and sensible and latent heat fluxes. These adaptations extend HydroGeoSphere to accommodate thermal energy transport in a fully-integrated manner, allowing for the analysis of both anthropogenic and non-anthropogenic impacts on the thermal conditions of the entire hydrologic regime while maintaining a thermal energy balance.

Chapter 3

Verification of Thermal Energy Transport Component

3.1 Introduction

The numerical implementation of thermal energy transport into HydroGeoSphere requires verification. Because there are no benchmarks available for fully-coupled thermal energy transport, demonstrating the correctness of the numerical solution of the surface and subsurface components will be performed separately. The formulation for subsurface thermal energy transport will be verified using the results of a case study by Molson *et al.,* (1992) involving the Borden thermal injection experiment. The surface thermal energy transport and atmospheric inputs are verified using a test problem previously simulated using CLASS (Verseghy, 1991). Once each component is verified separately, a proof of concept simulation will be performed for the fully-integrated surface/subsurface thermal energy regime.

3.2 Subsurface Verification: Borden Thermal Injection Experiment

Subsurface thermal energy transport is verified by comparing results from HydroGeoSphere with the published case study presented by Molson *et al.* (1992). This verification example involves a simulation of the Borden thermal injection experiment. A description of the experiment and the observed data are presented by Palmer *et al*. (1992). Unless otherwise stated, all parameters used in the HydroGeoSphere simulation are identical to those used by Molson *et al.,* (1992).

The domain size is 40 m x 30 m x 20 m, and is discretized in all directions using 0.5 m block elements. The initial temperature of the domain varies from 15 ^{o}C at ground surface to 9 ^{o}C six meters below the surface. The injection well is located at x=12 m, y=15 m, z=16 m and water is injected at a temperature of 37 ^{o}C for the first 6 days. The flow and transport parameters are given in Table 1. The aquifer thermal parameters are listed in Table 2. Molson *et al*., (1992) include a thermal retardation term (R) calculated by:

$$R = 1 + \frac{(1-\theta)c_s\rho_s + L_v\omega\rho_w(\partial W_u/\partial T)}{S_w\theta c_w\rho_w} \quad (28)$$

where ω is defined as the total aquifer moisture content, and $W_u(T)$ is the fraction of total moisture unfrozen, expressed as a function of temperature. HydroGeoSphere does not use a thermal retardation term, therefore, this term was forced in the Borden thermal injection verification example.

Table 1. Flow and transport properties and boundary conditions for the Borden thermal injection experiment simulations (values used for both Molson *et al.,* (1992) and HydroGeoSphere simulations). Data from Palmer *et al*. (1992).

PARAMETER	VALUE
Aquifer Flow System Parameters	
Porosity (θ)	0.35
Specific Storage (S_s)	0.001 m^{-1}
Hydraulic Conductivity (K)	9.0 x 10^{-5} m/s
Residual Saturation (θ_r)[1]	0.053
Hydrodynamic Dispersion Parameters	
Longitudinal Dispersivity (D_L)	0.100 m
Transverse Horizontal Dispersivity (D_{TH})	0.010 m
Transverse Vertical Dispersivity (D_{TV})	0.005 m
Effective Molecular Diffusion Coefficient (D^*)	6.0 x 10^{-10} m^2/s
Source Parameters	
Injected Fluid Temperature (T_i)	37.0 ^{o}C
Fluid Injection Rate ($\sum Q_i$)	0.103 L/s
Injection Period (t_i)	6 days
Flow Boundary Conditions	
y = 0 m, y = 30 m and z = 0 m	Zero gradient
x = 0 m	Dirchlet h = 0 m
x = 40 m	Specified Flux q = -15.2 m/yr
z = 20 m	Specified Flux q = 0.20 m/yr
Transport Boundary Conditions	
x = 0 m, y = 0 m, y = 30 m and z = 0 m	Zero gradient
x = 40 m	Free exit
z = 20 m	Flux based on varying air temperature

[1] Residual saturation value from ROSETTA class averages (USDA, 2008)

Table 2. Aquifer thermal parameters for the Borden thermal injection experiment simulations (values used for both Molson *et al.,* (1992) and HydroGeoSphere simulations). Data from Palmer *et al*. (1992).

PARAMETER	VALUE
Aquifer thermal conductivity (k_b)	2.0 J m^{-1} s^{-1} ^{o}C^{-1}
Matrix solids density (ρ_s)	2630 kg/m^3
Specific heat of water (c_w)	4174 J kg^{-1} ^{o}C^{-1}
Specific heat of solid matrix (c_s)	800 J kg^{-1} ^{o}C^{-1}
Latent heat of water (L_w)	3.33 x 10^{-5} J/kg
Thermal retardation factor (R)	1.9
Aquifer heat capacity (c_b)	2.84 x 10^6 J m^{-3} ^{o}C^{-1}

The simulation was run for 76 days, and the results are presented at 9 days, 27 days and 76 days for a two-dimensional longitudinal cross-section through the injection well (Figure 1). The results from the HydroGeoSphere simulation are compared to those presented in Molson *et al.* (1992) (Figure 1) and to the observed field data presented by Palmer *et al*., (1992) (Figure 2). Figure 1 shows that the temperature results from both models agree. The peak temperatures of the thermal plume are within 0.5 ^{o}C of each other, and the location and extent of the plume are very similar. The thermal plumes at the various times computed using HydroGeoSphere are slightly deeper in the domain, and closer to the input well as compared to the Molson *et al.,* (1992) results. In addition, the subsurface temperatures in the top layers of the subsurface differ between simulations. These minor differences are due to the different treatment of the temperature boundary condition at the surface of the domain. In the simulation results presented by Molson *et al.,* (1992) the atmosphere is directly connected to the subsurface, whereas HydroGeoSphere requires the surface domain be present to link the atmosphere to the subsurface, which is more representative of field conditions. To accommodate these differences, the air temperatures were applied to the top layer of the subsurface domain in the HydroGeoSphere simulation to best mimic the direct atmosphere-subsurface connection used in the Molson *et al.,* (1992) simulations. In addition, Molson *et al.,* (1992) used temperature-dependent density and viscosity terms, whereas the HydroGeoSphere simulation treated these parameters as constant under the given range in subsurface temperatures. Slightly different formulations for temperature-dependent density are used in HydroGeoSphere and Molson *et al.* (1992) respectively, so the differences between the model results may not be resolved by varying density in the HydroGeoSphere simulations.

22
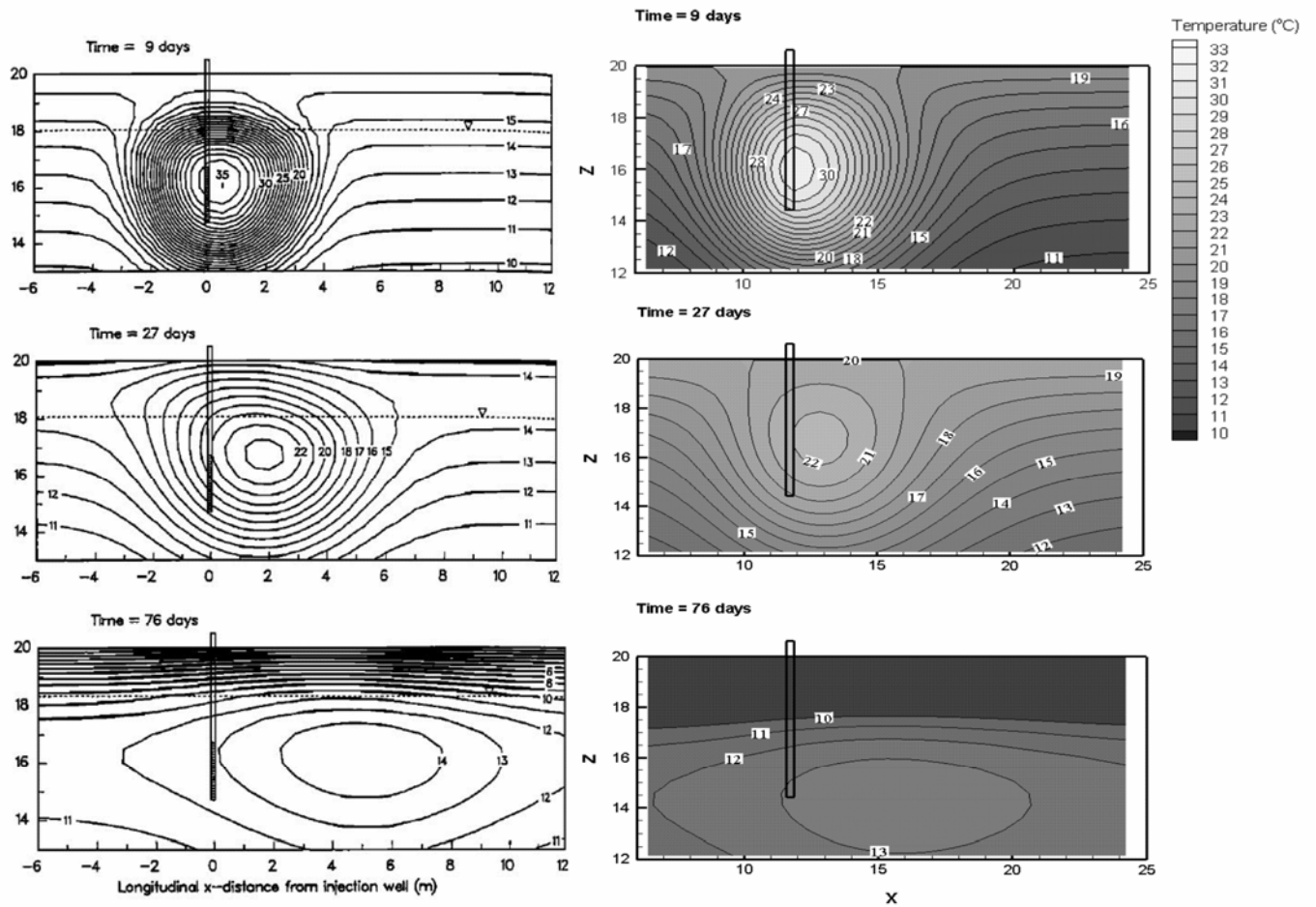
Figure 1. Simulated thermal plume along a longitudinal section for the Molson *et al.* (1992) simulations (left column) and HydroGeoSphere simulations (right column) at 9 days (top), 27 days (middle) and 76 days (bottom).
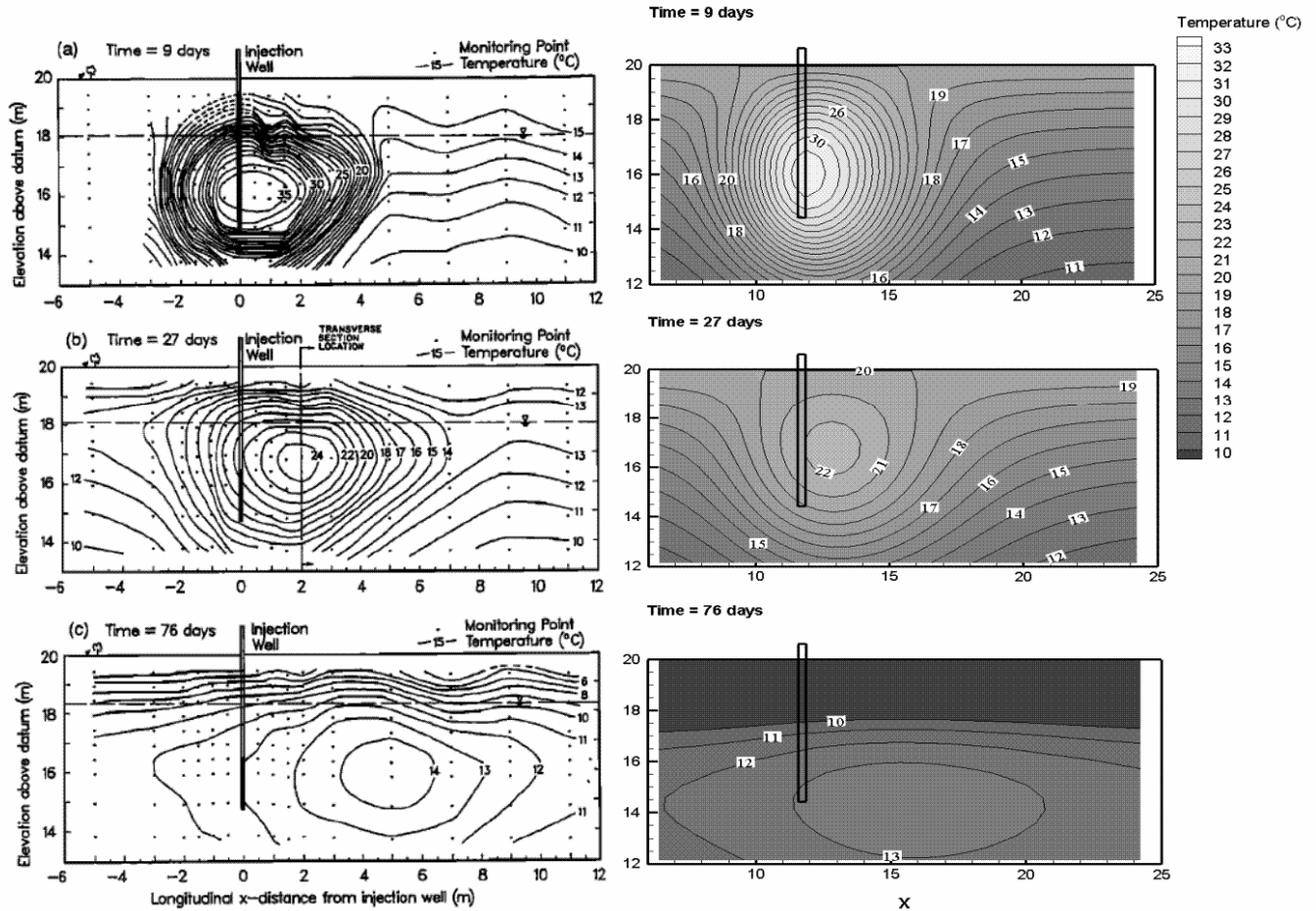
Figure 2. Observed thermal plume along a longitudinal section from Palmer *et al*., (1992) (left column) and the simulated thermal plume for the HydroGeoSphere simulation (right column) at 9 days (top), 27 days (middle) and 76 days (bottom).

3.3 Surface and Atmospheric Input Verification: CLASS Example

The surface-regime thermal energy transport and atmospheric inputs as implemented in HydroGeoSphere will now be verified using a 1D example from CLASS (Verseghy, 1991). The simulation used was Run 1 of the stand-alone test cases presented in Verseghy (1991). Run 1 simulates desert-like conditions; high air temperature and shortwave radiation, and low soil moisture and precipitation. CLASS and HydroGeoSphere employ different approaches for the movement of moisture; CLASS utilizes a modified

24

version of the Green-Ampt equation for infiltration, whereas infiltration is internally calculated within HydroGeoSphere based on the physical system and the fully-integrated surface/subsurface coupling relationships. CLASS uses the Clapp and Hornberger (1978) relation for unsaturated subsurface flow, and in this example a van Genuchten relationship is used in HydroGeoSphere. In addition, CLASS is limited to three layers within the subsurface, located at depths of 0.1 m, 0.35 m, and 4.1 m below the ground surface, and the surface moisture content is approximated using the moisture content of the first layer. This example is well-suited for comparing the temperature response between the two models because the simulated system does not have significant moisture movement, which is anticipated to cause some of the discrepancies between the results. Unless otherwise noted, all parameters used to define the HydroGeoSphere simulations are identical to those used by Verseghy (1991).

The HydroGeoSphere simulation uses a discretization of 0.1 m throughout the entire 4.1 m depth of the domain in order to ensure the stability of the heat transport solution and resolve the soil moisture profile. In addition, the depth of the surface/subsurface exchange zone was taken to be 0.01 m. The CLASS simulation uses a "layer" approach and has a top layer of 0.1 m in thickness, followed by a second layer that is 0.25 m in thickness, and a final layer that extends to a depth of 4.1 m. The physical and thermal parameters used for this simulation are given in Table 3.

A comparison between the HydroGeoSphere and CLASS simulation results is shown in Figure 3. The CLASS results consistently have lower temperatures compared to the HydroGeoSphere results at early time, and match well at late time when the system reaches steady state. These discrepancies occur due to the different subsurface discretization methods, and the different treatment of the surface and soil moisture regimes between CLASS and HydroGeoSphere. The large layers used in portions of the CLASS domain force the temperature profile within each layer to be represented by one average value, smearing the actual temperature profile. The finer discretization in HydroGeoSphere maintains more discrete temperature values throughout the same depth, allowing for a better representation of the actual temperature profile. HydroGeoSphere also uses a physically-based equation for variably-saturated flow whereas the moisture movement in CLASS is dependent upon empirically-based soil hydraulic properties and relationships. In addition, the temperature results from CLASS are strictly calculated as daily averages whereas the HydroGeoSphere model uses variable time stepping. Simulation results from HydroGeoSphere were averaged over each 24 hour period to provide results that could be compared to those from CLASS.

25

Table 3. Physical and thermal parameters for the CLASS stand-alone Test Run #1 (values used for both CLASS and HydroGeoSphere simulations from Verseghy (1991)).

PARAMETER	VALUE
Atmospheric Variables	
Maximum incoming shortwave radiation ($K^{\downarrow}$)	800 W/m^2
Incoming longwave radiation ($L^{\downarrow}$)	300 W/m^2
Diurnal air temperature range (T_a)	10 – 30 ^{o}C
Diurnal wind speed range (V_a)	1 – 5 m/s
Air pressure (P_a)	100 kPa
Relative humidity (RH)	25%
Rainfall	0 mm/d
Density of air (ρ_a)	1.225 kg/m^3
Specific heat of air (c_a)	7.17 x 10^2 J/kg ^{o}C
Drag Coefficient (c_D)	2.00 x 10^{-3}
Latent heat of vaporization (L_v)	2.26 x 10^6 J/kg
Soil Initial Data	
Initial soil temperature (T_g)	5 ^{o}C
Soil Properties	
Saturated soil albedo (α_{sat})	0.15
Dry soil albedo (α_{dry})	0.27
Saturated thermal conductivity (k_{sat})	1.7 W/m K
Dry thermal conductivity (k_{dry})	0.27 W/m K
Saturated hydraulic conductivity (K_s)	6.0 x 10^{-6} m/s
Porosity (θ)	0.45
Alpha (α)[1]	1.49
Beta (β)[1]	1.25
Residual saturation[1]	0.098
Soil texture parameter[2]	7.5

[1] Van Genuchten parameters used in HydroGeoSphere from ROSETTA averages (USDA, 2008)

[2] Parameter used for Clapp and Hornberger (1978) method used in CLASS
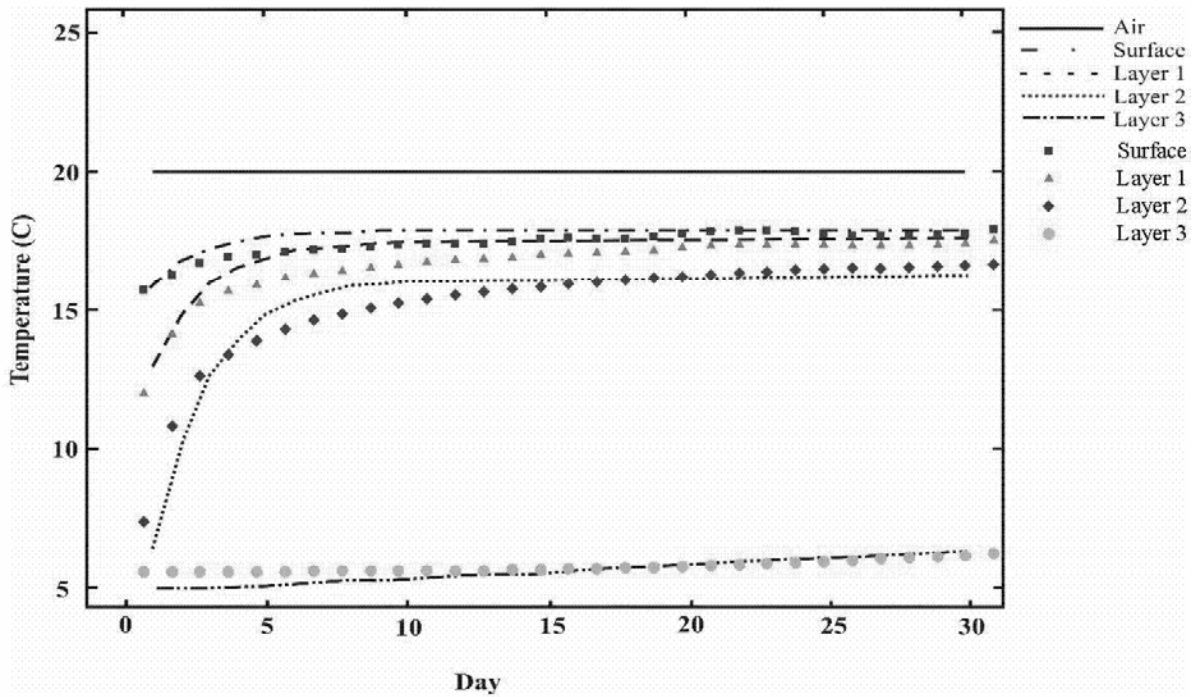
Figure 3. Results of the shallow surface thermal energy transport and atmospheric input verification simulation. Depth of the layers are 0.1 m (Layer 1), 0.35 m (layer 2) and 4.1 m (Layer 3) respectively. (lines: CLASS results; symbols: HydroGeoSphere results).

3.4 Proof of Concept Simulation

Because there are no benchmarks currently available to verify the fully-integrated surface/subsurface thermal energy transport capabilities, a proof of concept simulation is used instead. In a previous study, the flow system used was calibrated to field conditions (Jones *et al.,* 2006) and in this work the conceptual framework of the thermal energy transport is developed. The results of the fully-integrated thermal energy transport simulation are analyzed to ensure consistency with the conceptual framework.

The proof of concept simulation is a plot-scale example involving a rainfall runoff experiment conducted at Canadian Forces Base Borden in Ontario, Canada (Abdul, 1985). The three-dimensional domain is approximately 80 m long, 15 m wide and 4 m deep, and contains 21,952 nodes and 39,765 prism elements. The site is highly characterized, and the subsurface is comprised of a clean, uniform sand. The channel is initially dry, and the initial water table is located near the base of the channel. Rainfall was applied to the surface at a rate of 2 cm/hr for 50 minutes using an irrigation system. The parameters used in the thermal energy simulation are given in   Table 4; the remaining hydraulic properties of the surface and subsurface regime are provided in   Table 5. The volumetric water content-pressure head relationships given by Abdul and Gillham (1989) characterize the unsaturated zone flow conditions. The depth of the surface/subsurface exchange zone is 0.01 m. With the exception of the prescribed rainfall and the critical depth boundary condition at the stream outflow, all the surface and subsurface boundary conditions are no-flow. The flow simulation results indicate that the surface water depths at the end of the rainfall agree with the water depths recorded in the field (Figure 4). Although not shown here, the calculated hydrograph at the channel outlet and the simulated hydraulic response of the subsurface as presented by Jones et al. (2006) agree with the measured responses. This confirms that the flow system underlying the thermal energy transport is representative of the field conditions.

The surface and subsurface temperatures after 50 minutes of rainfall are given in Figure 5. The temperature patterns of the uppermost subsurface layer is similar to the surface temperature patterns, but a temperature gradient between the two regimes remains, indicating that the system has not reached complete equilibrium within 50 minutes. The subsurface temperatures decrease with depth, and the impact from the surface thermal inputs extend to less than one meter into the subsurface. The temperatures of the surface and subsurface along the upper portions of the slopes are within $1^{\circ}C$ of each other; however, along the channel the subsurface temperatures are significantly lower than in the channel water, indicating that the thermal exchange fluxes are not strong enough to cause equilibration between these two regimes.

Table 4. Thermal properties of Borden plot-scale simulation.

PARAMETER	UNITS	VALUE	SOURCE
Specific heat of soil solids (c_s)	J/(kg $^{\circ}$C)	1.25×10^3	Schmidt *et al.* (2007)
Specific heat of water (c_w)	J/(kg $^{\circ}$C)	4.19×10^3	Weast (1984)
Specific heat of air (c_p)	J/(kg $^{\circ}$C)	7.17×10^2	Weast (1984)
Density of air (ρ_a)	kg/m^3	1.22×10^0	Weast (1984)
Thermal conductivity of bulk soil (k_b)	W/(m K)	2.16×10^0	Markle *et al.* (2006)
Thermal conductivity of water (k_w)	W/(m K)	5.00×10^{-1}	Weast (1984)
Incoming shortwave radiation ($K^{\downarrow}$)	W/m	1.10×10^2	Environment Canada (2008)
Dry ground albedo (α_{dry})	(-)	3.50×10^{-1}	Verseghy (1991)
Saturated ground albedo (α_{sat})	(-)	1.80×10^{-1}	Verseghy (1991)
Incoming longwave radiation ($L^{\downarrow}$)	W/m	3.00×10^2	Verseghy (1991)
Stefan-Boltzmann constant (σ)	kg/(s^3 $^{\circ}$C^4)	5.67×10^{-8}	Weast (1984)
Wind speed (V_a)	m/s	1.00×10^0	
Drag coefficient (C_D)	(-)	2.00×10^{-3}	
Latent heat of vaporization (L_v)	J/kg	2.26×10^6	Weast (1984)
Soil-water suction head (Ψ)	m	1.38×10^{-1}	Verseghy (1991)
Ideal gas constant (R_w)	kg m^2/(s^2 $^{\circ}$C mol)	8.31×10^0	Weast (1984)
Air pressure (P_a)	Pa	1.01×10^5	Environment Canada (2008)
Saturation vapour pressure (e_{sat})	Pa	1.70×10^3	Verseghy (1991)
Air/Rain temperature (T_a)	$^{\circ}$C	1.20×10^1	Environment Canada (2008)
Initial groundwater temperature ($T_g(0)$)	$^{\circ}$C	8.00×10^0	Conant (2001)
Initial surface temperature ($T_o(0)$)	$^{\circ}$C	1.00×10^1	Conant (2001)

Table 5. Hydraulic properties of Borden plot-scale simulation.

PARAMETER	UNITS	VALUE	SOURCE
Surface			
Manning's roughness (channel)	$s/m^{1/3}$	0.03	VanderKwaak (1999)
Manning's roughness (slopes)	$s/m^{1/3}$	0.3	VanderKwaak (1999)
Microtopography height	M	1×10^{-2}	VanderKwaak (1999)
Mobile water depth	m	1×10^{-4}	VanderKwaak (1999)
Dispersivity (longitudinal and transverse)	m	0.1	VanderKwaak (1999)
Molecular diffusion coefficient	m^2/s	1.2×10^{-9}	VanderKwaak (1999)
Subsurface			
Porosity	(-)	0.37	MacFarlane *et al*., (1983)
Specific storage	m^{-1}	3.2×10^{-4}	VanderKwaak (1999)
Saturated hydraulic conductivity	m/s	1.0×10^{-5}	MacFarlane *et al*., (1983)
Longitudinal dispersivity	m	0.05	Sudicky *et al*., (1983)
Transverse dispersivity	m	0.005	Sudicky *et al*., (1983)
Effective molecular diffusion coefficient	m^2/s	8.0×10^{-10}	VanderKwaak (1999)
Initial water table depth (below ground surface)	m	0.22	VanderKwaak (1999)
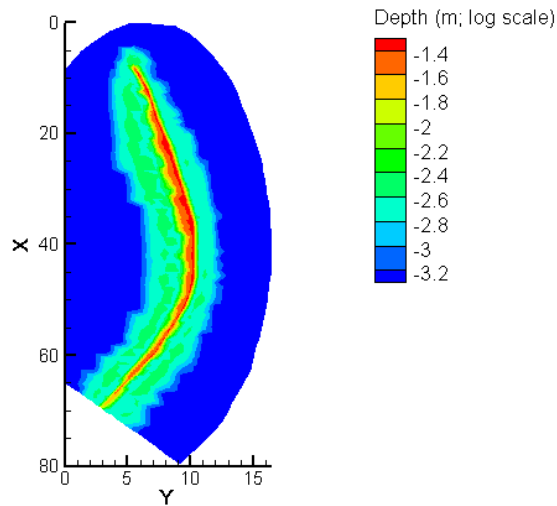
Figure 4. Surface water depths at 50 minutes.
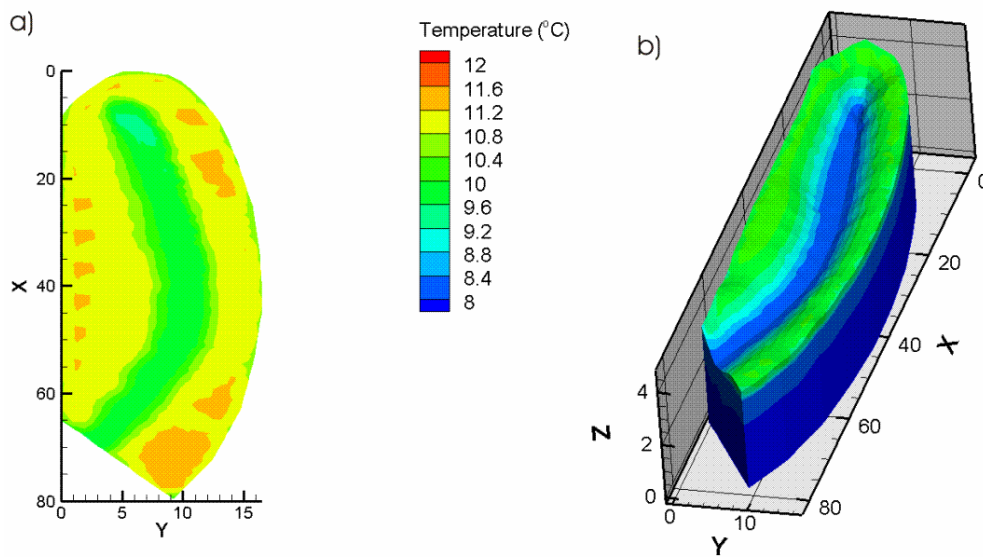
Figure 5. a) Surface water temperatures at 50 minutes; b) subsurface water temperatures at 50 minutes.

A major advantage of the fully-integrated surface/subsurface approach is that the exchange fluxes between the surface and subsurface are directly calculated as part of the numerical solution as opposed to being specified as a boundary condition. The advective and dispersive thermal energy exchange fluxes are given in Figure 6. A positive thermal energy exchange flux indicates that thermal energy is exchanging from the

31

subsurface to the surface; a negative thermal energy exchange flux indicates that thermal energy is exchanging from the surface to the subsurface. In Figure 6a, the advective thermal exchange flux at 50 minutes shows that along the upper portions of the hill slope, the heat exchange is strong from the surface into the subsurface, and along the stream channel the advective heat exchange is weak from the subsurface to the surface. This indicates that the subsurface is acting as a weak buffer on the surface thermal energy conditions. The magnitude of the dispersive thermal exchange fluxes (Figure 6b) are significantly less than the advective thermal exchange fluxes. However, it allows for the transfer of some thermal energy from the surface to the subsurface along the streambed, causing a slight increase in subsurface temperatures in these regions
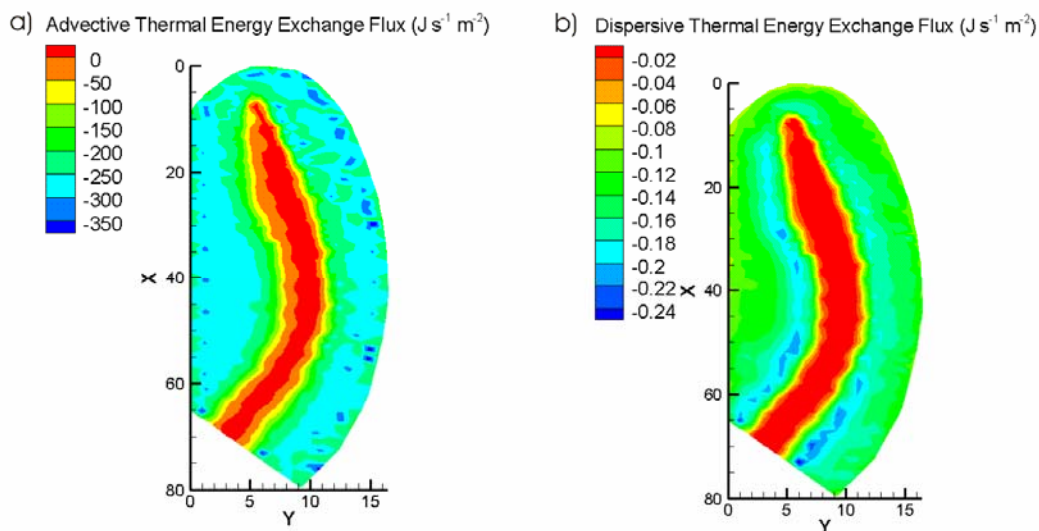
Figure 6. a) Advective thermal energy exchange flux at 50 minutes; b) Dispersive thermal energy exchange flux at 50 minutes.

The simulated temperature regime is similar to what is expected based upon the flow regime, with higher temperatures in the stream where the rainfall collects, and along the upper stream bank areas with shallow surface water depths where no cool groundwater discharges to the surface. Previous analysis of the flow system demonstrated that the capillary fringe effect is occurring along the edges of the stream during the rainfall event (Jones *et al.,* 2006). The capillary fringe effect occurs when the zone of tension-saturation extends to, or very near to, the ground surface near a stream. With a small amount of infiltration, the water stored in this zone rapidly achieves positive pressure-head conditions meaning that a sudden rise in the water table develops near the stream, thus increasing the hydraulic gradient to drive groundwater into the

stream. In the regions where the capillary fringe effect occurs, the surface temperature is low, due to the discharge of cooler groundwater to the surface water. In addition, the area with cooler temperatures in the subsurface along the channel is indicative of the dominant effect of the advective thermal energy flux from the subsurface to the surface.

The results of the plot-scale example indicate that HydroGeoSphere is able to capture the expected thermal energy responses. In addition, HydroGeoSphere was also able to represent small-scale details such as the thermal effects induced by the rapid response of the capillary fringe. In a later chapter, this example problem will be re-visited to explore the feasibility of using temperature signals in a stream in response to rainfall events to perform hydrograph separations.

3.5 Summary

Verification simulations were used to demonstrate that thermal energy transport was properly implemented into HydroGeoSphere. The subsurface component of HydroGeoSphere was verified by comparing simulation results for the Borden thermal injection experiment to those from a previously verified model. The comparison of results based on a CLASS test problem further demonstrated that atmospheric thermal inputs to the shallow subsurface are correctly implemented. A plot-scale proof of concept simulation demonstrated the new capabilities of HydroGeoSphere for thermal energy transport in a fully-integrated surface/subsurface thermal energy transport capabilities of HydroGeoSphere. In all of the verification simulations, the HydroGeoSphere results reasonably matched the results from other models, and for the proof of concept simulation, intuitively expected results were obtained.

Chapter 4
Pine River Simulations

In this chapter, simulations of a section of the Pine River, located in Angus, Ontario, Canada are presented and the results are compared to field data collected by Conant (2001). This site was chosen because extensive site characterization and monitoring data are available.

4.1 Study Area

The thermal energy transport capabilities of HydroGeoSphere will be further tested by simulating a reach of the Pine River, located in Angus, Ontario, Canada. The site is approximately 75 km north-northwest of Toronto (Figure 7a). The Pine River drains a basin that is approximately 348 km^2 in area and discharges into the Nottawasaga River, approximately 2.3 km downstream of the study site (Conant, 2001). The modeled portion of the study domain is 60 m by 80 m and includes a 60 m long reach of the river. This location was chosen because the groundwater/surface water exchanges and thermal conditions in the riverbed, groundwater, and surface water were highly-characterized spatially along this reach (Figure 7b, Figure 8a; see also Conant, 2001; Conant, 2004; Conant *et al*., 2004; Schmidt *et al.,* 2007). Extensive hydrogeological data were also collected at the site in an effort to characterize the subsurface migration of a tetracholoroethene plume discharging into the Pine River (Conant, 2001; Conant *et al.*, 2004).

The area in the vicinity of the site is primarily residential with some commercial properties and undeveloped land. The surface elevation ranges between 183 masl at the top of the riverbed to 189 masl in the fields away from the riverbanks, yielding only 6 m of topographic relief at the site. The north flowing river has a net slope of 0.0007 m/m, and varies in width between 11 and 14 m with an average depth of 0.5 m (maximum of 1.1 m) in the summer. The stream flow rates vary between 1.4 and 2.0 m^3/s during the summer months (Conant, 2001).

The geology of the study site is depicted in Figure 8b. The surficial geology of the riverbed is composed primarily of sand with some gravel and cobbles (Conant, 2004). At various locations beneath the riverbed, the deposits contain interbedded semi-confining layers of peat, silt and silty clay. Some geological windows exist through the semi-confining deposits that allow groundwater to preferentially discharge into the river. The semi-confining units overlie a fine sand aquifer that is continuous across the entire domain. To the east of the river, the semi-confining deposits are absent and are replaced by a 1.5 m thick silt and clay aquitard that is overlain by a sand layer of approximately 4 m thickness that extends to the ground surface. The fine

sand aquifer beneath the aquitard is confined in these areas (Conant, 2001; see also Figure 8). A detailed discussion of the geology of the site can be found in Conant (2001) and Conant *et al*., (2004).

The climate of the region is considered semi-humid and receives an average of approximately 88 mm/month of rain during the summer. About 74 mm of rainfall occurred during the July simulation period based on data collected at Barrie, Ontario (Environment Canada, 2008). The overall recharge rate for the region is estimated at 21 cm/year (Neff *et al.,* 2005).
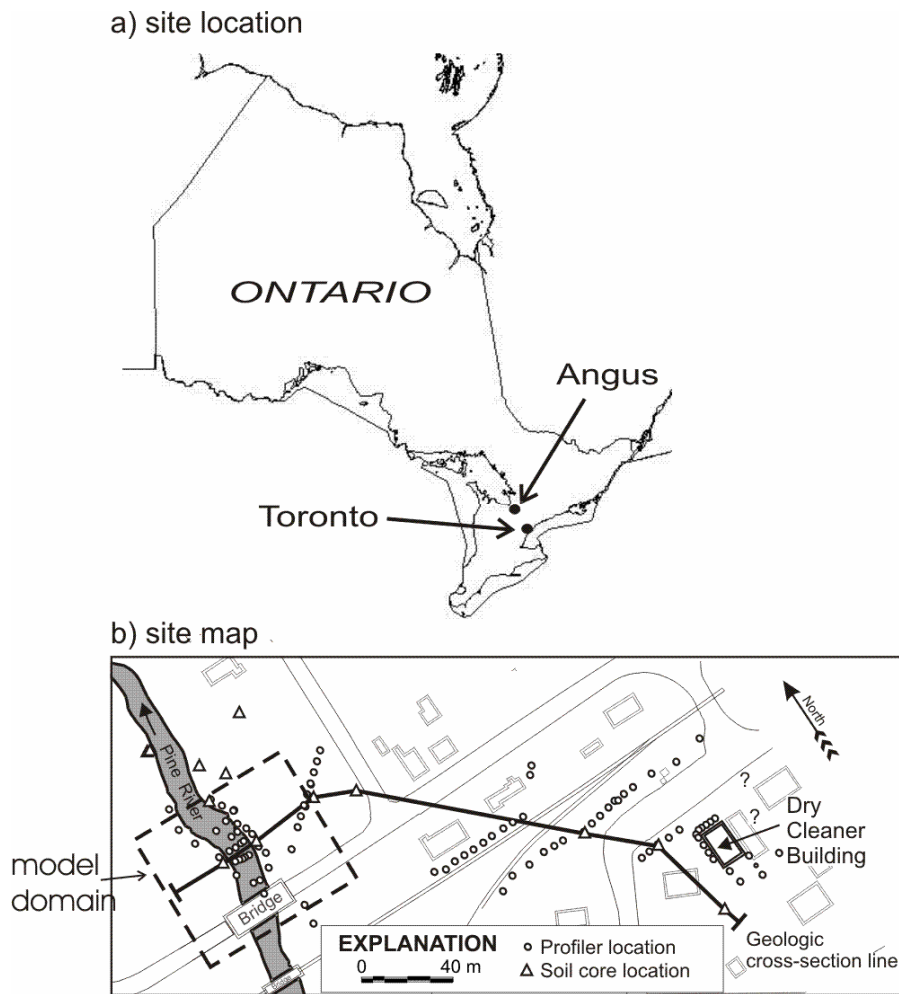
Figure 7. Pine river simulation: a) location of Angus, Ontario, b) plan view site map of the Pine River study site (modified from Conant, 2001).
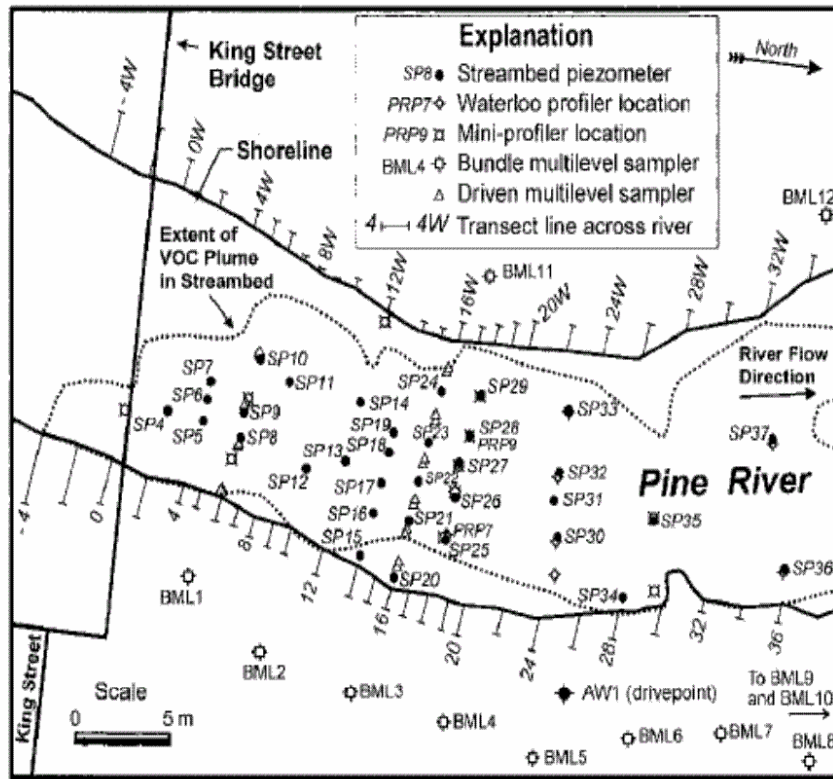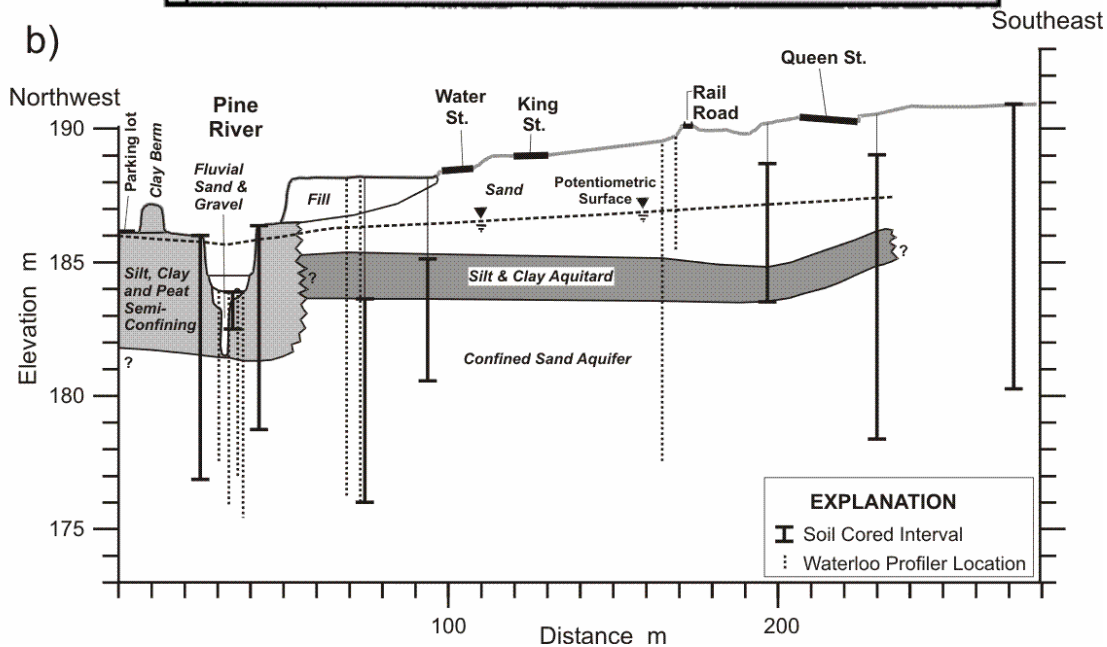
Figure 8. a) Field instrumentation at the Pine River site; b) geological cross section of the subsurface, east of Pine River (modified from Conant, 2001).

4.2 Physical System

The topography in the 60 m long by 80 m wide domain is based upon relatively sparse DEM data, and survey results completed by Conant (2001) (Figure 9). This data was used to define a 2D triangular-element mesh representing the top of the model domain (ground and riverbed surfaces). The mesh was designed so that element dimensions near the river are significantly smaller than those further from the river (Figure 9). This allows a more accurate rendering of the near-stream hydrodynamic processes while reducing the overall computational effort.
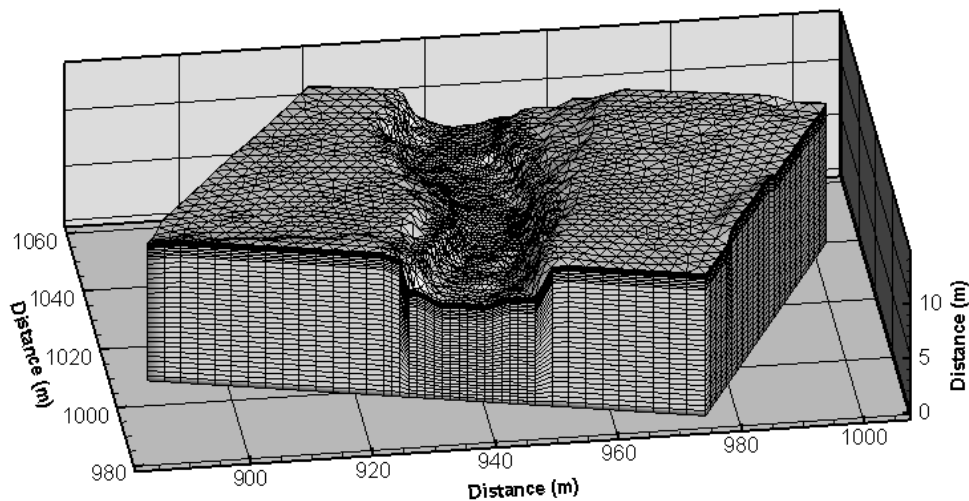
Figure 9. Domain discretization and topography of the Pine River simulation domain (2x exaggeration for z axis).

In the fully-integrated simulation framework applied here, surface water flow and thermal energy transport is simulated using a 2D mesh, which is superimposed onto a 3D finite-element mesh used for subsurface flow and transport. The domain is discretized into 95,040 nodes and 180,320 elements. Thirty-six layers separate the surface and the base of the 3D mesh, located at 175 masl. The vertical discretization is 0.1 m for the uppermost five layers, and doubles to approximately 0.2 m at depth.

The side hydraulic boundaries (parallel to the river) were prescribed head boundaries, based upon monthly hydraulic head measurements taken during the summer. A downward-directed water flux boundary was

used at the bottom of the domain, determined through calibration, which ensured that the total discharge into the stream is representative of conditions observed in the field. The surface boundary conditions include a constant head boundary for the river inlet, using river stage measurements (Conant, 2001), a critical depth outflow boundary at the river outlet, and a prescribed net mean monthly rainfall rate applied to the surface. This rate corresponds to the average for the month of July at the field site (Neff *et al.,* 2005). All other boundaries are considered no flow, reflecting the general direction of flow perpendicular to the river.

Subsurface hydraulic conductivities were defined based upon extensive permeameter and slug test measurements performed by Conant (2001, 2004) and Writt (1996). The simulated subsurface geology is given in Figure 10. The conductivities and other physical properties used for each unit are given in Table 6. The unsaturated zone properties were based upon the ROSETTA class-average hydraulic parameters (United States Department of Agriculture (USDA), 2008). Surface flow properties were simplified into two general groups, overland flow and river channel, and the properties used were taken from VanderKwaak (1999) for a nearby stream section in Borden, Ontario (Table 7). The depth of the surface/subsurface exchange zone is 0.01 m.
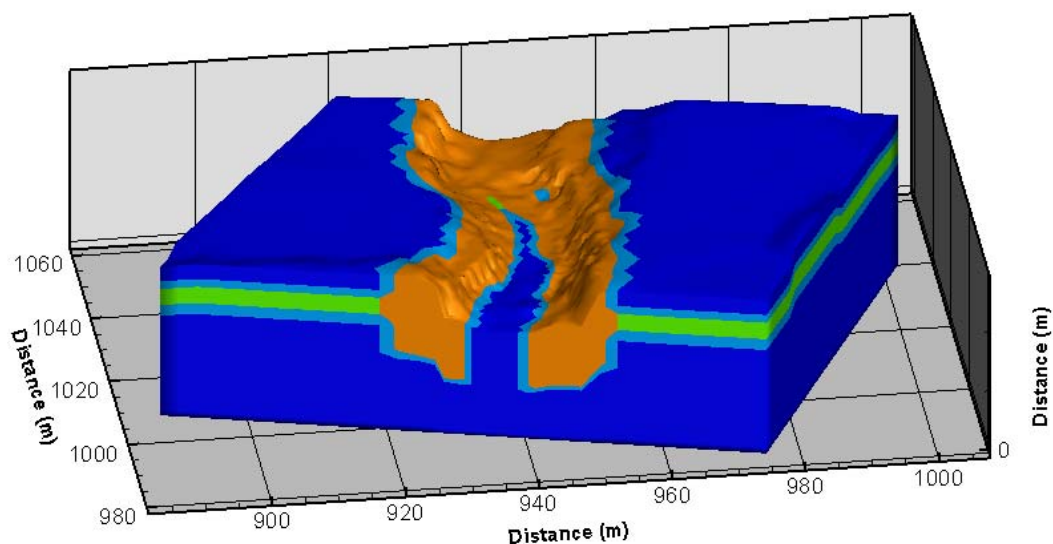
Figure 10. Simulated subsurface geology for the Pine River. Blue represents sand units, green represents the aquitard, and orange represents the semi-confining unit.

Table 6. Subsurface physical properties used in the Pine River simulation.

PARAMETER	VALUES			UNITS	SOURCE
	Stratigraphic Unit				
	Sand	**Aquitard**	**Semi-Confining**		
Hydraulic Parameters					
Hydraulic Conductivity (K)	3×10^{-4}	8×10^{-7}	2×10^{-6}	m/s	Conant (2004)
Porosity (θ)	0.37	0.45	0.55	-	Conant (2004)
Hydrodynamic Dispersion Parameters					
Longitudinal Dispersivity (D_L)	0.1			m	Palmer *et al*. (1992)
Transverse Dispersivity (D_{TH} & D_{TV})	0.01			m	Palmer *et al*. (1992)
Effective Molecular Diffusion Coefficient (D^*)	1.2×10^{-9}			m^2/s	Palmer *et al*. (1992)
Van Genuchten Parameters					
Residual Saturation (θ_r)	0.053	0.11	0.1	-	USDA (2008)
Alpha (α)	3.52	1.62	1.26	-	USDA (2008)
Beta (β)	3.18	1.32	1.27	-	USDA (2008)

Table 7. Overland flow properties used in the Pine River simulation (all values from VanderKwaak (1999)).

PARAMETER	VALUE	UNITS
Manning's Roughness		
Channel	0.03	$s/m^{1/3}$
Slope	0.3	$s/m^{1/3}$
Microtopography Height	0.01	m
Mobile Water Depth	0.0003	m

The Pine River thermal energy regime is taken to reflect average conditions during the month of July although the measured temperatures represent a snapshot in time during this month. Thermal conductivities of the solids (k_s) assigned to each subsurface material type are consistent with the measured saturated thermal conductivity values presented by Schmidt *et al.,* (2007); see Table 8. Other thermal properties are taken from Markle *et al.* (2006) and Verseghy (1991). A constant temperature was assigned below the water table for the lateral boundaries of the domain as well as to the bottom of the domain. This ensured that the water entering over these boundaries are maintained at 10°C, the average annual groundwater temperature measured at the field site (Conant, 2001). The surface thermal boundary conditions include a rainfall temperature equal to the air temperature ($20\ ^{\circ}$C), a stream inflow temperature of $18.5\ ^{\circ}$C, and a free-exit stream outflow boundary. All other boundaries are considered to be zero thermal flux boundaries.

4.3 Flow and Thermal Energy Transport Results

A uniform and constant rainfall rate, equal to 17 mm/month which corresponds to the July average less the average evapotranspiration, was applied to the surface of the initially saturated system until steady-state equilibrium was achieved in both the surface and subsurface flow regimes. The computed steady-state water depths are presented in Figure 11. The steady-state river depths are representative of those measured in the field which averages 0.5 m (Conant, 2004). In addition, the simulated river outflow is 1.91 m^3/s and is within the range of 1.4 to 2.0 m^3/s observed in the field (Conant, 2001). The calculated hydraulic head patterns indicate that groundwater from both sides of the river discharges into the river (Figure 12), which is consistent with the flow conditions observed in the field (Conant, 2001).

Table 8. Thermal transport properties used in the Pine River simulation.

| PARAMETER	VALUE	UNITS	SOURCE
Thermal Conductivity of Solids (k_s)			
Sand	2.0	W m^{-1} $^{\circ}$C^{-1}	Schmidt *et al.* (2007)
Aquitard	1.1	W m^{-1} $^{\circ}$C^{-1}	Schmidt *et al.* (2007)
Semi-confining	1.3	W m^{-1} $^{\circ}$C^{-1}	Schmidt *et al.* (2007)
Atmospheric Parameters			
Air temperature (T_a)	20	$^{\circ}$C	Environment Canada (2008)
Incoming shortwave radiation ($K_{\downarrow}$)	55	W m^{-2}	Environment Canada (2008)
Cloud Cover (C_c)	0.50		Environment Canada (2008)
Surface vapour pressure (e_a)	1704	Pa	Weast (1984)
Density of air (ρ_a)	1.225	kg m^{-3}	Weast (1984)
Specific heat of air (c_a)	7.17 x 10^2	J kg^{-1} $^{\circ}$C^{-1}	Weast (1984)
Wind speed (V_a)	1.0	m s^{-1}	Environment Canada (2008)
Drag coefficient (c_D)	2.0 x 10^{-3}		MacFarlane & Laprise (1985)
Latent heat of vaporization (L_v)	2.26 x 10^6	J kg^{-1}	Weast (1984)
Soil-water suction at surface (ψ_g)	0.138	m	Verseghy (1991)
Air pressure (p_a)	101.3	kPa	Environment Canada (2008)
Matrix Solids and Water Properties			
Matrix solids density (ρ_s)	2630	kg/m^3	Schmidt *et al.* (2007)
Specific heat of water (c_w)	4185	J kg^{-1} $^{\circ}$C^{-1}	Weast (1984)
Specific heat of matrix solids (c_s)	1254	J kg^{-1} $^{\circ}$C^{-1}	Schmidt *et al.* (2007)
Latent heat of water (L_w)	3.33 x 10^{-5}	J/kg	Weast (1984)
Dry surface albedo (α_{dry})	0.35		Verseghy (1991)
Saturated surface albedo (α_{sat})	0.18		Verseghy (1991)
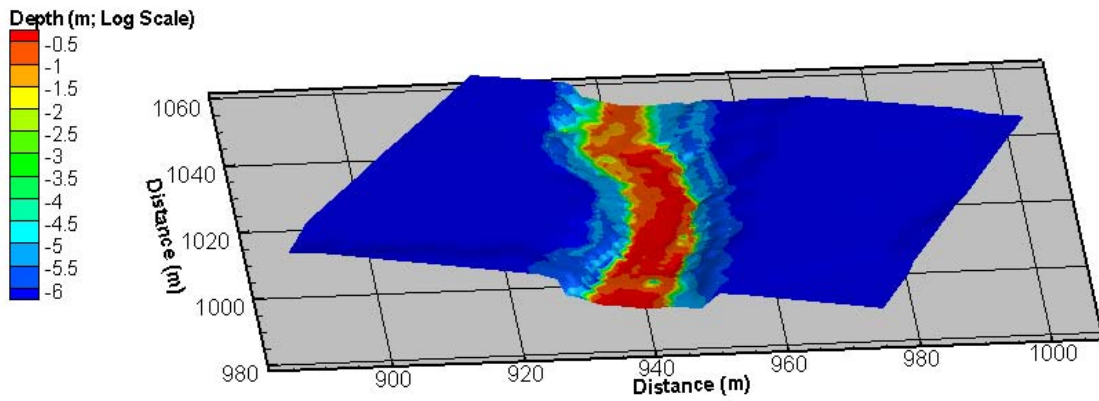
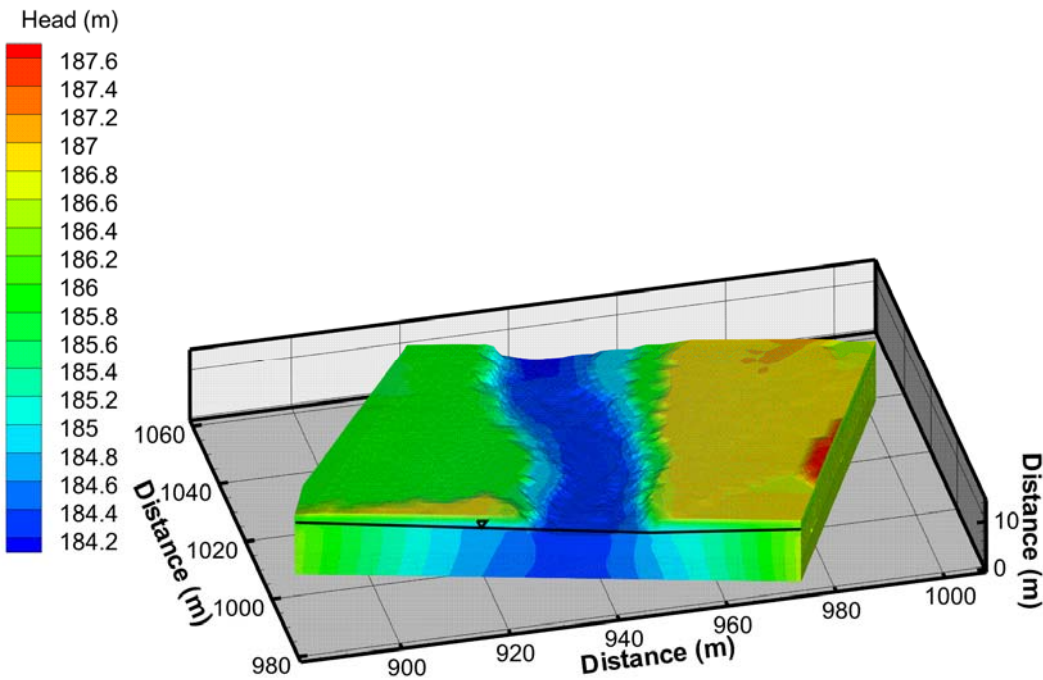**Figure 11. Simulation results for water depths in the Pine River.**

Figure 12. Hydraulic head results for the Pine River simulation.

The fully-integrated modelling approach allows for the calculation of the water exchange fluxes across the entire surface of the domain, including the groundwater-surface water interactions over the riverbed reach.

42

The calculated rates for the Pine River simulations are given in Figure 13. As part of the field-based study, Conant (2004) estimated the groundwater discharge/recharge rate (Figure 13) based upon riverbed temperature measurements and Darcy fluxes calculated using streambed piezometer measurements (Figure 8a depicts piezometer locations). In comparing the results provided in Figure 13, it can be seen that HydroGeoSphere is able to simulate the general groundwater discharge/recharge patterns over the stream bed. The field-based observations indicate several regions of high discharge into the stream where the fluxes are greater than 200 $L/m^2/d$. These high discharge regions are captured within the simulation results. The simulated results exhibit some regions with slightly higher discharge rates into the river compared to the field-based observations. This is a result of estimating the groundwater fluxes over the bottom boundary of the simulation domain in addition to simplifying the heterogeneity of the subsurface geology. The low flow discharge zones were also well simulated, matching both location and flux rates. As concluded by Conant (2004), the groundwater discharge patterns in the riverbed are more dependent on the subsurface geology, and less so on the surficial riverbed geology for this site. This conclusion is confirmed by the HydroGeoSphere simulation because it was necessary to incorporate the general subsurface geology patterns in order to obtain a reasonable match with the observed riverbed fluxes. The windows in the semi-confining layer beneath the stream regulate the discharge of groundwater to the subsurface and the regions without windows through the semi-confining layer have significantly lower discharge rates to the subsurface. As such, incorporating the general subsurface geological patterns was necessary to properly reflect the exchange fluxes between the surface and subsurface.

The simulated thermal energy regime presented in this work is representative of steady-state conditions during a typical July at the Angus site. The simulated temperature distribution over the surface of the domain area is given in Figure 14. The temperatures in the upper banks are high, due to the high rainfall temperature and because of the incoming thermal radiation fluxes. Within the river, the temperature is approximately 18.4^oC, which matches the average field-based stream temperatures recorded by Conant (2004) for the summer months. It should be noted that the surface thermal conditions are depth integrated and cannot represent thermal stratification that may be present in the field. In addition, the air temperatures and incoming radiation values were not varied diurnally in the simulation, as they are representative of near steady-state conditions. In a later chapter, exploratory computations will be made to elucidate the impact of diurnal atmospheric inputs on the surface and subsurface temperature fields.
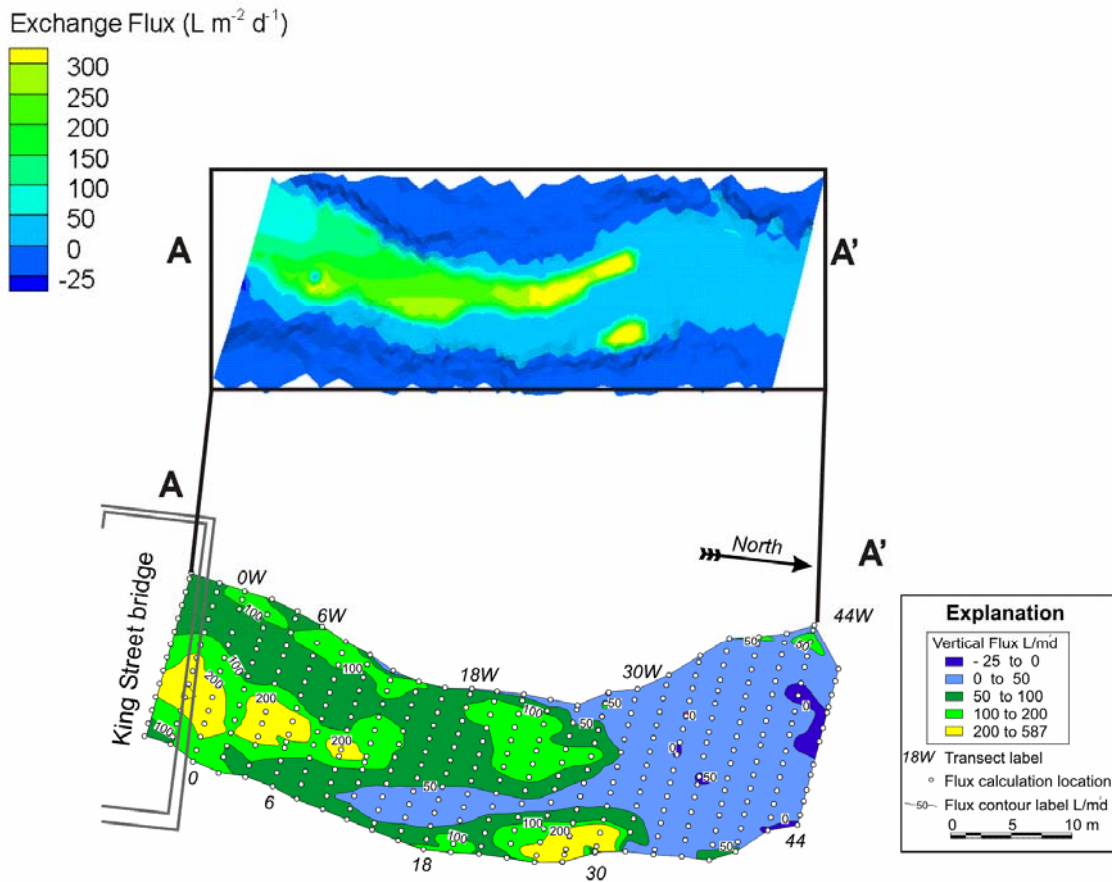
Figure 13. Plan views of the simulated (top) and field-based (bottom) riverbed water exchange fluxes for the Pine River. Positive fluxes mean water is flowing from the subsurface to the surface. The river flows from A to A'. Field-based data are from Conant, 2004.
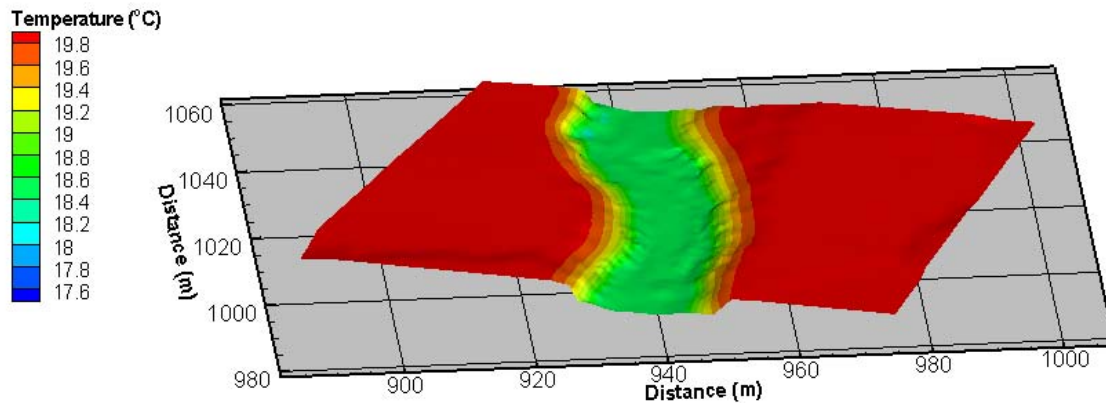
Figure 14. Surface temperature distribution for the Pine River simulation.

The calculated subsurface temperature distribution is given in Figure 15. As expected, the temperature of the top layer of the subsurface, located 0 to 10 cm below the riverbed, does not correspond to the surface water temperatures due to the high non-equilibrium exchange fluxes from the subsurface into the surface along the stream. The rate of groundwater flux from the subsurface determines the temperature patterns in the shallow riverbed deposits. The warmer areas in the riverbed reflect zones where groundwater inputs are low and the dispersive/diffusive movement of the incoming thermal energy is relatively important. Conversely, the lower temperature regions in the riverbed are dominated by the advective movement of thermal energy caused by the discharging groundwater. The impact of the temperature of the surface water in the river on the subsurface temperatures is limited, for the most part, to the top two or so meters of the subsurface.

In comparing the field-based streambed temperatures to the calculated temperatures for the top layer of the subsurface (Figure 16), it can be seen that the thermal patterns are similar. The high temperature zones in regions of low groundwater discharge, and low temperature zones in regions of high groundwater discharge are present in the simulation results. The regions with overestimated groundwater discharge to the surface also have underestimated streambed temperatures because a higher flux of cool groundwater is moving towards the surface in the simulated results than in the field-based observations, as discussed previously. While there are differences between the calculated temperatures in the subsurface and those observed in the field, the thermal patterns and temperature ranges compare reasonably well, indicating that

45

HydroGeoSphere is capable of capturing the salient spatio-thermal patterns. The field-based observations are a snapshot of streambed temperatures measured over two days and are likely influenced by temporally variable atmospheric and hydrological conditions. Thus, all the details cannot be captured in the steady-state simulations and exact matches were not expected.
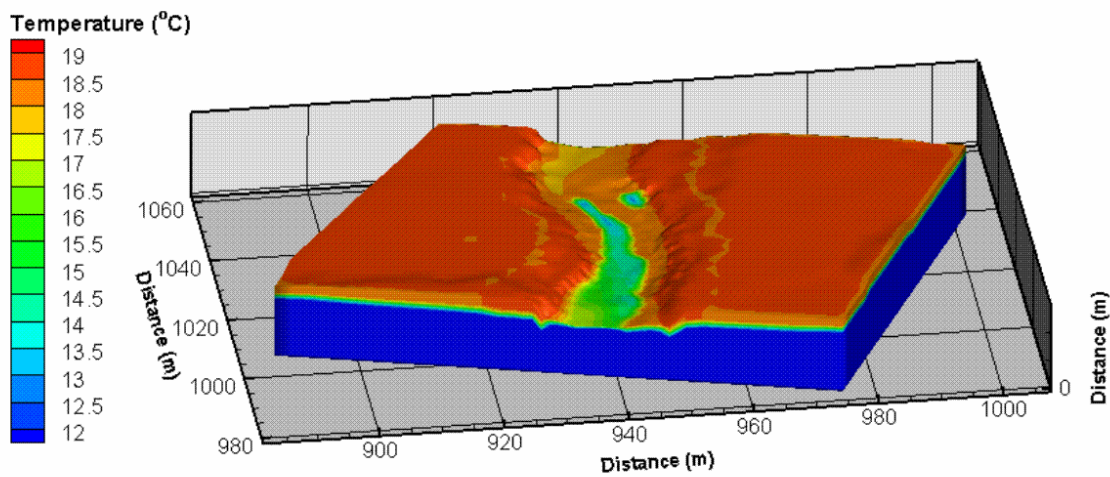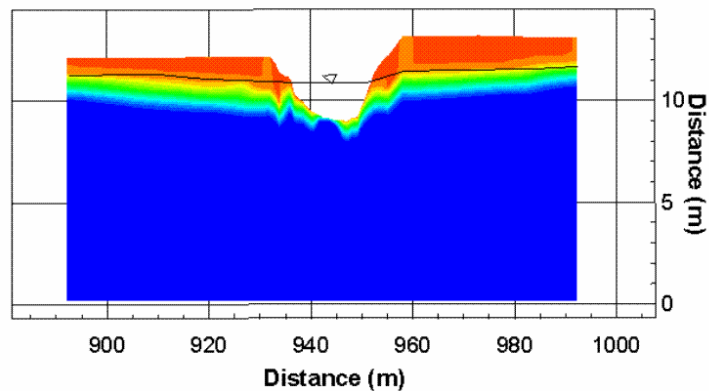
Figure 15. Subsurface temperature distribution for the Pine River simulation for a) the entire 3D domain, and b) through a cross section at y = 1020 m (4x vertical exaggeration).

46
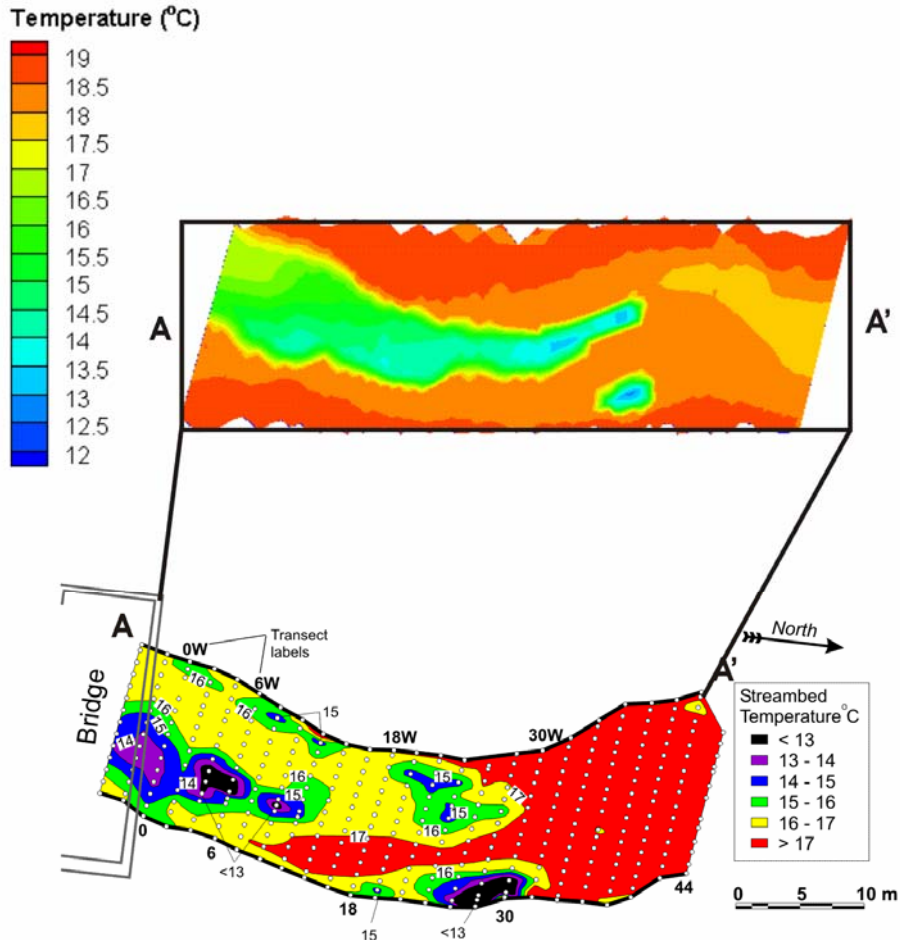
Figure 16. Plan views of the simulated (top) and field-based (bottom) riverbed temperatures for the Pine River. The river flows from A to A'. Field-based data are from Conant, 2001.

An advantage of the fully-integrated approach for simulating thermal energy transport is that the advective and dispersive thermal energy exchange fluxes between the surface and the subsurface are directly calculated by the model. Figure 17 shows both the advective and dispersive thermal energy exchange fluxes. In Figure 17a, a positive thermal energy exchange flux indicates that the thermal energy is moving from the subsurface to the surface, and a negative value indicates that thermal energy is moving from the surface to the subsurface. The advective thermal energy exchange flux is much larger than the dispersive flux and thus dominates the net thermal energy exchange. This demonstrates why the regions below the river where the high advective discharge occurs remain at a lower temperature compared to the river itself.

The positive advective thermal energy exchange flux within the river shows that the thermal energy is moving from the cooler subsurface to the warmer surface water in the river. The slightly negative dispersive thermal energy exchange flux indicates that some surface thermal energy is moving into the subsurface, slightly increasing the temperature of the geologic media and the groundwater.
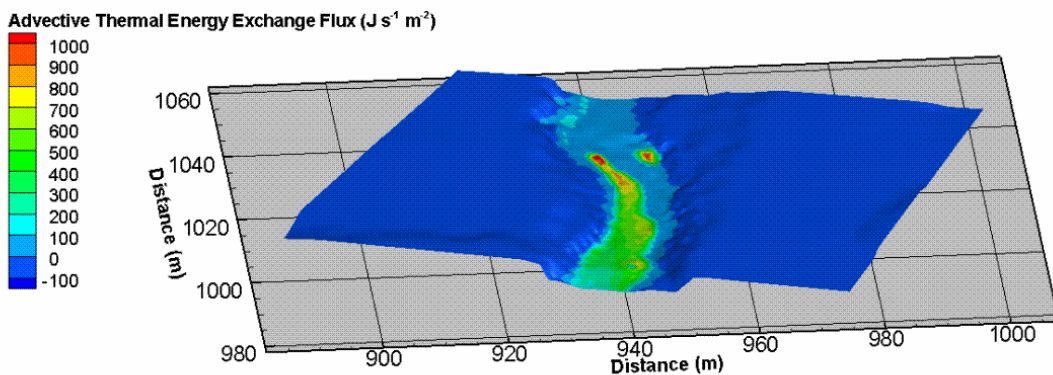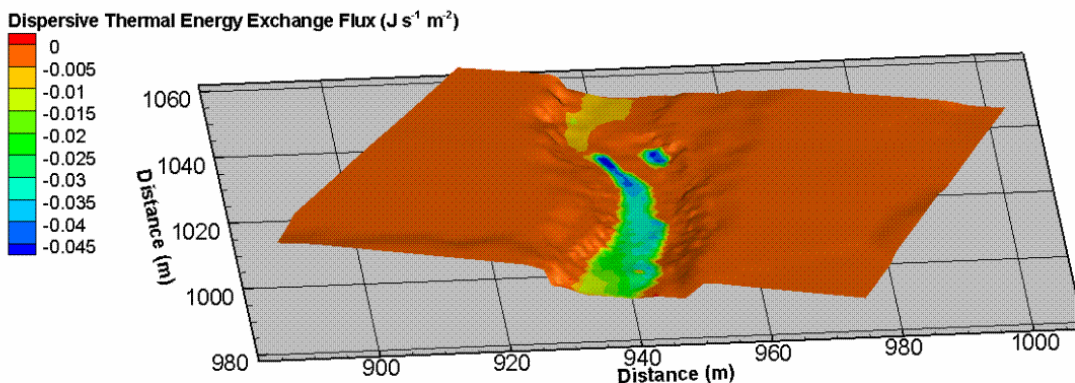
Figure 17. a) Advective thermal energy exchange flux and b) dispersive thermal energy exchange flux patterns for the Pine River simulation.

4.4 Summary

The Pine River was intensively characterized and monitored for surface and subsurface hydraulic interactions, in addition to streambed and stream temperatures, by Conant (2001). HydroGeoSphere

simulations of the Pine River site were conducted in order to compare the thermal energy transport results to the field observations.

Overall, the simulation results for the Pine River site are believed to be representative of the field-based observations. Exact agreement was not achieved, nor expected, for several reasons. Perhaps most importantly, the simulation results are based on a steady-state assumption, whereas the field observations represent a snapshot in time of the transient processes occurring at the time the measurements were taken. Other discrepancies between the simulated results and the field observations can also be attributed to using a simplified representation of the complex geology at depth (e.g. discretization of the semi-confining deposits) and, to a lesser extent, reduced data availability for the area to the west of the Pine River. In the next chapter, a suite of transient simulations will be performed to explore the impacts of both transient hydraulic conditions, as driven by discrete rainfall events, and diurnal atmospheric energy inputs on the thermal responses. These transient simulations will be based on the Pine River setting.

Chapter 5

Transient Simulation of Thermal Energy Transport

5.1 Introduction

The steady-state simulation of the Pine River site demonstrates the ability of HydroGeoSphere to match field observations; however, it is also important to consider transient conditions. Several parameters used in the Pine River simulation can vary over a variety of scales with time. Diurnal fluctuations of some atmospheric input parameters, in addition to discrete rainfall events, will be applied to the Pine River example. These simulations will be used to investigate how the thermal energy regime reacts to the transient atmospheric conditions and precipitation events, respectively.

5.2 Diurnal Fluxes

Many atmospheric energy inputs vary significantly over the course of a day. Two parameters with large diurnal variability include incoming shortwave radiation and air temperature. Transient simulations of the Pine River example will be conducted for a time-frame of several days with these two energy drivers fluctuating diurnally.

The inclusion of a positive incoming shortwave radiation term will increase the surface and subsurface temperatures. While the daily average for incoming shortwave radiation is usually a positive value, it can fluctuate to below zero at night, when solar radiation is essentially non-existent. Therefore, it is anticipated that including diurnal fluctuations of shortwave radiation will impact the thermal conditions of the hydrologic system.

The impact of air temperature on the surface and subsurface thermal regimes is intuitive; the warmer the air temperature, the warmer the ground surface. However, air temperature can fluctuate by over 15°C over a 24 hour period. Air temperature plays an important role in many of the atmospheric contributions to the hydrologic regime. The longwave radiation and sensible and latent heat fluxes are all directly related to air temperature in HydroGeoSphere. In addition, the temperature of the precipitation is assumed to equal the air temperature. Therefore, the diurnal fluctuations of air temperature are believed to have a significant impact on the thermal conditions of the hydrologic regime.

For the Pine River transient simulations presented in this chapter, sinusoidal input functions are used for both incoming shortwave radiation and air temperature. Respectively, air temperature and incoming

shortwave radiation were set to vary from 15°C to 25°C, and from -5 W/m^2 to 115 W/m^2, over each 24 hour period (Figure 18). The remainder of the parameters describing the physical system are identical to those described in Chapter 4. The steady-state flow system also remains identical to that presented in Chapter 4 for the simulations presented below in which the air temperature and incoming shortwave radiation is allowed to vary diurnally. Later in this chapter, cases in which discrete rainfall events are applied, but constant-in-time atmospheric energy inputs are assumed, will be presented.
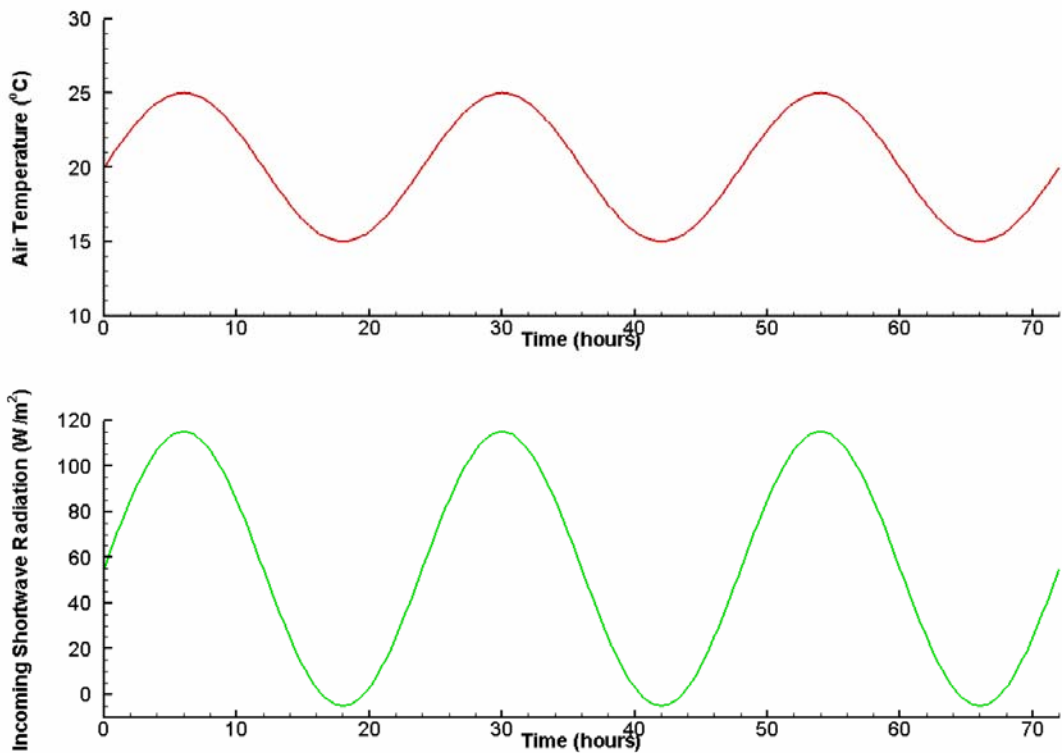
Figure 18. Diurnal fluctuations for air temperature (top) and incoming shortwave radiation (bottom).

5.2.1 Surface and Subsurface Temperature

The surface temperature responds rapidly to the changes in both air temperature and shortwave radiation (Figure 19). At the peak of the cycle, when the air temperature is 25 $^{\circ}$C and the incoming shortwave radiation is 115 W/m^2, the temperature in the higher topographical regions is approximately 24.9 $^{\circ}$C. The stream temperature, however, remains at just under 18.5 $^{\circ}$C because it is controlled by the inlet boundary condition of the stream and is depth-averaged (Figure 19a).

Figure 19. Surface temperatures at: a) the peak of the diurnal cycle (t = 6 hours) ; b) the trough of the diurnal cycle (t = 18 hours).

When the air temperature and incoming shortwave radiation terms are at their minimum (15 $^{\circ}$C and -5 W/m^2 respectively), the surface temperature is lowered to between 15 $^{\circ}$C and 16 $^{\circ}$C everywhere except in the streambed, demonstrating the rapid response of the surface to atmospheric fluctuations. (Figure 19b). In Figure 19, it can be seen that the highest topographical locations undergo the most rapid temperature changes, because there is no advective heat flux from the subsurface to the surface to buffer the temperature (Figure 13). As previously mentioned, the stream temperature itself does not change significantly because of its dependence on the inlet boundary condition. The surface areas adjacent to the stream have a dampened reaction to the change in atmospheric conditions because overland flow transmits the warm rainfall water towards the river before it can cause significant heating of the ground surface.

The stream temperature changes only slightly between the maximum and minimum values of air temperature and incoming shortwave radiation. The variation in temperature is less than 0.1 ^{o}C, which indicates that the calculated stream temperature is controlled mainly by the prescribed inlet temperature, rather than the diurnal nature of the incoming thermal fluxes. If the headwaters of the stream had been included in the simulated domain, thus removing the need for an inlet boundary condition, the effect of the diurnal fluxes would have been more apparent.

The energy storage attributes of the top layer of the subsurface (depths less than 10 cm) buffers the effects of the diurnal changes in air temperature and incoming shortwave radiation (Figure 20). The maximum subsurface temperature is only 20.3^{o}C, almost 5 ^{o}C less than the peak air temperatures, and the minimum temperature in the top layer of the domain is 15.9 ^{o}C when the air temperature is the lowest (15 ^{o}C). The lower maximum and higher minimum subsurface temperatures compared to the atmospheric conditions at the same time indicate that the thermal energy exchange fluxes across the land surface are not sufficient to transfer all of the energy rapidly to depths more than a few centimeters to ten centimeters.

The top subsurface layer below the streambed varies in temperature throughout the period of diurnal atmospheric fluctuations significantly more than the stream temperatures, as the stream temperatures are regulated by the prescribed input temperature. This is because the dispersive flux of thermal energy from the surface to the streambed is larger in this region than elsewhere on account of the larger temperature differences between the surface water and the groundwater. The regions with the highest groundwater discharge to the stream exhibit, however, the smallest change in temperature due to the atmospheric fluctuations. These results are consistent with the streambed thermal responses described by Constantz (2008). Constantz (2008) proposed that for a high inflow of groundwater, the streambed sediment temperature will have less diurnal fluctuations than regions with lower groundwater discharge.

In addition to lower maximum and higher minimum subsurface temperatures compared to the atmospheric conditions, the timings of the maximum and minimum temperatures in the subsurface are delayed. As the thermal energy from the atmospheric inputs is transferred first to the surface via shortwave and longwave radiation, and then to the subsurface through advective and/or dispersive thermal energy exchange fluxes, it takes longer for the subsurface to react to the changes in atmospheric conditions. Figure 21 shows the calculated maximum and minimum subsurface temperatures which occur one hour after the maximum and minimum atmospheric inputs.
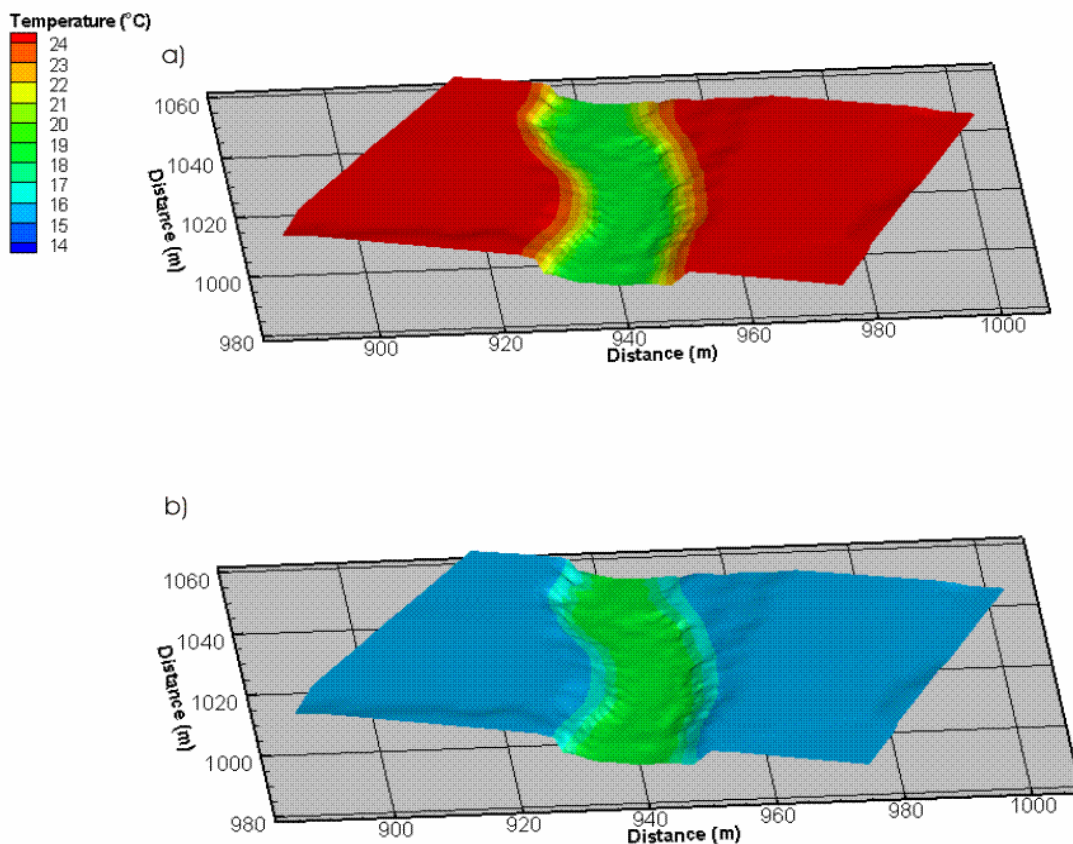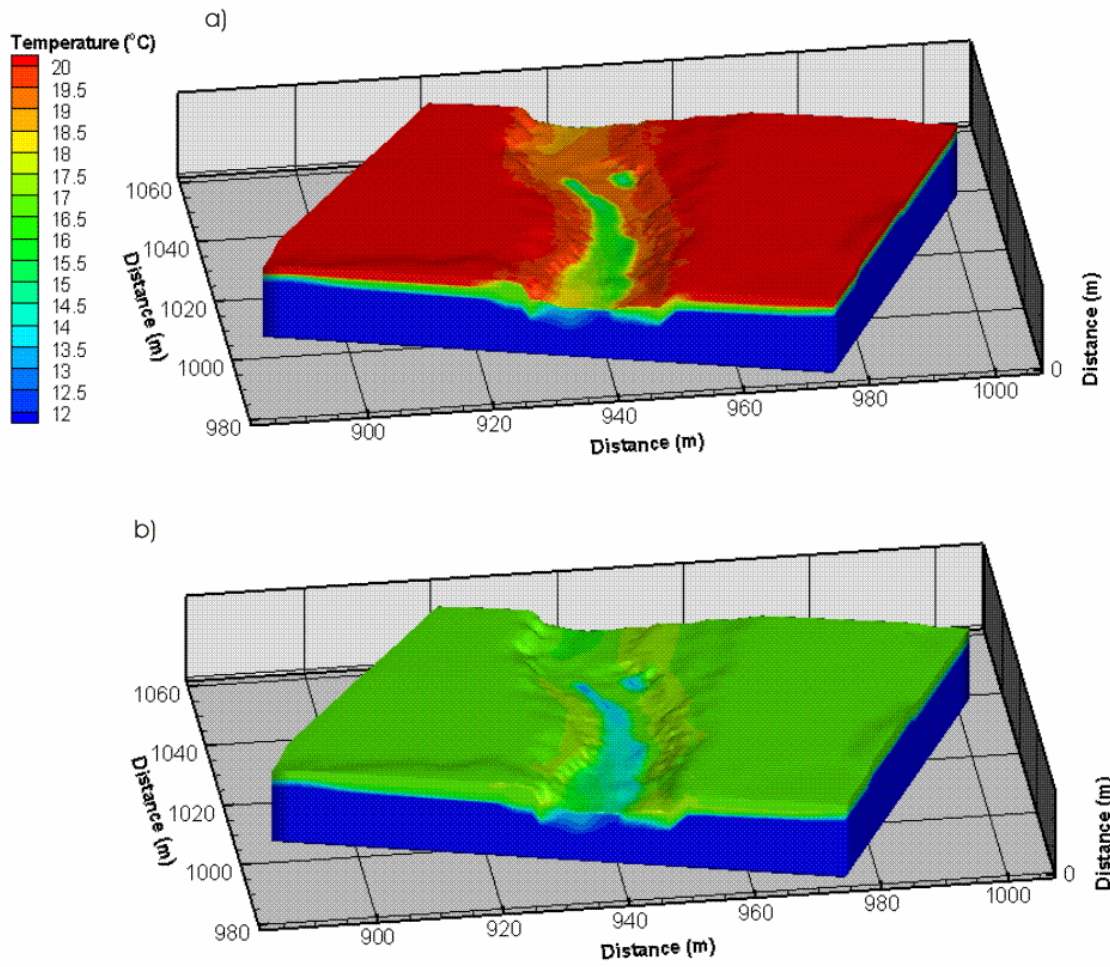
Figure 20. Subsurface temperatures at: a) the peak of the diurnal cycle (t = 6 hours); b) the trough of the diurnal cycle (t = 18 hours).
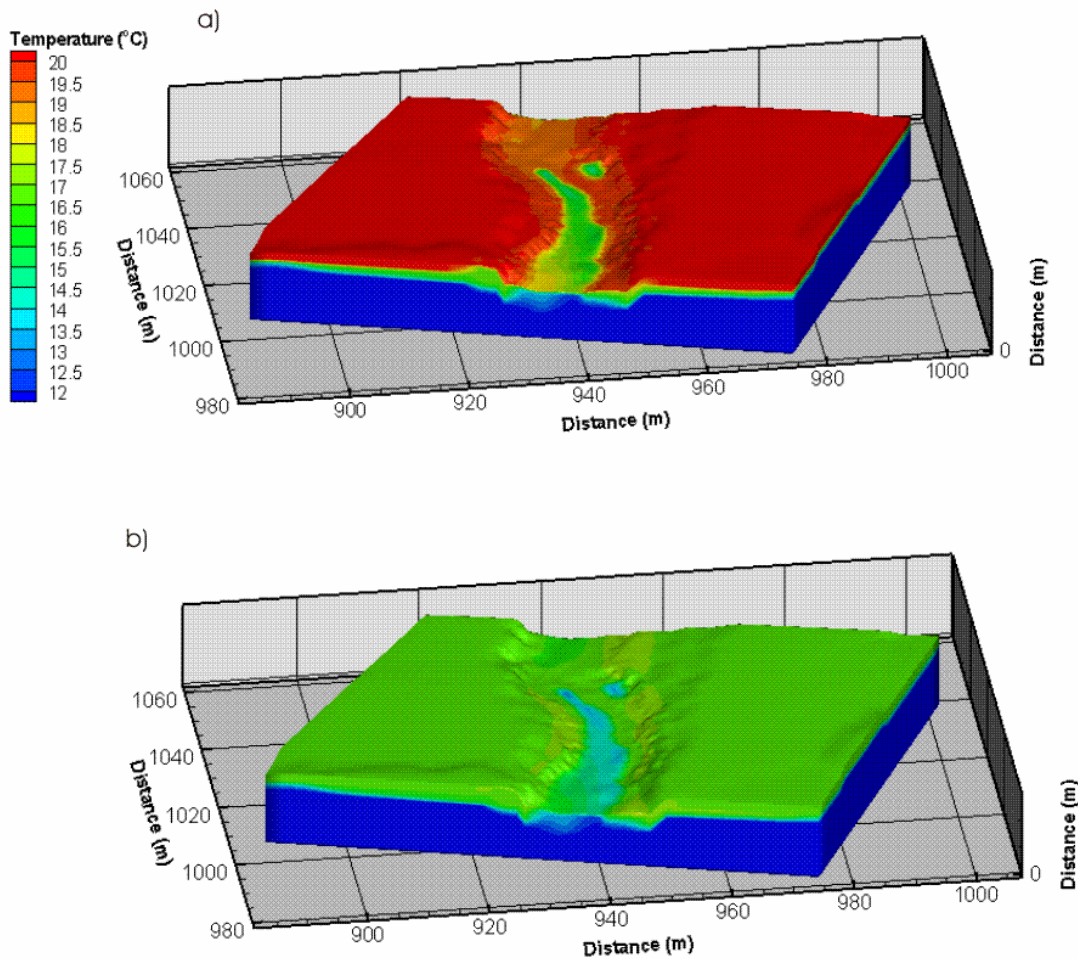
Figure 21. Diurnal simulations: a) The maximum subsurface temperatures, one hour after the peak atmospheric conditions (t = 7 hours); b) the minimum subsurface temperatures, one hour after the lowest atmospheric conditions (t = 19 hours).

5.2.2 Advective and Dispersive Thermal Energy Exchange Flux

The advective and dispersive thermal energy exchange fluxes are the connection between the surface and subsurface thermal energy regimes. The transient thermal transport simulations incorporating diurnal atmospheric fluctuations utilize the steady-state water flow system as presented in Chapter 4. As such, any changes in the advective thermal energy exchange flux is a result of a change in the temperature of the water exchanging between the two regimes and not the quantity of water exchanging. In Figure 22 it can be seen that the advective thermal energy exchange flux changes between the peak and the trough of the

55

diurnal cycle predominantly in the regions of high groundwater discharge to the stream. Note the change in scale above 0 J s^{-1} m^{-1}. It was shown in Figure 19 that the surface temperatures in the higher topographical regions corresponded to the maximum and minimum air temperatures of the diurnal cycle. As such, the advective thermal energy exchange flux in these regions was highest at the peak of the cycle, and lowest at the trough.
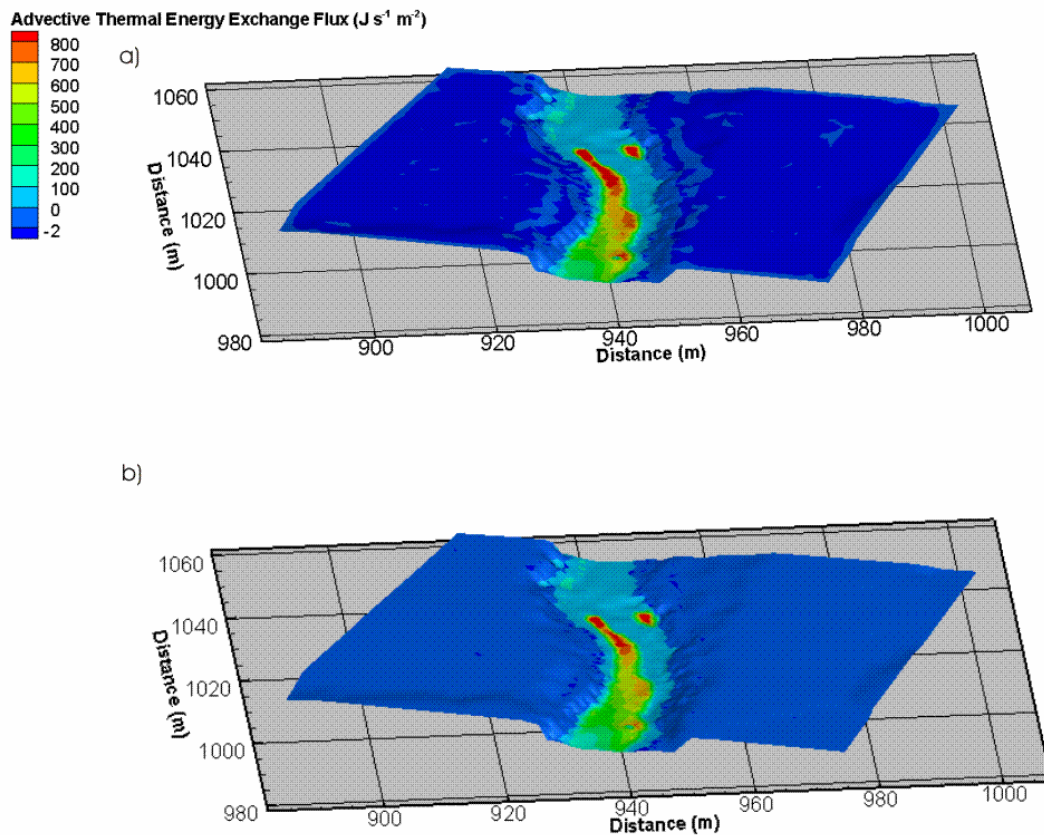
Figure 22. Advective thermal energy exchange flux at: a) the peak of the diurnal cycle (t = 6 hours); b) the trough of the diurnal cycle (t = 18 hours). Note the change in scale at zero J s^{-1} m^{-1}.

The advective thermal energy exchange flux is dependent upon both the quantity and the temperature of the water exchanging between the two regimes. The advective flux of water exchanging from the surface to the subsurface in the higher topographical regions is significantly less than the groundwater discharge into the stream (Figure 13). However, the temperature of the water exchanging in the higher topographical regions

is greater than that discharging into the stream. Nevertheless, the magnitude of the advective thermal energy exchange flux in the higher topographical regions is significantly lower than that discharging into the stream. This clearly illustrates that the quantity of water exchanging between the surface and subsurface regimes controls the magnitude of the advective thermal energy exchange fluxes.

The dispersive thermal energy exchange flux given in Figure 23 varies both spatially and temporally, acting either as a source or a sink of thermal energy to the subsurface regime. At the peak of the diurnal cycle, the dispersive energy exchange flux is negative in the higher topographical regions (transferring thermal energy from the surface to the subsurface) because the surface temperature is higher than in the subsurface. However, within the low groundwater discharge regions along the streambed, the subsurface temperatures are higher than the surface values, and therefore the dispersive thermal energy exchange flux is positive, thus transferring thermal energy from the subsurface to the surface. Because the air temperature changes throughout the day, these thermal fluxes reverse in direction (e.g. the dispersive thermal energy exchange flux in the higher topographical regions becomes a positive value when the surface temperatures are lower than those in the subsurface). In the low groundwater discharge zones within the streambed, the dispersive thermal energy exchange flux is negative when the stream temperature is higher than the subsurface value.

Overall, the transient nature of the atmospheric inputs induces noticeable changes in the thermal energy transport regime. The surface temperatures change quickly in response to the atmospheric conditions, whereas the subsurface temperatures were found to lag in time. The advective thermal energy exchange flux also changed over the course of the diurnal cycle, increasing and decreasing with changes in the corresponding surface and subsurface temperatures. In addition, the dispersive thermal energy exchange flux fluctuated both spatially and temporally between a source and a sink of thermal energy to both the surface and subsurface as the atmospheric conditions changed.
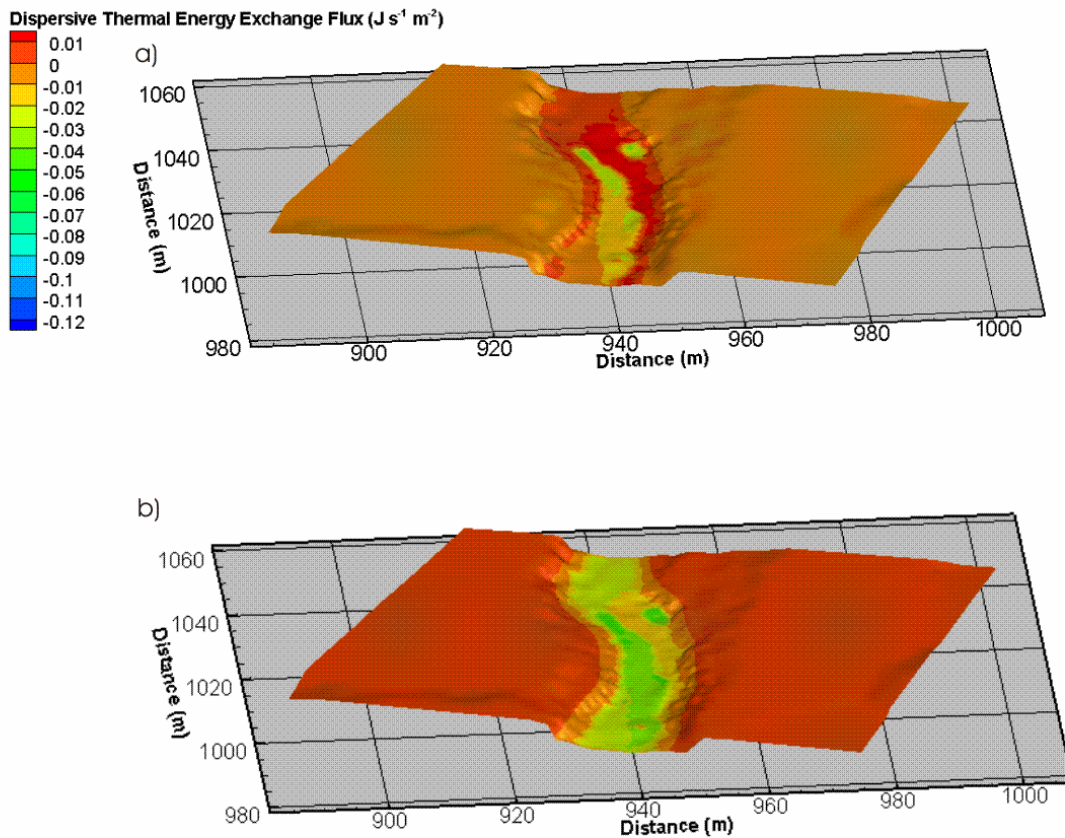
Figure 23. Dispersive thermal energy exchange flux at: a) the peak of the diurnal cycle (t = 6 hours); b) the trough of the diurnal cycle (t = 18 hours).

5.3 Transient Precipitation Events

Three separate simulations involving different individual precipitation events were conducted to investigate the impacts of a transient flow system on the thermal energy conditions: a low rainfall rate (2 mm/hr), a medium rainfall rate (1 cm/hr), and a high rainfall rate (5 cm/hr). The duration of the rainfall is one hour for each case, followed by a 5-day recession period, ensuring that all three simulations return to essentially the same hydraulic conditions. The initial flow system is given by the steady-state results presented in Chapter 4. The atmospheric energy inputs are held constant throughout the entire rainfall event and recession period as given in Chapter 4. The results for the hydraulic heads, water depths, water exchange fluxes, surface and

subsurface temperatures, and advective and dispersive thermal energy exchange fluxes at the end of each rainfall event, and the end of the recession period, are presented and discussed below.

5.3.1 Flow System

The discrete rainfall events applied to the Pine River setting will change the flow system during and shortly after the rainfall, in addition to the temperature patterns. Hydraulic heads will increase as more precipitation is added to the surface of the domain (Figure 24). The most significant changes in hydraulic head are limited to the top 0.4 m of the domain in the higher topographical regions and along the stream banks (Figure 25). The water saturation in the top 0.4 m of the subsurface also increases with increasing rainfall rate along the stream banks and over the higher topographical regions (Figure 26). The higher rainfall rate also increases the overland flow water depths in the seepage faces along the river (Figure 27). The water exchange flux increases with the rainfall rate from the surface to the subsurface most noticeably away from the stream in the higher topographical areas (Figure 28) which causes the increase in water saturations.

The Pine River domain can be divided into three different regions based on the hydraulic response to the rainfall events: the higher topographical regions, the stream banks and the streambed region. The higher topographical regions are located furthest from the stream, where the terrain is relatively flat, thus inhibiting overland flow (Figure 29). As such, the applied rainfall remains on the surface until it infiltrates into the subsurface. As the rainfall rates increase, the difference between the rainfall rate and the infiltration rate also increases. This causes an increase in the overland water depths, water exchange fluxes, hydraulic heads, and saturations in the higher topographical regions (Figure 24 - Figure 28).

The stream banks are steep in comparison to the slopes furthest from the stream. As such, the overland flow is significantly higher in the bank region than in the higher topographical areas (Figure 29). The infiltration to the subsurface along the higher regions of the stream banks not influenced by the capillary fringe effect increases slightly as the rainfall rates increase (Figure 28). This results in a slight increase in saturation and hydraulic head in these regions with the higher rainfall rates (Figure 24 and Figure 26). The infiltration along the higher regions of the stream banks is less than that infiltrating in the higher topographical regions, and therefore the changes in saturation and hydraulic head are also less along the stream banks than further away from the stream. The water depths increase slightly as the rainfall rates are increased; however, no significant amount of water accumulates due to the rapid runoff over the slopes (Figure 27).

The streambed region appears to change very little as the rainfall rates increase with regard to subsurface hydraulic heads, water depths, water exchange fluxes and flow rates (Figure 24 - Figure 29). As mentioned

in Chapter 4, the hydraulic and thermal conditions of the stream are dominated by the prescribed inflow boundary condition. The simulated stream discharge rate, which corresponds to the field observations, is approximately 1.9 m^3/sec and, therefore, the addition up to 5 cm of rainfall to the domain over a one hour period is relatively insignificant, causing less than 0.01 mm increase in the stream depth.

5.3.2 Surface Temperatures

At the end of all three rainfall events (t = 1 hour), differences in surface temperature can be seen between each case involving the different rainfall rates, and between the higher topographical regions and the stream banks (Figure 30). The surface temperatures in the higher topographical regions reach the air/rainfall temperature of 20 ^{o}C in all three simulations because the rainfall does not runoff in these regions, but instead infiltrates to the subsurface. The temperature regime in the stream bank region of the surface responds slower than the higher topographical regions to the rainfall events because most of the rainfall rapidly runs off the slopes, rather than remaining on the surface and heating it. The thermal energy transferring from the rainwater to the stream banks is not sufficiently high to dominate over the dispersive thermal energy flux from the surface to the subsurface, therefore reducing the apparent impact of the rainwater on the surface stream bank temperature regime. As the rainfall rate increases, the temperature of the stream banks increase more quickly relative to the lower rainfall rates as more thermal energy is added to this region, and the transfer of thermal energy to the surface becomes significantly larger than the dispersive thermal energy exchange flux from the surface to the subsurface. At the end of the simulation (t = 5 days), the stream temperature remains the same, at 18.5 ^{o}C, and the temperature of the higher topographical regions and stream banks have decreased, because the effects from the rainfall event have dissipated. The banded temperature pattern shown in Figure 28d at the end of the simulation period simply reflects the variations in the depth to the water table and the changes in water saturations in the unsaturated zone with distance from the stream.

Figure 24. Hydraulic heads at: a) the end of the high rainfall event; b) the end of the medium rainfall event; c) the end of the low rainfall event; d) the end of all simulations (t = 5 days).

Figure 25. Cross-section of hydraulic heads at y = 1020 m at: a) the end of the high rainfall event; b) the end of the medium rainfall event; c) the end of the low rainfall event; d) the end of all simulations (t = 5 days).

Figure 26. Water saturation at: a) the end of the high rainfall event; b) the end of the medium rainfall event; c) the end of the low rainfall event; d) the end of all simulations (t = 5 days).

Figure 27. Water depths at: a) the end of the high rainfall event; b) the end of the medium rainfall event; c) the end of the low rainfall event; d) the end of all simulations (t = 5 days).

Figure 28. Water exchange fluxes at: a) the end of the high rainfall event; b) the end of the medium rainfall event; c) the end of the low rainfall event; d) the end of all simulations (t = 5 days). Positive flux indicates water discharging to the surface.

65

Figure 29. Magnitude of overland flow at: a) the end of the high rainfall event; b) the end of the medium rainfall event; c) the end of the low rainfall event; d) the end of all simulations (t = 5 days).

Figure 30. Surface temperatures at: a) the end of the high rainfall event; b) the end of the medium rainfall event; c) the end of the low rainfall event; d) the end of all simulations (t = 5 days).

5.3.3 Subsurface Temperatures

The subsurface temperatures are also affected by the different intensities of the three discrete rainfall events (Figure 31). The subsurface temperatures in the top 0.1 m at the end of the high and medium rainfall simulations appear similar, while the low rainfall event produces lower temperatures along the stream bank compared to the other simulations. In the unsaturated zone of the regions furthest from the stream (the top 1.2 m), there remains no discernable difference between the subsurface temperature profiles at the end of the medium and high rainfall events (Figure 32). This indicates that the one hour rainfall period was sufficiently long for the shallow subsurface thermal conditions in these regions to reach equilibrium with the rainfall temperature. The temperature in the top 1.2 m of the subsurface for the low rainfall event is lower compared to the other simulations. This is because the infiltration rate is not high enough to bring the top 1.2 m of the subsurface to equilibrium with the atmospheric conditions.

The temperatures along the stream banks are different for all three rainfall rates (Figure 31 and Figure 32). For the medium and high rainfall events, the top 0.2 m of the subsurface has the same temperature profile along the stream banks. However, at depth, it is evident that the increased infiltration into the subsurface for a high rainfall rate transports warmer water further into the subsurface compared to both the medium and low rainfall rates (Figure 32). Additional differences along the stream banks between the calculated subsurface temperatures for the three different rainfall cases are observed earlier in each rainfall event, at 20 minutes (Figure 33 and Figure 34). Insufficient time has elapsed for the subsurface conditions to reach equilibrium with the surface conditions, as was observed in the top 0.2 m of the subsurface at the end of the medium and high rainfall events.

The subsurface temperatures below the stream do not significantly change between the three simulations at both 20 minutes into the rainfall event, and at the end of the rainfall event (Figure 31 to Figure 34). The water exchange in these regions is from the subsurface to the surface, and therefore any change in subsurface temperature below the stream is due to a change in the dispersive thermal energy exchange. It was previously shown that the temperature of the stream does not change with increased rainfall rates, and therefore the main driver of the dispersive thermal energy exchange flux, the difference between the surface and subsurface temperatures, also does not change with increased rainfall rates. Because the dispersive thermal energy exchange flux does not change, the subsurface temperatures below the stream also do not change.

Figure 31. Subsurface temperatures at: a) the end of the high rainfall event; b) the end of the medium rainfall event; c) the end of the low rainfall event; d) the end of all simulations (t = 5 days).
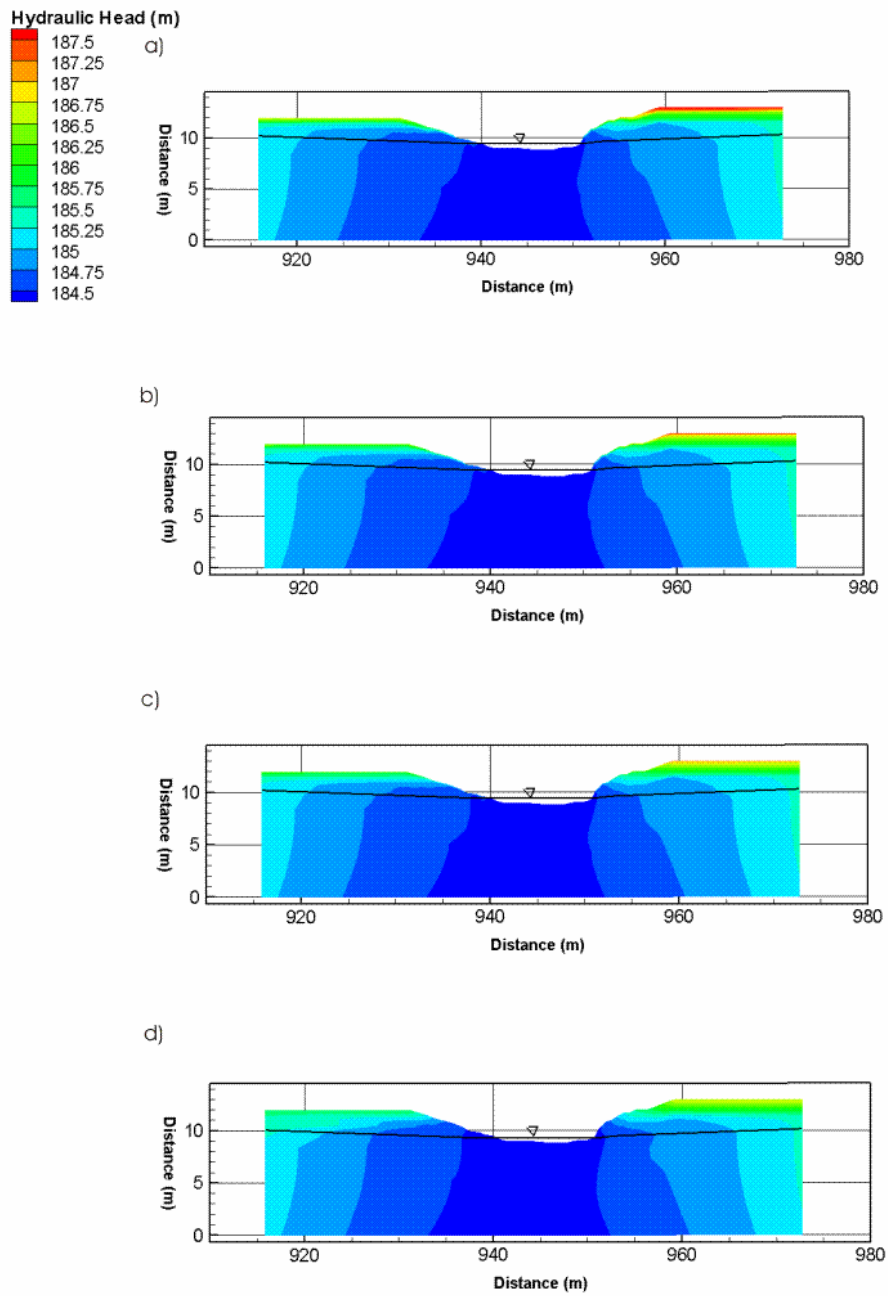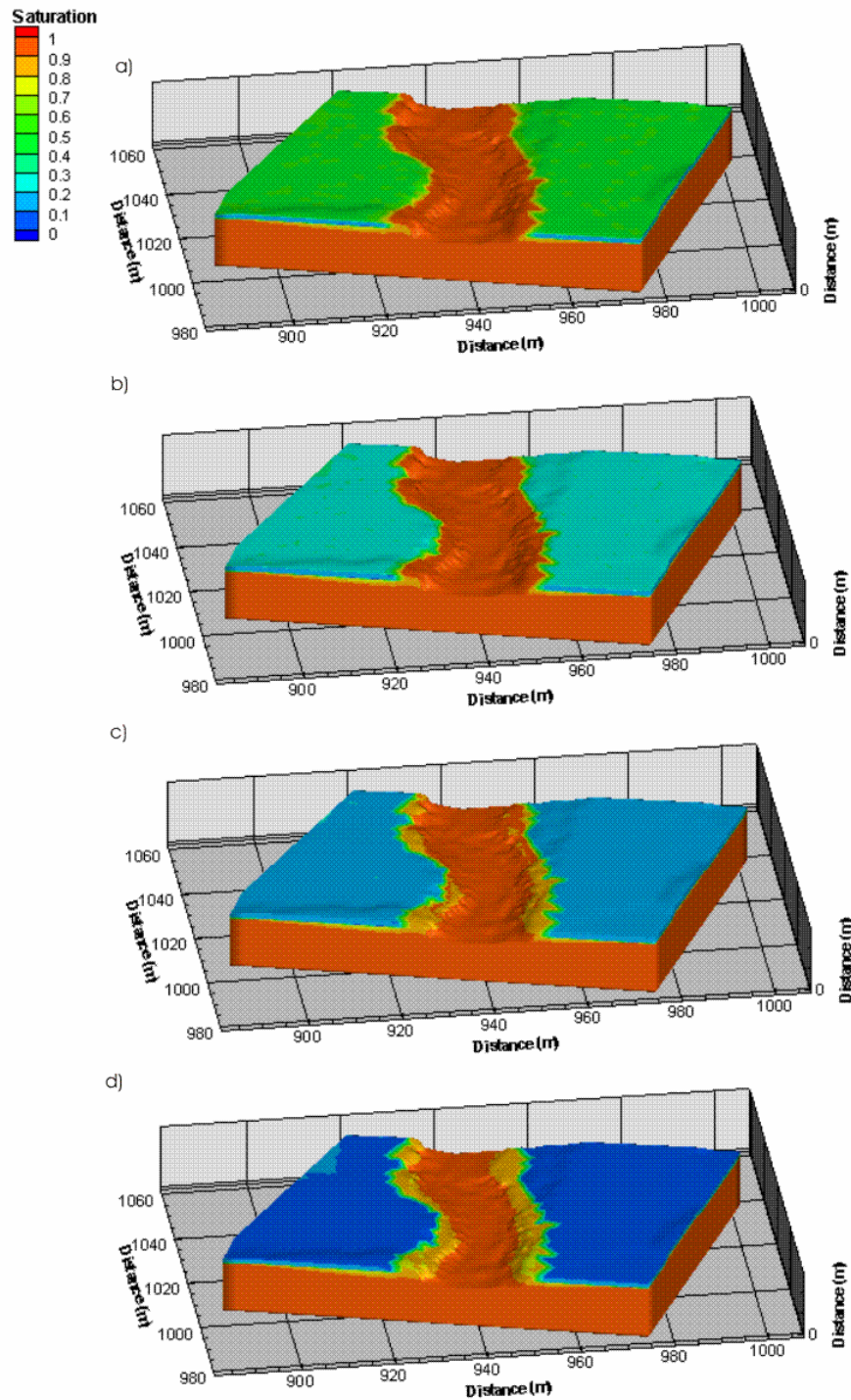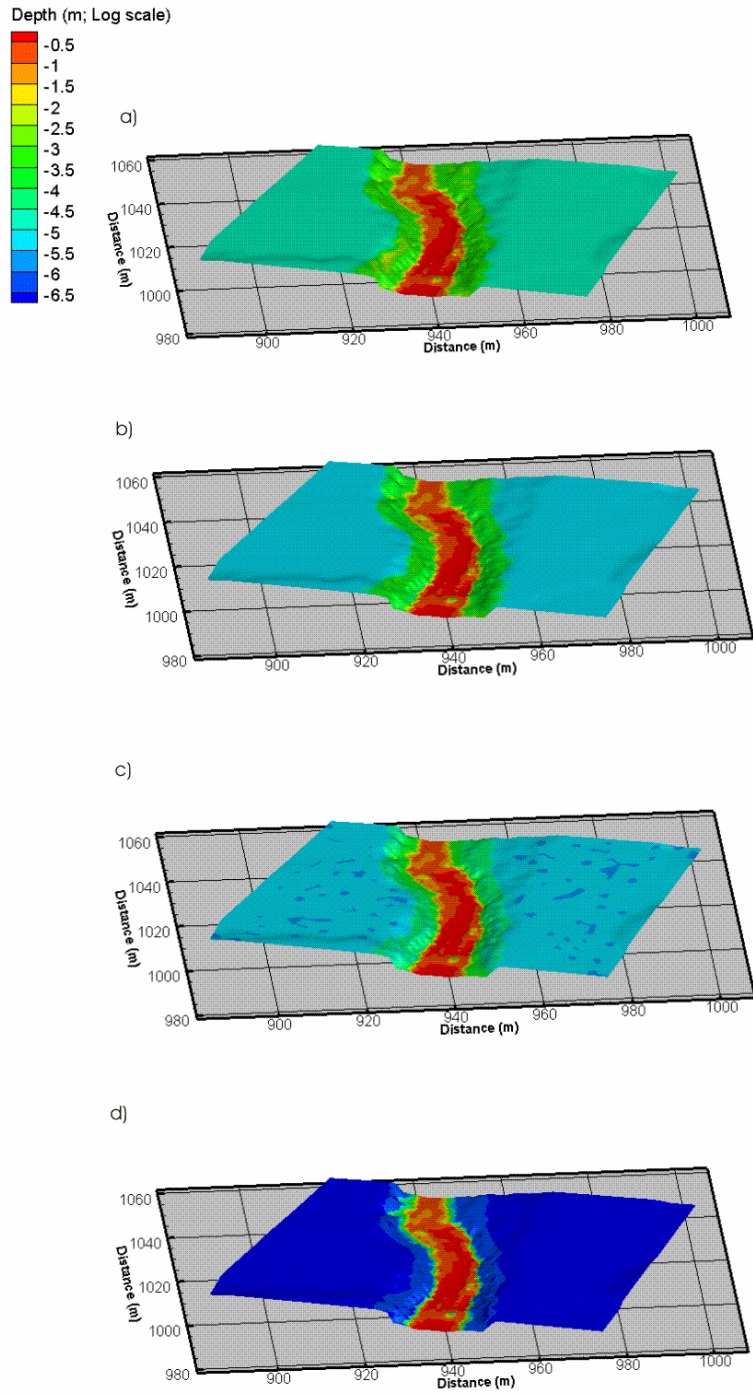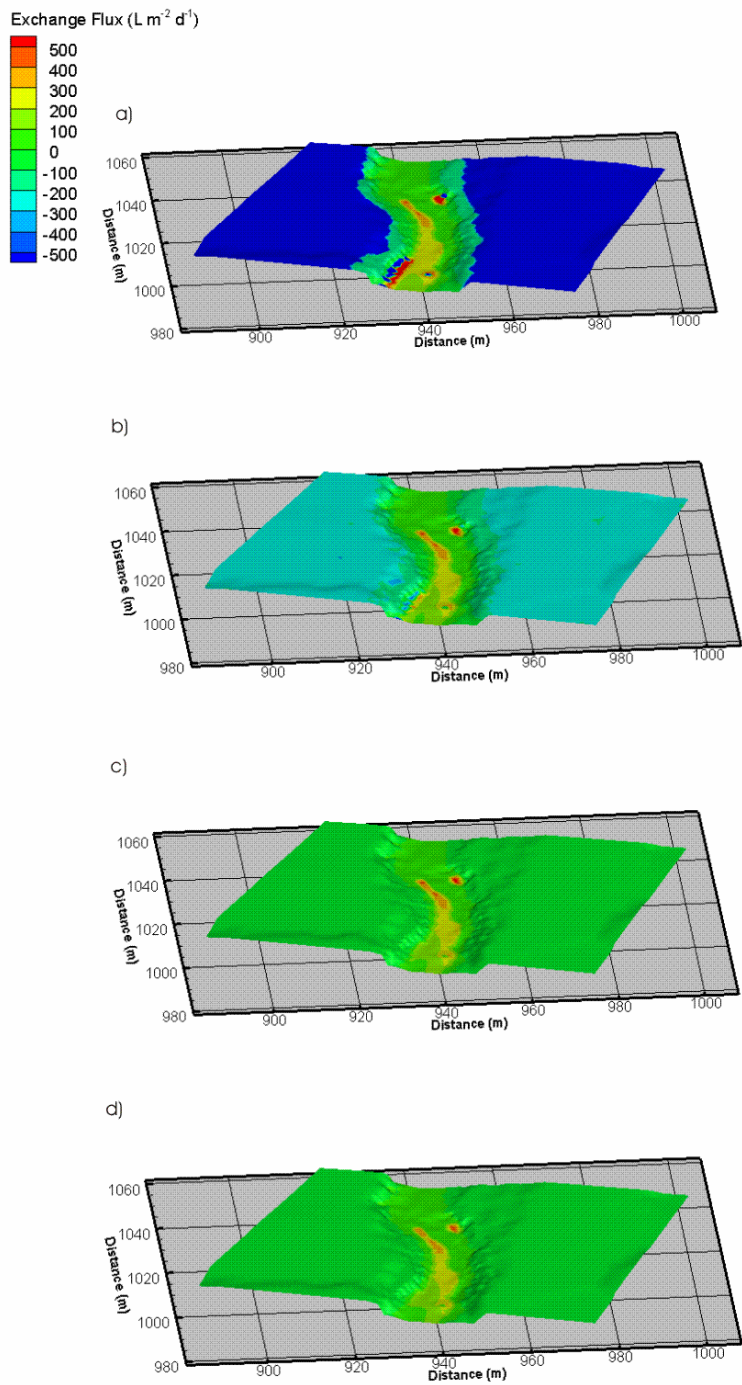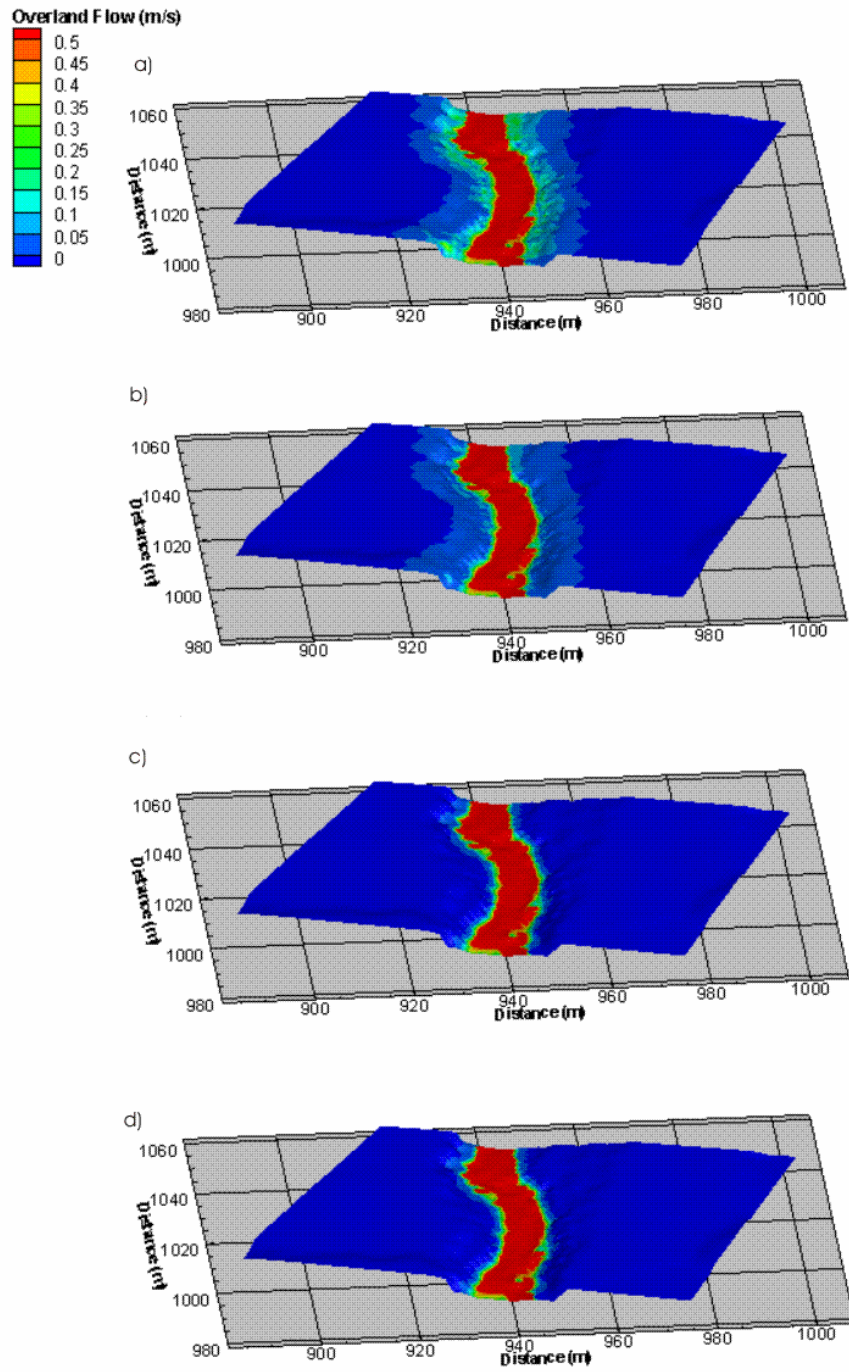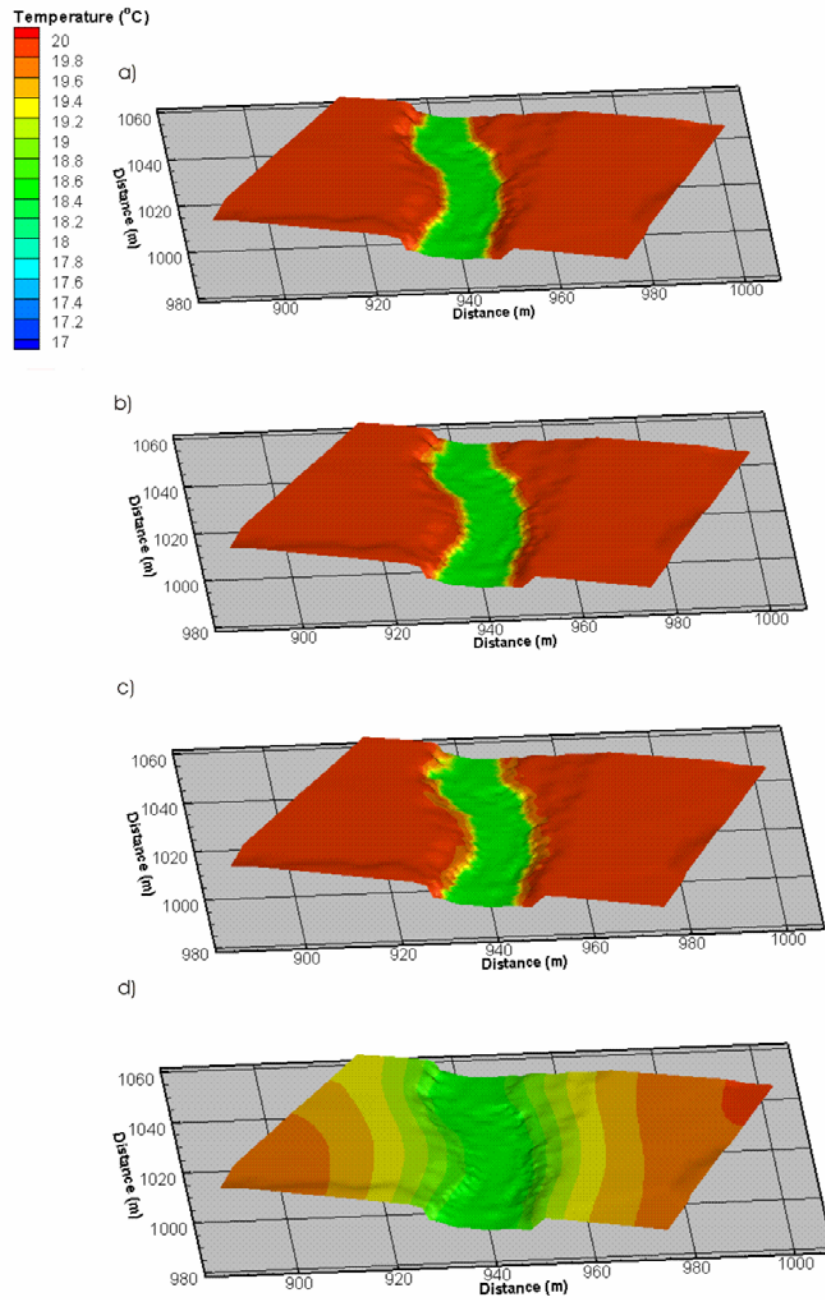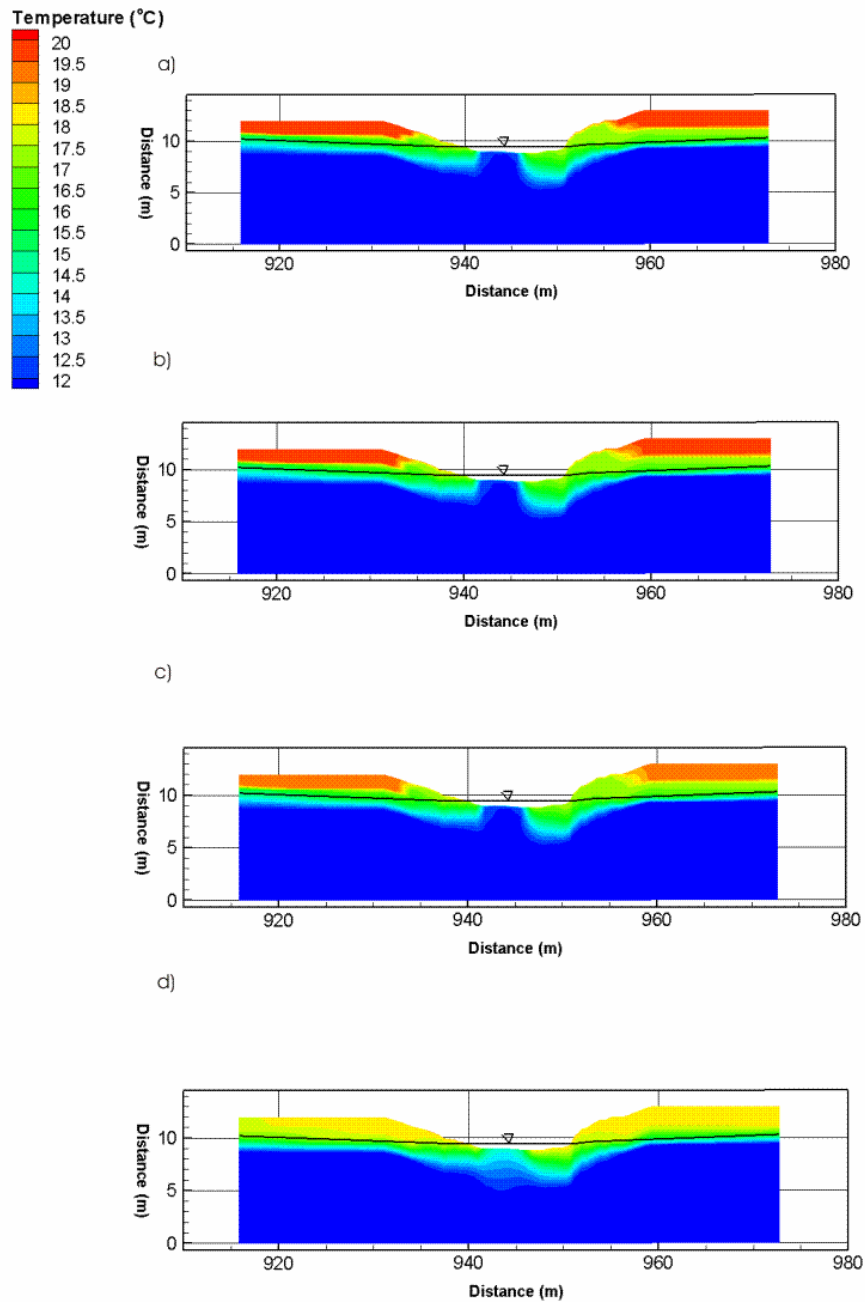
Figure 32. Cross-section of subsurface temperatures at y = 1020 m at: a) the end of the high rainfall event; b) the end of the medium rainfall event; c) the end of the low rainfall event; d) the end of all simulations (t = 5 days).

70

Figure 33. Subsurface temperatures 20 minutes into the: a) high rainfall event; b) medium rainfall event; c) low rainfall event.
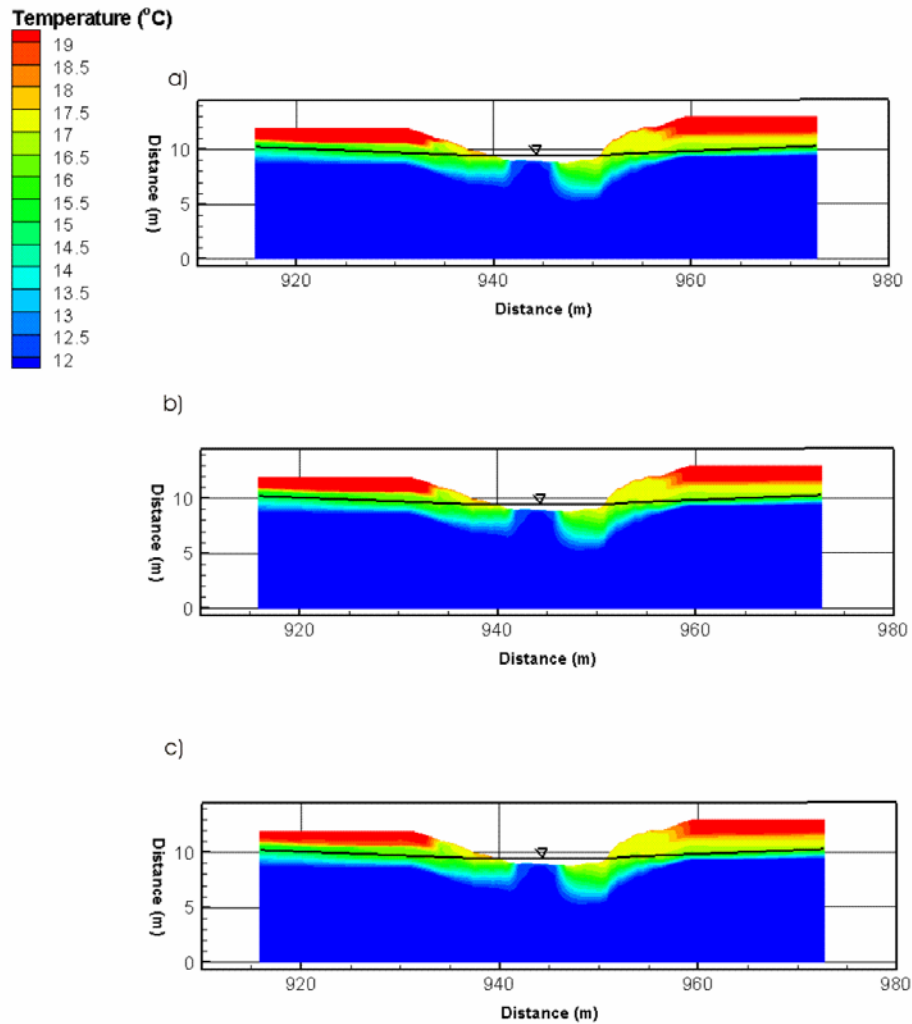
Figure 34. Cross-section of subsurface temperatures at y = 1020 m 20 minutes into the: a) the high rainfall event; b) the medium rainfall event; c) the low rainfall event.

At the end of the simulations, the subsurface temperatures reduce throughout the entire domain. Because the constant atmospheric thermal inputs from shortwave and longwave radiation and the latent and sensible heat flux continue to influence the temperature regime, the subsurface temperatures in the shallow depths of the higher topographical regions and over stream banks remain elevated. However, the high temperature signature associated with the precipitation event is no longer evident. This indicates that there may be

potential for temperature to be used as an indicator to discern the origins of groundwater, and possibly for hydrograph separation. The following chapter will investigate the use of a thermal energy tracer for hydrograph separation.

5.3.4 Advective Thermal Energy Exchange Flux

In the regions furthest from the stream, the advective thermal energy exchange flux increases with the applied rainfall (Figure 35) as more water is exchanging from the surface to the subsurface (Figure 28). Along the stream banks in regions devoid of capillary fringe effects, both the water infiltration to the subsurface and the surface temperatures increase with increased rainfall rates. Hence, the advective thermal energy exchange fluxes also increases. Along the stream, the groundwater discharge from the subsurface to the surface increases only slightly as the rainfall rate increases. In addition, the temperature of the water exchanging from the subsurface to the surface does not change significantly between the three cases involving different rainfall rates. Because of this there is little change in the advective thermal energy exchange fluxes along the streambed with an increase in the rainfall rate.

5.3.5 Dispersive Thermal Energy Exchange Flux

The magnitude and direction of the dispersive thermal energy exchange flux is driven by the difference between the surface and subsurface temperatures. Because the temperature regimes for each of the three rainfall simulations are similar to each other at the end of each precipitation event, it is expected that the dispersive thermal energy exchange fluxes would also be similar. However, as observed in Figure 36, the dispersive thermal energy exchange fluxes increase as the rainfall rate increases, as can be seen when comparing results at the end of each rainfall event. This is due to the dependence of the thermal energy transfer coefficient on other factors that vary in the transient flow simulations, such as water saturation. The ability of air to conduct heat is significantly lower than for water or the porous medium solids. As such, an increase in saturation can increase the dispersive transfer of the thermal energy between the surface and subsurface regimes. The saturation in the top layers of the subsurface increase significantly as the rainfall rate increases (Figure 26), thus increasing the dispersive thermal energy exchange flux. The dispersive thermal energy exchange fluxes after the 5 day recession period decrease compared to those at the immediately after all three rainfall events. This is because the difference between the surface and subsurface temperatures decrease with time and because the water saturation also diminishes in the shallow subsurface (Figure 36).

Figure 35. Advective thermal energy exchange fluxes at: a) the end of the high rainfall event; b) the end of the medium rainfall event; c) the end of the low rainfall event; d) the end of all simulations (t = 5 days).
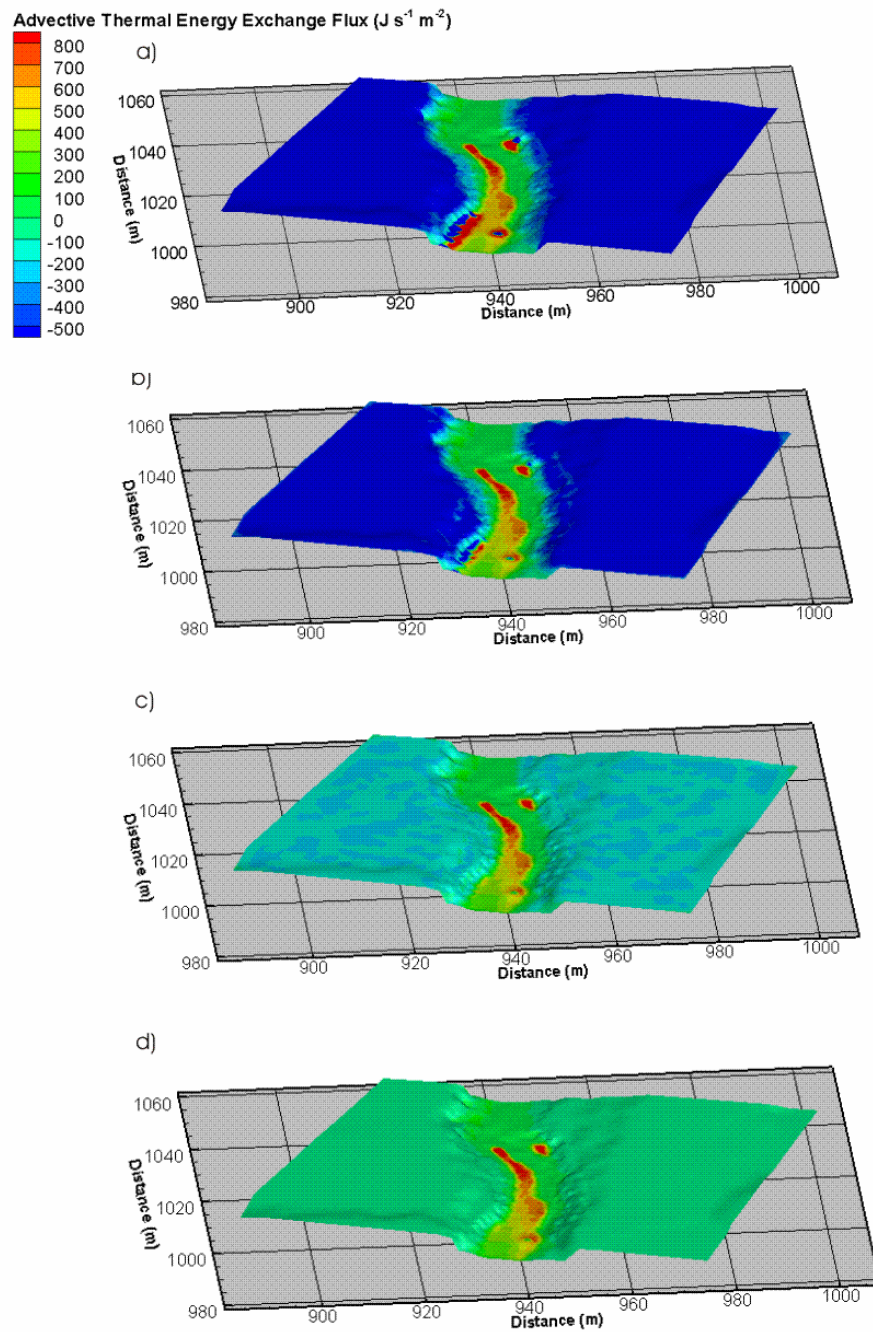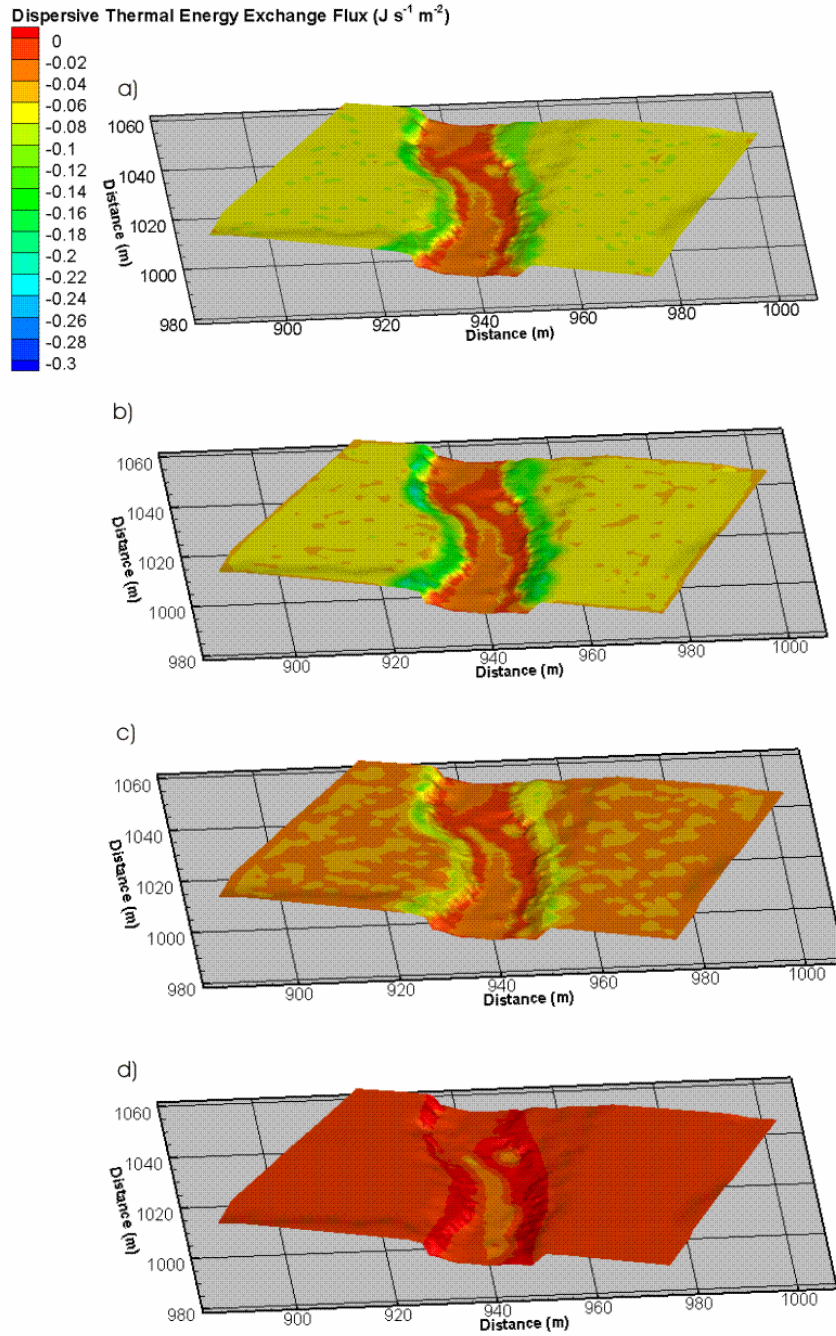
Figure 36. Dispersive thermal energy exchange fluxes at: a) the end of the high rainfall event; b) the end of the medium rainfall event; c) the end of the low rainfall event; d) the end of all simulations (t = 5 days).

5.4 Summary

The Pine River simulations with diurnal atmospheric inputs and transient precipitation events demonstrated the complex interactions between the atmosphere, the surface and the subsurface thermal energy regimes. The simulations with diurnal atmospheric inputs showed that the surface regime responds quickly to changes in atmospheric conditions and that the subsurface thermal conditions are dampened and delayed. In addition, the diurnal fluxes can play an important role in the movement of thermal energy from the surface to the subsurface. The change in surface and subsurface temperatures as a result of fluctuating atmospheric conditions altered the advective thermal energy exchange fluxes between the two regimes. The dispersive thermal energy exchange fluxes can fluctuate spatially and temporally between acting as either a source or a sink term throughout the diurnal cycle, due to the rapid response of the surface temperatures, and the dampened and delayed response of the subsurface temperatures.

The three transient rainfall events simulated for the Pine River example demonstrated how the rainfall rate can impact the most of the thermal energy regime. The surface temperatures responded quickly to the rainfall event and, except along stream banks, were similar between all three simulated rainfall cases. The subsurface temperatures were also similar at the end of the rainfall events; however, they differed between the low, medium and high rainfall events at early times. The advective thermal energy exchange flux varied between the three simulated rainfall cases; the increased rainfall rates increased the overland flow water depths, which in turn increased the hydraulic gradient between the surface and the subsurface. This increase in hydraulic gradient increases the quantity of water exchanging from the surface to the subsurface, causing more thermal energy to be transferred between the regimes. The dispersive thermal energy exchange fluxes were also impacted by the different rainfall rates. Despite the difference between the surface and subsurface temperatures being similar at the end of all three rainfall-rate simulations, the dispersive thermal energy exchange fluxes increased with higher rainfall rates. An increase in rainfall rate also increases the saturation of the top layers of the subsurface. Because the dispersive thermal energy exchange flux is also dependent on saturation the dispersive thermal energy exchange flux also increases with higher rainfall rates. When the subsurface temperatures at the end of the rainfall event were compared to those at the end of the recession period, it was evident that, despite maintaining the same atmospheric conditions throughout the simulation, the thermal signature of the precipitation events had dissipated. This indicates that there is potential for using temperature to determine the origins of groundwater, and for hydrograph separation.

Chapter 6

The Use of Temperature as a Tracer for Hydrograph Separation

6.1 Introduction

The previous chapter alluded to the possibility of using temperature for hydrograph separation. Temperature, for example, has been previously used to determine groundwater discharge patterns in streambeds (i.e. Conant, 2004; Blume *et al*., 2008; Barlow and Coupe, 2009). This is because there is a sufficient difference between groundwater and surface water temperatures in most climates to enable the distinction of discharge and recharge patterns along a streambed. In several of these studies, temperature was used to characterize the groundwater-surface water interactions, and a separate geochemical or isotopic tracer was used for hydrograph separation. There have been a limited number of field studies that examine temperature as a tracer for hydrograph separation, such as Kobayashi *et al*.(1999). The results of these studies indicate that temperature has the potential to be used as a simple and inexpensive tracer for hydrograph separation. The new capabilities of HydroGeoSphere can be used to examine this potential, and to evaluate its limitations in a variety of environments. This chapter will present results that show the use of a temperature tracer in a small intermittent channel and the sensitivity of the hydrograph separation results to the selection of the pre-event temperature.

The mass balance approach is a widely used method for hydrograph separation, despite some inherent limitations (Jones *et* al., 2006; Renaud *et al*., 2007; Sudicky *et al*., 2007). The mass balance approach for hydrograph separation of a two-component system is written as:

$$Q_{meas} = Q_{event} + Q_{pre-event} \ (29a)$$

$$(CQ)_{meas} = (CQ)_{event} + (CQ)_{pre-event} \ (29b)$$

Where *Q* is discharge, *C* is concentration of a conservative tracer, and the subscripts indicate the measured (*meas*) streamflow quantities, the *event* (precipitation) signals, and the *pre-event* (groundwater) components. If the initial concentration of each tracer for the event and pre-event zones (C_{event} and $C_{pre-event}$) is known and the concentrations are measured over time in the stream (C_{meas}), then the tracer mass balance relationships given by equations 29a and 29b are presumed to provide estimates of the pre-event ($Q_{pre-event}$) and event (Q_{event}) contributions to the total stream discharge (Q_{meas}).

In this chapter, a hypothetical hydrograph separation using temperature as the tracer is performed using the new capabilities of HydroGeoSphere. The Borden rainfall-runoff experiment (Abdul, 1985) will be used as an example to test the applicability of temperature to permit hydrograph separation. This rainfall-runoff experiment was a detailed and intensively monitored study that was previously simulated using several fully-integrated surface-subsurface hydrological models (see e.g. VanderKwaak, 1999; Jones *et al*., 2006). Hydrograph separation results from both the field data and from previous model simulations will be compared to the results performed in this work using temperature as the tracer.

6.2 Borden Rainfall Runoff Experiment

The Borden rainfall-runoff experiment was previously described in Chapter 3 as the topic of the proof of concept simulation. In the field study, artificial rainfall was applied to the surface of the site at a rate of 2 cm/hr for 50 minutes. A bromide tracer (90 mg/L) was added to the artificial rainfall water in order to discern the event contribution to streamflow from the pre-event contribution. The discharge at the channel outlet and the bromide concentrations were measured, and a two-component mass-balance-based hydrograph separation was used to determine the event and pre-event contributions to the streamflow. This rainfall-runoff experiment was unique in that the hydrogeological characteristics and parameters describing the site were well characterized and the experiment was performed under controlled conditions (Abdul, 1985). Simulations of the Borden rainfall-runoff experiment previously presented by VanderKwaak (1999) and Jones *et al*., (2006) showed that the transport regime and hydrograph separation results could be well simulated with a fully-integrated surface-subsurface hydrological model (Figure 37). Although temperatures were not monitored by Abdul (1985), this experiment serves as a suitable test problem to explore the viability of using temperature for hydrograph separation because previous integrated modelling was successful in reproducing the flow regime and the bromide tracer transport.

The flow conditions and the surface and subsurface thermal properties used for the hydrograph separation simulations are the same as those given in Chapter 3 (Table 1 and Table 2). An initial simulation was conducted to bring the thermal energy regime to steady state with the imposed atmospheric conditions (Table 9). The steady-state thermal conditions are important for the hydrograph separation; these temperatures will be used as the pre-event signal for the temperature-based hydrograph separation calculations.

The initial flow conditions for the rainfall-runoff simulations are identical to those used by Jones *et al*., (2006), with a dry surface and a water table located at the base of the stream (0.22 m below ground surface

78

at the channel). The initial thermal conditions included a surface temperature of 15 ^{o}C, in equilibrium with the air temperature, and subsurface temperatures from the steady-state simulations that vary with depth between approximately 13.5 ^{o}C near the surface to 10 ^{o}C at depth (Figure 38).
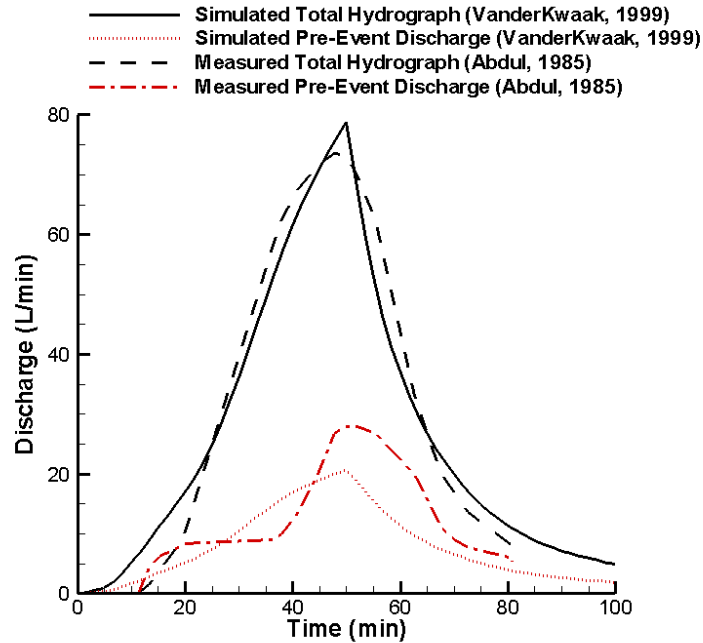
Figure 37. Hydrograph separation results for measured (Abdul, 1985) and simulated (VanderKwaak, 1999) data.

Table 9. Atmospheric conditions of the Borden hydrograph separation simulation.

Parameter	Units	Value	Source
Incoming shortwave radiation ($K^\downarrow$)	W/m	5.50×10^1	Verseghy (1991)
Incoming longwave radiation ($L^\downarrow$)	W/m	3.00×10^2	Verseghy (1991)
Stefan-Boltzmann constant (σ)	kg/(s^3 ^{o}C^4)	5.67×10^{-8}	Weast (1984)
Wind speed (V_a)	m/s	1.00×10^0	Verseghy (1991)
Air pressure (P_a)	Pa	1.01×10^5	Environment Canada (2008)
Air/Rain temperature (T_a)	^{o}C	1.50×10^1	Environment Canada (2008)
Subsurface temperature (T_g)	^{o}C	1.00×10^1	Conant (2001)
Surface temperature (T_o)	^{o}C	1.50×10^1	Conant (2001)

79
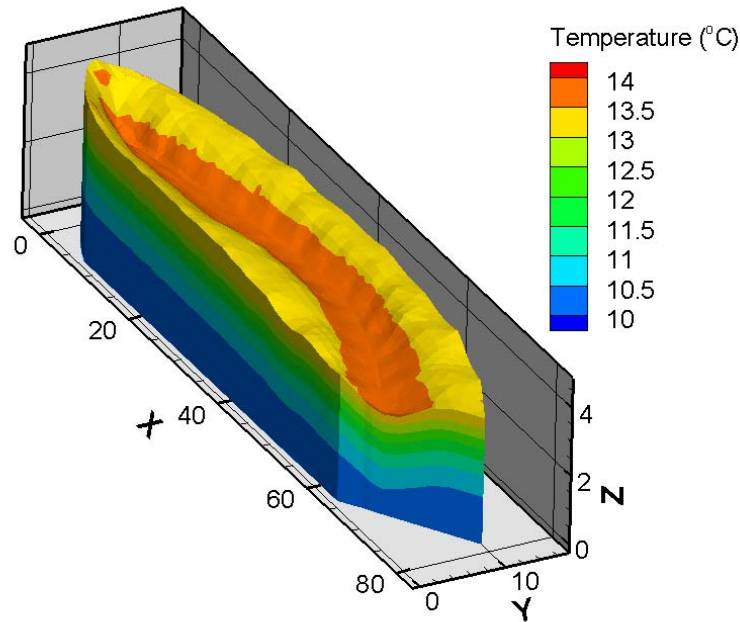
Figure 38. Initial subsurface temperature distribution for the Borden temperature-based hydrograph separation.

6.3 Hydrograph Separation Results

The rainfall-runoff experiment was simulated by applying a rainfall of 2 cm/hr to the surface, followed by 50 minutes of recession. The rainfall is applied at a temperature of 15 ^{o}C (the same as the air temperature), and the atmospheric inputs did not change throughout the simulation. As the surface component of HydroGeoSphere is depth-integrated, changes in the thermal stratification of the channel are not captured. The temperature results indicate only slight changes in the channel discharge temperature over the course of the applied rainfall and following the 50 minute recession period (Figure 39). In addition, the temperature breakthrough curve is unlike the traditional geochemical or isotopic breakthrough curves measured in streams, which normally include a steady rise to a peak concentration, followed by a return to a background value. The temperature breakthrough curve begins with a rapid decline in temperature. Because the surface was initially dry, with a temperature of 15 ^{o}C, the steep decline represents the discharge of cool groundwater to the surface when the rainfall is first applied. The following increase in temperature, from approximately 10 minutes into the event until the end of the rainfall, indicates the movement of water influenced by the precipitation event into the stream. The decline at the end of the rainfall event represents

the discharge of the 15 ^{o}C input water (precipitation), which is followed by a slight increase in temperature at approximately 70 minutes as the channel flow ceases, and the atmospheric conditions again heat the surface.
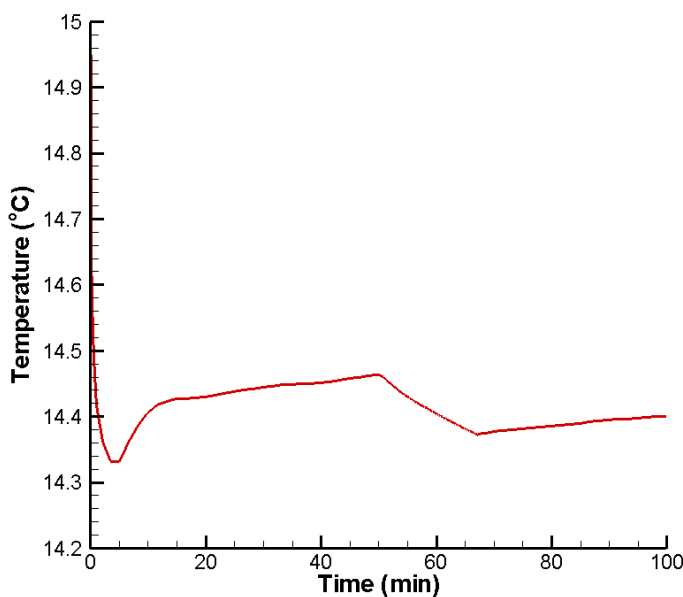
Figure 39. Stream discharge temperature over time for the Borden rainfall-runoff simulation.

A hydrograph separation was performed using the simulated temperatures and channel discharges, using a methodology analogous to the two-component mass-balance approach given in equations 28a and 28b. These results match well with the results given by Abdul (1985) based on the measured bromide concentrations at the channel outlet (Figure 40). Using the steady-state subsurface temperatures given in Figure 38, a pre-event temperature of 13.5 ^{o}C was chosen for this analysis. The sensitivity of this selection is discussed in the following section.

The results of the temperature-based hydrograph separation indicate that the use of temperature as a tracer is feasible, and that it has the potential to provide results as representative as traditional geochemical or isotopic tracers. However, this hypothesis is based upon simulation results alone, and further studies should be conducted in the field to further test the feasibility. In addition, further simulations should be conducted to determine the applicability of temperature tracers for hydrograph separation on larger scale domains and under different hydrological conditions (including continuous base flow).

Previous modelling studies have compared simulated and measured results for hydrograph separation using a bromide tracer for the Borden rainfall-runoff experiment (VanderKwaak, 1999; Jones *et al*., 2006). A comparison between the results from the previous model simulations, and those from this study indicate that temperature provides the same, if not a better match, to the measured results than the bromide tracer (Figure 41). Again, this indicates the potential use of a temperature tracer in hydrograph separation studies.
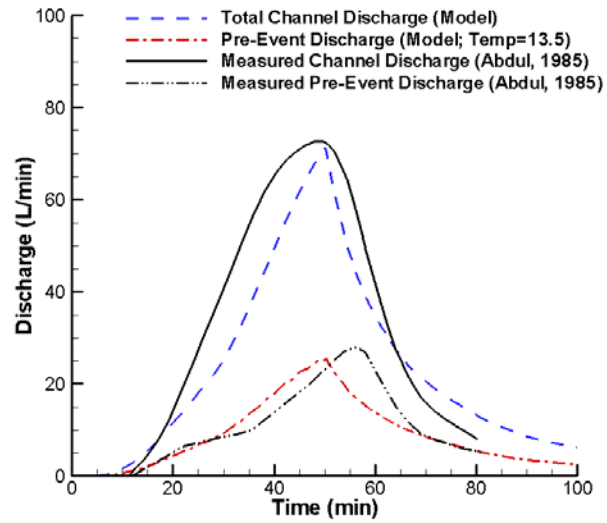

Figure 40. Hydrograph separation results based on temperature as a tracer, and the measured field results based on bromide as a tracer (Abdul, 1985).
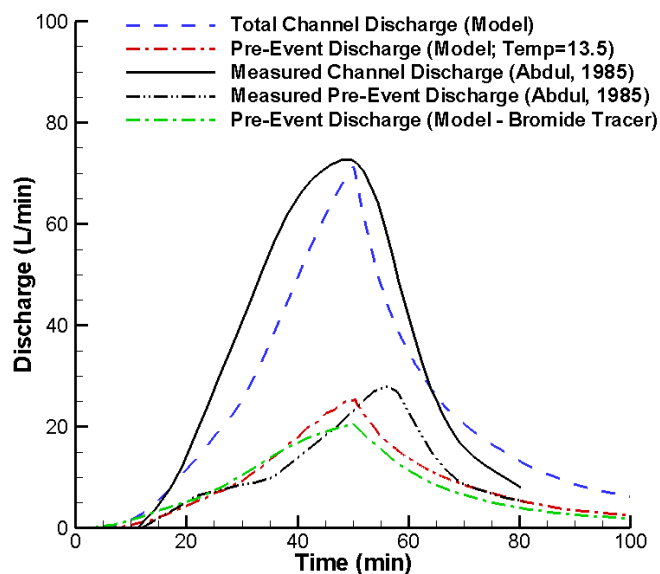
Figure 41. Hydrograph separation results for the temperature tracer simulation, bromide tracer simulation (Jones *et* al., 2006) and the measured field results (Abdul, 1985).

6.3.1 Sensitivity to Pre-Event Temperature

As previously mentioned, the initial subsurface temperatures of the Borden domain vary spatially. To permit an energy-balance approach for hydrograph separation, the pre-event temperature is an important factor, and is represented by a single value in a simple two-component mixing model. The variation in subsurface temperatures is problematic for choosing a single unique value. This is no different from the subsurface spatial (or temporal) variability exhibited by any geochemical or isotopic concentration in the hydrologic system; the variability of temperature may indeed be even more pronounced in the regions near the streambed, but may be more predictable and consistent between sites.

The calculated subsurface temperature distribution at the Borden site allows for a variety of possible pre-event temperatures, between 10 ^{o}C to 14 ^{o}C (Figure 38). The origin of the groundwater that could rapidly discharge to the surface is naturally closer to the surface, and thus a subsurface temperature of 13.5 ^{o}C was used for the initial analysis. Two other selections, pre-event temperatures equal to 13 ^{o}C and 14 ^{o}C respectively, were used to test the sensitivity of the hydrograph separation results to the pre-event temperature choice. The results indicate, as expected, that a greater pre-event temperature leads to a higher pre-event contribution to the channel discharge, and a lower pre-event temperature leads to a lower pre-

event contribution (Figure 42). The difference in pre-event contributions between the 13.5 $^{\circ}$C and 14 $^{\circ}$C cases is greater than that from 13.5 $^{\circ}$C and 13 $^{\circ}$C selections. This is because the energy-balance approach to hydrograph separation is dependent upon the difference between the temperature signals in the event and pre-event water, in addition to the signal in the stream discharge. As the pre-event and event signals become closer (i.e. 14 $^{\circ}$C to 15°C vs. 13.5 $^{\circ}$C to 15°C), the calculated contributions become more sensitive to change. This relationship is evident when the solution to equations 29a and 29b are given for the pre-event contribution:

$$Q_{pre-event} = \frac{Q_{meas}(C_{meas} - C_{event})}{(C_{pre-event} - C_{event})} \ (30)$$

It is clear from Figure 42 that the selection of pre-event subsurface temperature plays an important role in the hydrograph separation using temperature as a tracer, especially under conditions where the pre-event and event temperatures are similar. The use of temperature as a tracer for hydrograph separation is likely best suited for sites where the difference between the event and pre-event temperatures are significant, as the calculation of the pre-event and event discharge contributions will be less sensitive to the variability of the subsurface temperatures.
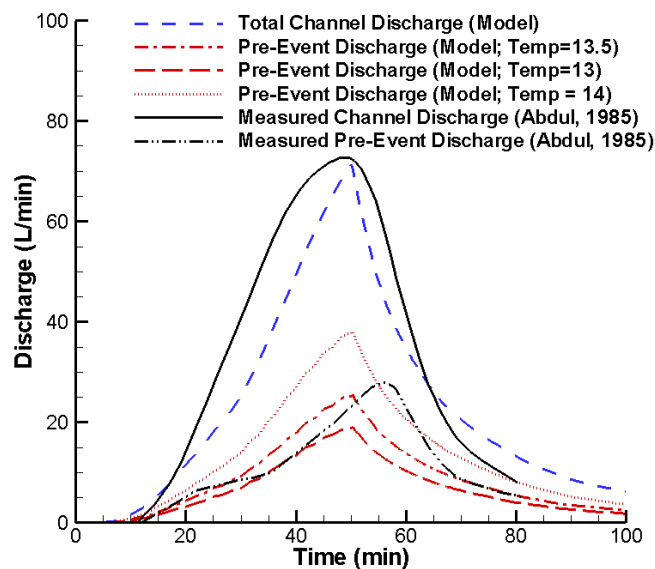

Figure 42. Hydrograph separation using a variety of pre-event temperatures.

6.4 Summary

The use of temperature as a tracer for hydrograph separation was investigated by simulating the Borden rainfall-runoff experiment (Abdul, 1985). The estimated pre-event contributions to stream discharge based on temperature matched both the measured and simulated bromide tracer results, indicating that temperature can be used as a tracer for hydrograph separation. Subsurface temperatures are often spatially variable, which could lead to difficulties in interpreting the data. It was shown that an understanding of the hydrological system, and the origin of any water that may enter the stream from the subsurface can help in selecting the appropriate temperature for the pre-event signal. In addition, the pre-event and event discharge contributions were found to be less sensitive to variability in the pre-event temperature when the difference between the event and pre-event temperatures were greater. It is suggested that thermal tracers be used for hydrograph separation when the difference between the event and pre-event temperatures is sufficiently large to minimize the sensitivity of results due to pre-event temperature variability. These conclusions are based only upon simulation results, and additional work should be conducted to determine the feasibility of using temperature as a tracer for hydrograph separation in the field. In addition, further simulations should be conducted to determine the applicability of this method to larger scale domains and under different flow conditions.

Chapter 7

Impact of Atmospheric Thermal Inputs

7.1 Introduction

The previous chapters presented the results of flow and thermal transport simulations for a section of the Pine River. In order to properly represent the thermal energy conditions within the hydrological regime, these simulations included atmospheric inputs; however, the relative importance of each of the atmospheric inputs was not explored. The Earth's climate, and hence the temperature of the Earth's surface, is dependent upon the transfer of thermal energy between the atmosphere and the land surface (Dingman, 1994; Hidore and Oliver, 1993). Atmospheric thermal contributions to the Earth's surface include shortwave and longwave radiation, and sensible and latent heat fluxes. Previous research has highlighted the importance of these inputs to the hydrologic regime; predominantly for estimating evapotranspiration and precipitation (e.g. Sellers *et al*., 1986; Mengelkamp *et al*., 1999; Lindsey and Farnsworth, 1997; Hostetler and Bartlein, 1990), for calculating snow melt (e.g. Jin *et al*,. 1999; Jordan, 1991), and for determining the effects of changing atmospheric conditions on vegetation and ecosystem health (e.g. Dickinson *et al*., 1998; Chen *et al*., 1998). However, little to no research has been conducted to determine the direct impact of each thermal atmospheric component on both surface and subsurface temperatures. This chapter will investigate the contributions of each of the atmospheric thermal inputs to the overall thermal conditions of the Pine River case study under warm weather conditions. In each of the following sections, the physical system is identical to that presented in Chapter 4.

7.2 Surface and Subsurface Temperature

The atmospheric thermal contributions are input directly into the surface thermal energy equation (equation 8) and will affect the temperature of the surface waters. The subsurface thermal energy equation (equation 1), however, is not directly dependent on the atmospheric inputs, but instead relies upon the thermal energy exchange fluxes from the surface in response to the changes in the atmospheric conditions. The surface and subsurface temperatures for the Pine River example are examined when each atmospheric component is neglected, and are compared to the results provided in Chapter 4.

7.2.1 Net Shortwave Radiation

Shortwave radiation is the radiant energy in the visible, near-ultraviolet and near-infrared wavelengths from the atmosphere to the Earth's surface. The daily average incoming shortwave radiation is usually a positive value, meaning that it increases the temperature of the Earth's surface. In the Pine River example, the incoming shortwave radiation was set to 55 W/m^2, a typical value for a partially cloudy day in Southern Ontario (data from the University of Waterloo Weather Station). Net shortwave radiation is dependent upon not only incoming shortwave radiation, but also the ground albedo (a function of soil cover and soil moisture), and cloud and canopy cover. Ground albedo is the only parameter in the net shortwave radiation calculations that is allowed to vary spatially within the Pine River simulations. In order to determine the effect of shortwave radiation on the simulation results, it will be removed from the atmospheric input calculations and the results will be compared to those provided in Chapter 4.

Because the incoming shortwave radiation term in the Pine River example is positive, removing it decreases both the surface and subsurface temperatures (Figure 43 and Figure 44). The surface temperatures decrease most significantly in the higher topographical regions and along the stream banks, but not noticeably within the stream (Figure 43). There is no perceptible change in the stream temperature because the thermal conditions of the stream are dominated by the temperature associated with the stream inlet boundary condition. The subsurface temperatures decrease throughout the top 0.5 m of the entire domain by up to 2.0 ^{o}C; however, under the streambed, in regions with high groundwater discharge to the surface, the decline in temperature is significantly less (< 0.5 ^{o}C) (Figure 44). These regions of high groundwater discharge to the stream are the least impacted by atmospheric changes, such as the removal of shortwave radiation, as the dominant movement of thermal energy is from the subsurface to the surface.

Figure 43. Pine River steady-state simulation results for surface temperature: a) without net shortwave radiation, b) with net shortwave radiation.
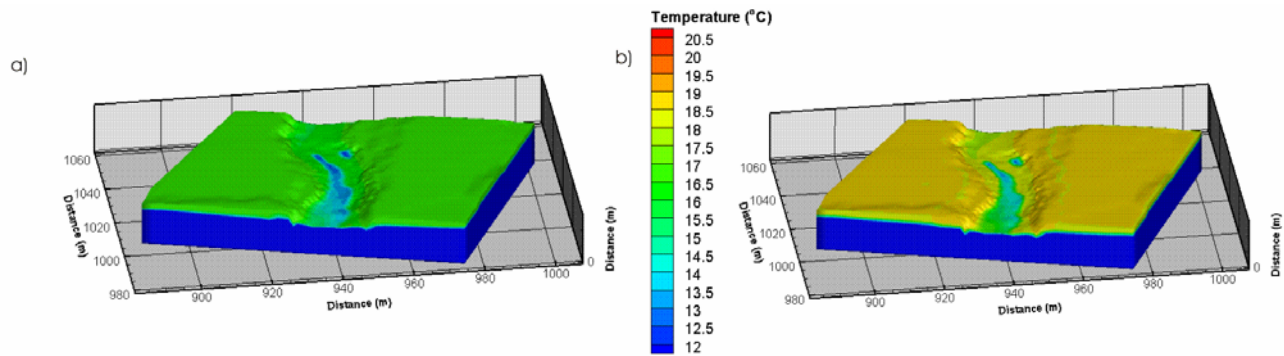
Figure 44. Pine River steady-state simulation results for subsurface temperature: a) without net shortwave radiation, b) with net shortwave radiation.

7.2.2 Net Longwave Radiation

Longwave radiation is the infrared energy emitted by the Earth and atmosphere at wavelengths between approximately 5 and 25 μm. As demonstrated in equations 15, 16 and 17, longwave radiation is dependent upon the ground surface temperature, and incoming longwave radiation can be a function of air temperature, near surface vapour pressure, and emissivity. The incoming longwave radiation can also be a specified constant. In the Pine River example, the incoming radiation is calculated using equations 16 and 17. The parameters that vary spatially in the Pine River example are the ground surface temperatures and emissivity. In order to determine the effect of net longwave radiation on the simulation results, it is

88

neglected from the atmospheric input calculations and the results are compared to those provided in Chapter 4.

Neglecting longwave radiation from the steady-state Pine River example increases the surface temperatures from the range of 18.13 $^{\circ}$C – 19.98 $^{\circ}$C with longwave radiation, to 18.50 $^{\circ}$C – 20.13 $^{\circ}$C without longwave radiation (Figure 45). This increase in surface temperatures indicates that the calculated incoming longwave radiation is less than the longwave radiation emitted by the Earth back to the atmosphere.
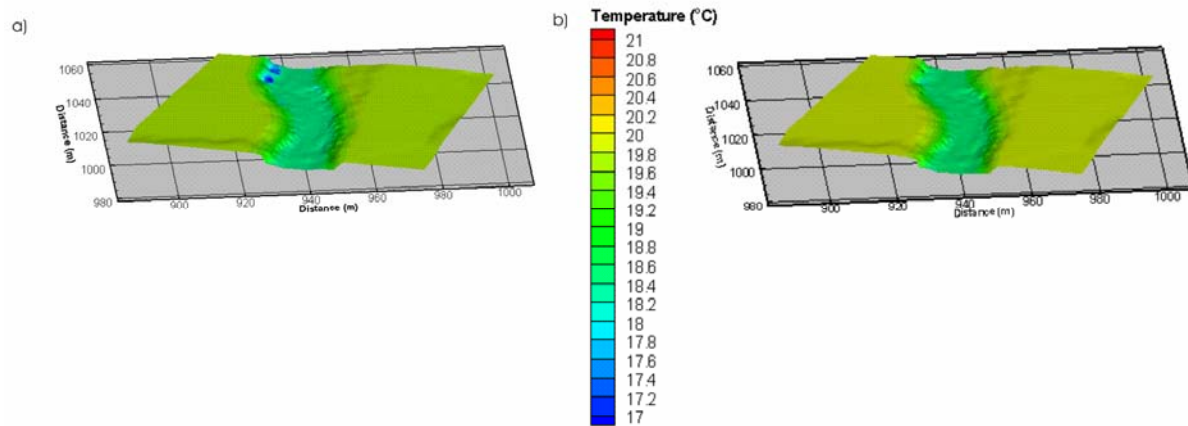

Figure 45. Pine River steady-state simulation results for surface temperature: a) without net longwave radiation, b) with net longwave radiation.

The subsurface temperatures also increase when longwave radiation is neglected (Figure 46). The increase is greater than 2 $^{\circ}$C to an approximate depth of 0.2 m in the regions furthest from the stream, while the zone beneath the stream increases by less than 1 $^{\circ}$C. The regions furthest from the stream receive thermal energy from the surface both advectively and dispersively, whereas the zones beneath the streambed only receive dispersive thermal energy flux from the surface. This causes a larger increase in subsurface temperatures in regions further from the stream compared to beneath the stream when net longwave radiation is neglected.
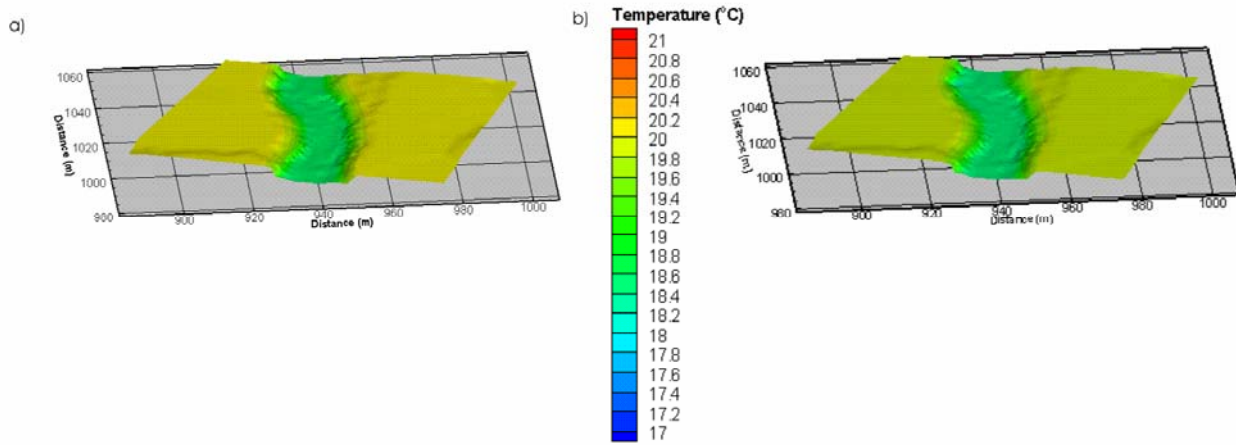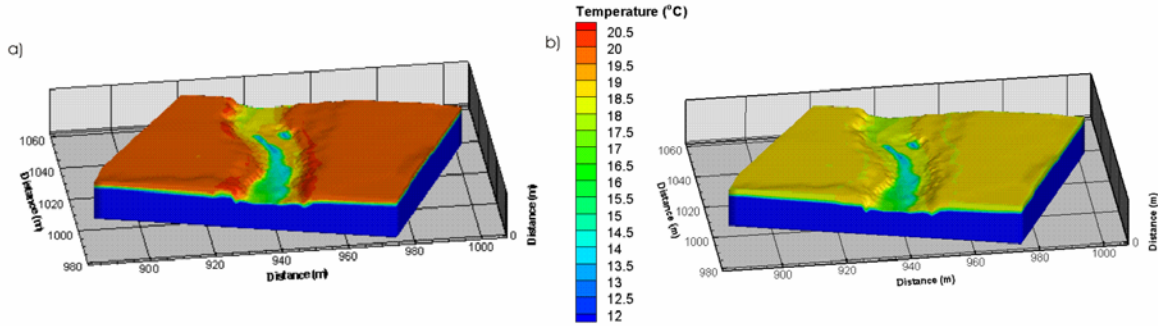
Figure 46. Pine River steady-state simulation results for subsurface temperature: a) without net longwave radiation, b) with net longwave radiation.

7.2.3 Sensible Heat Flux

Sensible heat flux represents the movement of energy from the Earth to the air above, typically via conduction. Sensible heat flux in HydroGeoSphere is dependent upon several factors, as illustrated in equation 18. Of these factors, only the calculated ground surface temperature varies spatially in the Pine River example. In order to determine the effect of sensible heat flux on the simulation results, it will be neglected from the atmospheric input calculations and the results will again be compared to those provided in Chapter 4.

Neglecting sensible heat flux decreases both the surface and subsurface temperatures slightly in the Pine River example (Figure 47 and Figure 48). Based on equation 18, it is apparent that the sensible heat flux is a source of thermal energy to the surface when the air temperature is higher than the surface temperatures, as in the Pine River example. The surface temperatures decrease from a range of 18.13 ^{o}C - 19.98 ^{o}C to 17.74 ^{o}C – 19.98 ^{o}C, indicating that the cooler regions of groundwater discharge along the stream banks are affected the most.

The subsurface temperatures also decrease from a range of 9.96 ^{o}C - 18.92 ^{o}C to 9.95 ^{o}C - 18.62 ^{o}C; the warmer regions of the subsurface, located furthest from the stream and to a depth of approximately 0.2 m, are the zones most impacted by neglecting sensible heat flux. Thermal energy is transferred from the surface to the subsurface in the regions furthest from the stream via advective and dispersive thermal energy exchange flux. Therefore, the impact of neglecting any atmospheric input on temperature is greater in these regions than below the streambed where only the dispersive thermal exchange flux transfers energy from the surface to the subsurface.

Figure 47. Pine River steady-state simulation results for surface temperature: a) without sensible heat flux, b) with sensible heat flux.

Figure 48. Pine River steady-state simulation results for subsurface temperature: a) without sensible heat flux, b) with sensible heat flux.

7.2.4 Latent Heat Flux

Latent heat flux represents the transfer of thermal energy during the evaporation/condensation process. Latent heat flux in HydroGeoSphere is dependent upon several parameters, as illustrated in equations 19 to 23. Of the parameters appearing in these equations, the humidity of the ground surface is the only parameter that varies spatially because of its dependence on the available soil moisture. To determine the effect of latent heat flux on the simulation results, it will be neglected from the atmospheric input calculations in the Pine River example and the results will be compared to those provided in Chapter 4.

91

Neglecting the latent heat flux increases the temperature in the surface and subsurface regimes, most notably in the regions furthest from the stream (Figure 49 and Figure 50). A decrease in temperature as a result of including the latent heat flux is indicative of evaporation over the surface of the domain because the specific humidity of the air is less than that of the ground surface. The temperature change is less significant under the streambed because the stream temperature is dominated by the inlet thermal boundary condition.
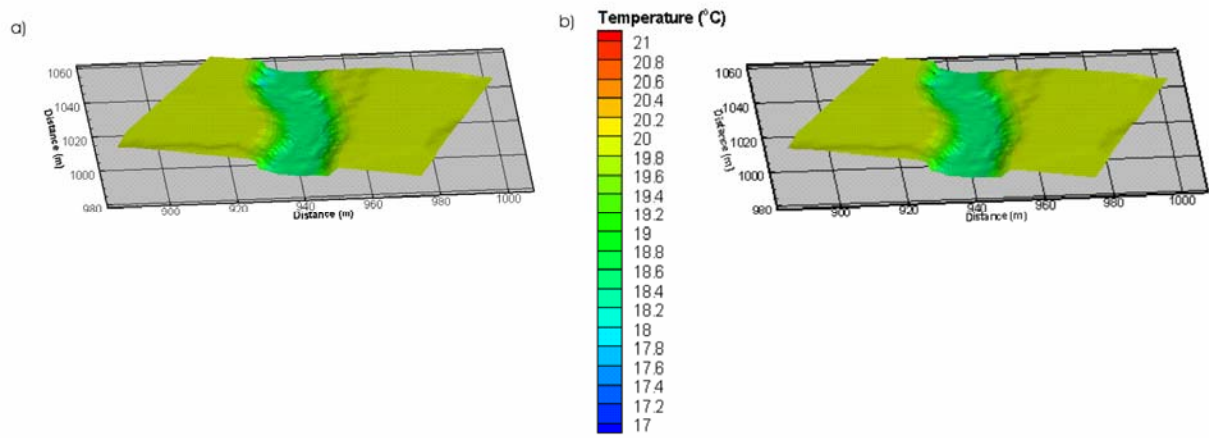

Figure 49. Pine River steady-state simulation results for surface temperature: a) without latent heat flux, b) with latent heat flux.
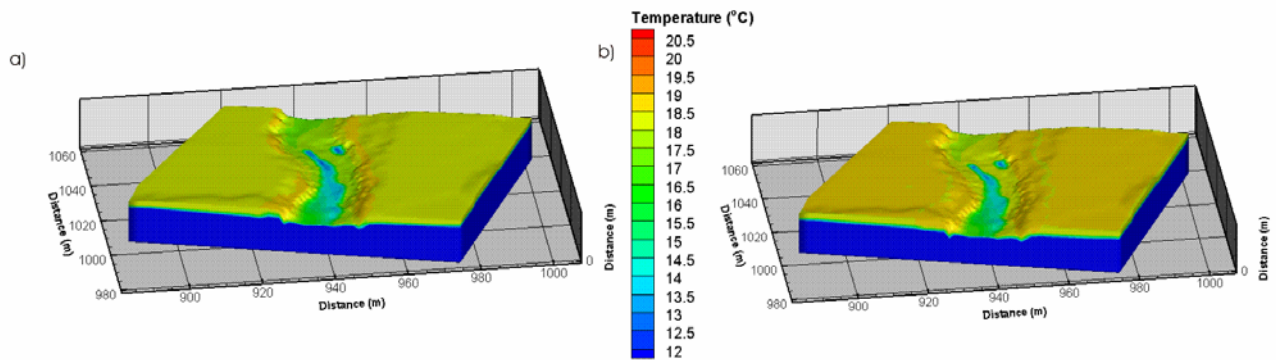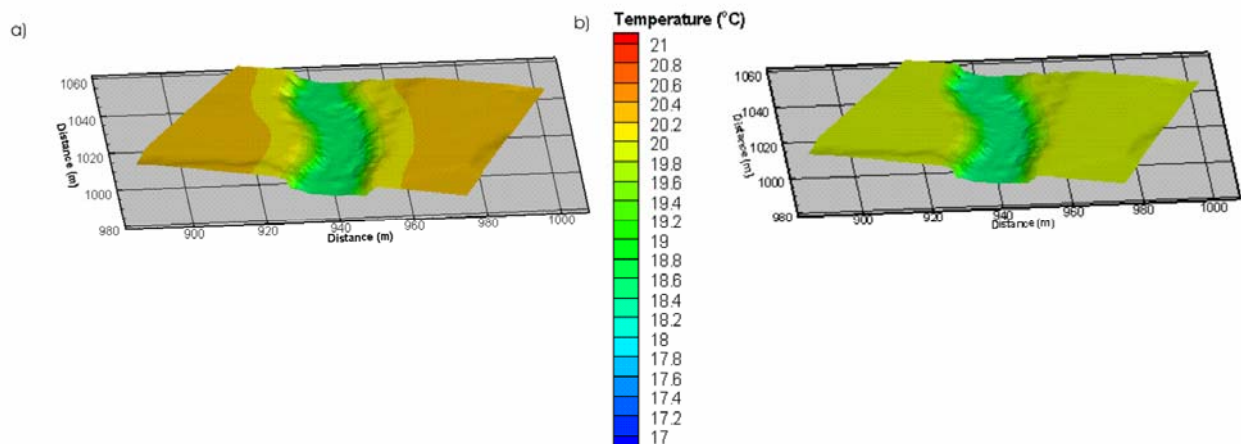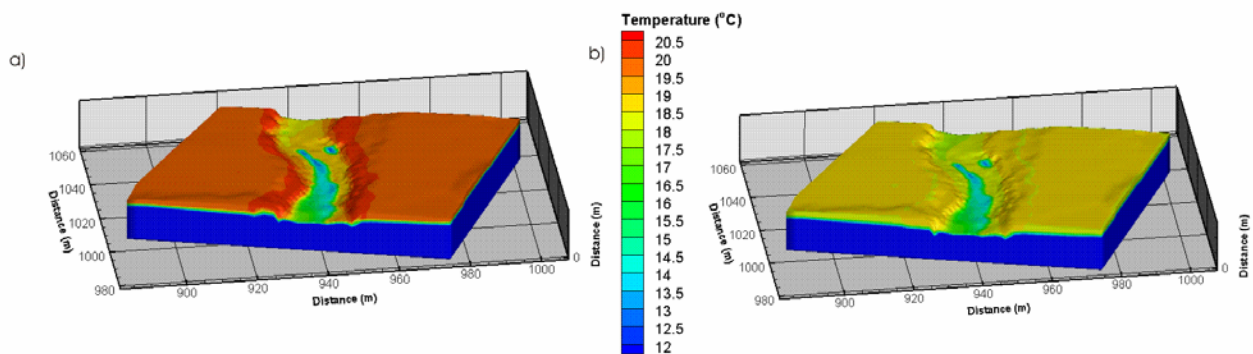

Figure 50. Pine River steady-state simulation results for subsurface temperature: a) without latent heat flux, b) with latent heat flux.

7.2.5 Total Atmospheric Thermal Contributions

Because groundwater heat transport models typically ignore all atmospheric thermal contributions, the importance of accounting for these terms will be highlighted by comparing the simulation results when atmospheric contributions are neglected to the results presented in Chapters 4. The neglect of all atmospheric thermal contributions causes the surface and subsurface temperatures to decrease in the Pine River example (Figure 51 and Figure 52). Individually neglecting shortwave radiation and sensible heat flux caused the surface and subsurface temperatures to decrease (Figure 43 and Figure 44; Figure 47 and Figure 48), indicating that these atmospheric inputs are dominant over the longwave radiation and latent heat fluxes in this example. Neglecting all of the atmospheric inputs results in significantly lower temperatures for both the surface and subsurface than when either the shortwave radiation or sensible heat fluxes are removed independently. This indicates that all of the atmospheric components must be accounted for to properly simulate the thermal energy regime of the entire hydrological system.

Figure 51. Pine River steady-state simulation results for surface temperature: a) without atmospheric thermal contributions, b) with atmospheric thermal contributions.
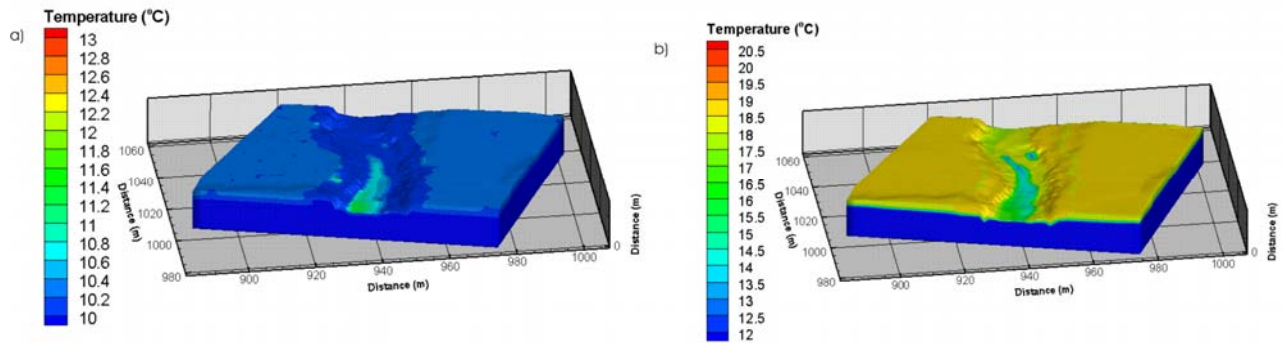
Figure 52. Pine River steady-state simulation results for subsurface temperature: a) without thermal atmospheric contributions, b) with atmospheric thermal contributions.

The hydraulic and thermal characteristics of each site play an important role in determining the effects of the atmospheric thermal contributions. For example, when all atmospheric thermal contributions are removed from the Borden rainfall-runoff case study given in Chapter 3, the trend in results is significantly different from that of the Pine River example. The surface and subsurface temperatures increase for the Borden example (Figure 53 and Figure 54), as opposed to the decrease in temperatures observed for the Pine River case (Figure 51 and Figure 52). In the Borden example, the effects of the net longwave radiation dominate the other atmospheric thermal contributions, whereas the net shortwave and sensible heat fluxes are the dominant atmospheric contributions for the Pine River example.

.

Figure 53. Borden simulation results for surface temperature at 50 minutes: a) without atmospheric thermal contributions, b) with atmospheric thermal contributions.
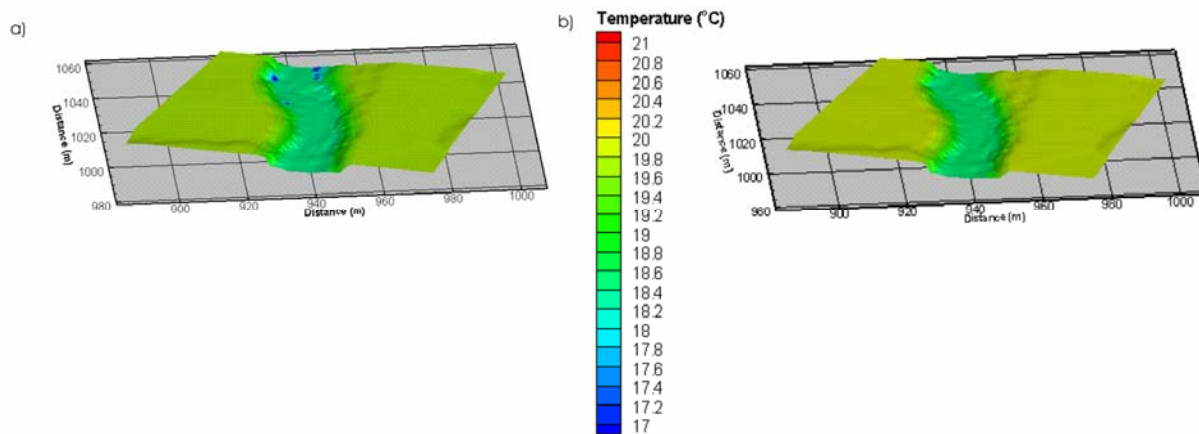
94
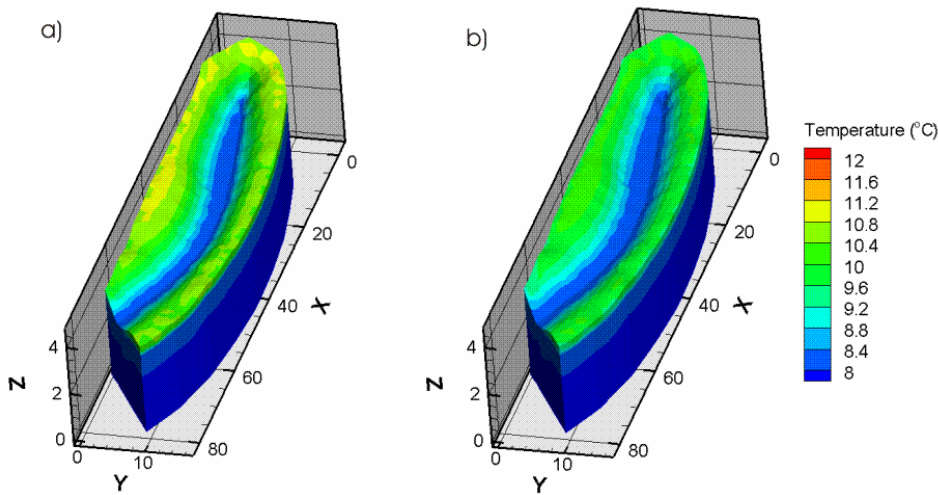
Figure 54. Borden simulation results for subsurface temperature at 50 minutes: a) without atmospheric thermal contributions, b) with atmospheric thermal contributions.
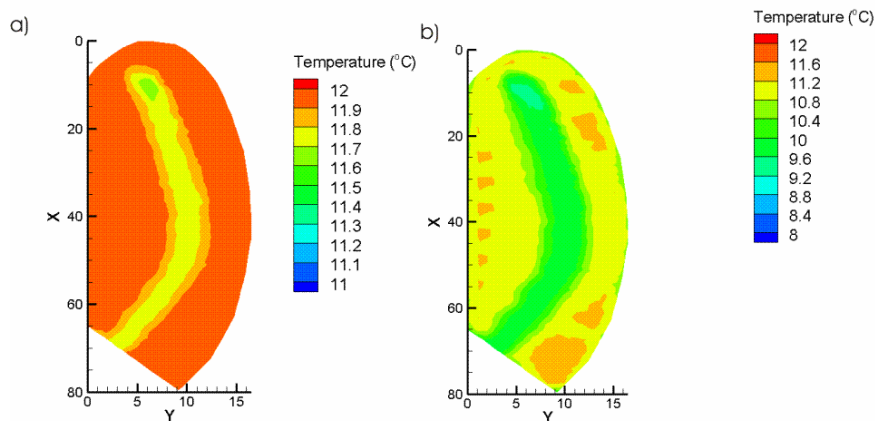
7.3 Advective and Thermal Energy Exchange Fluxes

The advective thermal energy exchange flux is dependent upon the rate of water exchanging between the surface and subsurface flow regimes and the temperature of the water that is being transferred. When atmospheric thermal conditions are altered, only the thermal regime, and not the flow system, is affected. Therefore, only a change in the surface and/or subsurface temperatures will cause a change in the advective temperature exchange fluxes. For example, when all the atmospheric contributions are neglected in the Pine River case study, both the surface and subsurface temperatures decrease compared to when they are included (Figure 51 and Figure 52). Because the temperature of the water exchanging between the two regimes decreased, the advective thermal energy exchange flux also decreased (Figure 55).

The dispersive thermal energy exchange flux is dependent on the temperature difference between the surface and subsurface. Therefore, a change in this exchange flux due to the removal of atmospheric thermal inputs will be dependent on specific site characteristics and flow regime conditions. For example, when all the atmospheric thermal contributions are removed from the Pine River simulations, the changes in the dispersive temperature exchange fluxes are isolated to the streambed, when compared to results from Chapter 4 (Figure 56). When the atmospheric contributions are neglected, the stream temperature does not change as it is dependent upon the inlet thermal boundary condition. However, the subsurface temperature under the stream decreases causing a larger difference between the surface and subsurface temperatures

which then increases the dispersive thermal energy exchange flux. In the regions furthest from the stream the difference between the surface and subsurface temperatures remain the same when atmospheric inputs are neglected, and therefore dispersive thermal energy exchange fluxes are unchanged.
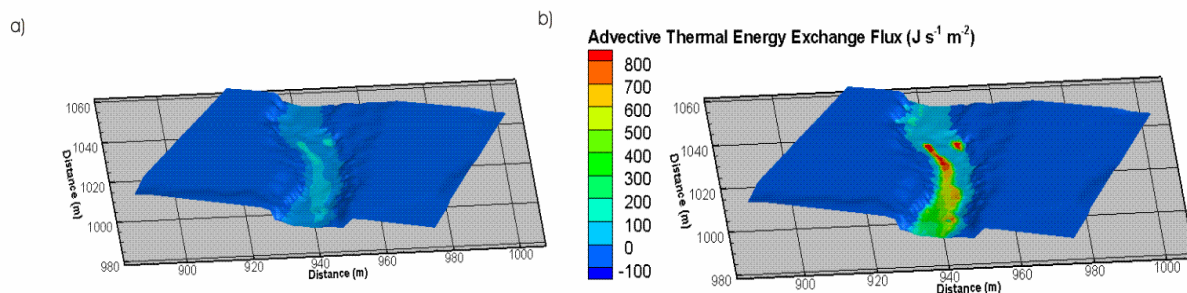
Figure 55. Pine River steady-state simulation results for advective thermal energy exchange flux: a) without atmospheric contributions, b) with atmospheric contributions.
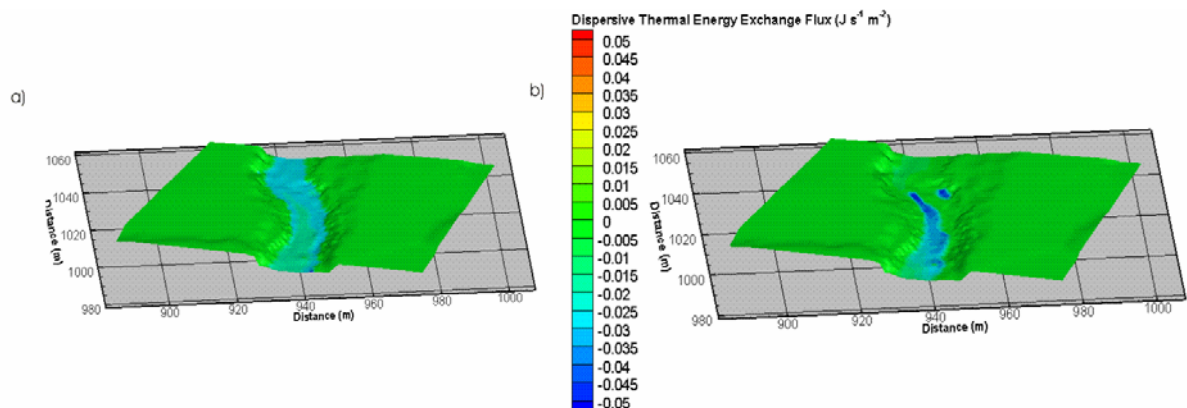
Figure 56. Pine River steady-state simulation results for dispersive thermal energy exchange flux: a) without atmospheric contributions, b) with atmospheric contributions.

7.4 Summary

This chapter demonstrated that each atmospheric contribution to the hydrologic system can affect the entire thermal regime, and is dependent on site-specific hydraulic and atmospheric characteristics. The total atmospheric contributions for warm weather conditions were found to increase surface and subsurface temperatures in the Pine Rive example; however, the atmospheric thermal contributions caused the surface

and subsurface temperatures to decrease in the Borden rainfall-runoff case study. In addition, no specific atmospheric contribution dominates the thermal conditions of the Pine River example, whereas the effect of the net longwave radiation dominated in the Borden example. These differences in behaviour demonstrate that no atmospheric contributions can be ignored when simulating both the surface and subsurface thermal systems, because the effect of each atmospheric input is site specific. As such, when simulating thermal energy transport in the surface and/or subsurface, it is important to not only collect information to properly characterize the hydrologic system, but also to characterize the atmospheric thermal inputs.

Chapter 8

Conclusions

Thermal energy transport within the fully-integrated framework provided by HydroGeoSphere provides a tool that has a wide variety of applications. As the focus on total ecosystem health increases, thermal conditions are playing a more important role in river restoration planning and the evaluation of land use changes and climate change impacts on basin-scale hydrology. In addition, the development of thermal Total Maximum Daily Load (TMDL) regulations such as in California may require the capability to predict temperature conditions for many stream networks, particularly those impacted by anthropogenic activities.

The objectives of this work were: (1) to incorporate thermal energy transport equations into HydroGeoSphere to extend its capabilities to handle temperature in a fully-integrated surface/subsurface context, (2) to verify this new capability through numerical test problems, (3) to demonstrate the use of the fully-integrated surface/subsurface framework to simulate the thermal patterns observed in the surface water and the groundwater along a river reach at a highly-characterized field site, (4) to investigate the impact of transient atmospheric heat inputs and rainfall rates on thermal energy transport characteristics, (5) to explore the potential use of temperature as a tracer for hydrograph separation, and (6) to determine the impact of each atmospheric component on the calculated surface/subsurface thermal energy conditions.

The governing equations and the numerical implementation describing two-dimensional depth-integrated surface and three-dimensional subsurface thermal energy transport, together with the handling of atmospheric energy inputs, were presented. The verification simulations demonstrated that they were properly implemented. The subsurface component of HydroGeoSphere was verified by comparing simulation results for the Borden thermal injection experiment to those from a previously verified model. The comparison of results based on a CLASS test problem further demonstrated that atmospheric thermal inputs to the surface and shallow subsurface are correctly implemented. The Borden rainfall-runoff experiment was used as a proof of concept example to verify the fully-integrated surface/subsurface capabilities.

The new capabilities of HydroGeoSphere were then demonstrated by successfully reproducing the thermal patterns observed in the surface and subsurface for a 60 m long section of the Pine River. The steady-state, high-resolution, 3D numerical simulation of the site indicated that not only could HydroGeoSphere reasonably match the thermal energy conditions within the surface and subsurface flow regimes, but it

could also represent the transfer of thermal energy between the two domains without the use of artificial boundary conditions. The simulations confirmed that the stratigraphy at depth controlled the groundwater discharge and the patterns of heat flow into the riverbed. The advective thermal energy exchange flux associated with the discharging groundwater was also shown to be far greater in magnitude than the dispersive thermal energy exchange flux even in locations where the discharge of groundwater is weak.

Varying the air temperature and shortwave radiation to mimic diurnal fluctuations affected the entire surface and subsurface thermal energy regime in the Pine River example. While the surface temperatures of most of the domain responded quickly in higher topographical areas to the changes in atmospheric conditions, the stream temperature was mainly determined by the inlet boundary condition. The impact of atmospheric fluctuations on the subsurface temperatures are dampened, and lagged in time, compared to the surface temperatures. Changes in the subsurface thermal regime due to atmospheric inputs require the transfer of thermal energy from the surface to the subsurface, as the atmosphere is not directly connected to the deeper subsurface. For the case of Pine River this transfer of thermal energy is not instantaneous; the shallow subsurface temperatures were found to lag by at least an hour and are dampened by over 1 ^{o}C, compared to the associated surface temperatures. The advective thermal energy exchange flux is dominant over the dispersive thermal energy exchange flux in the Pine River example. The advective thermal energy exchange flux varied throughout the transient simulation as the temperature of the water exchanging between the surface and the subsurface changed. The magnitude of the advective thermal energy exchange flux was always significantly greater than the dispersive thermal energy exchange flux. However, the dispersive thermal energy exchange flux has the potential to play an important role in the surface and subsurface temperature distribution. The direction of the dispersive thermal energy exchange flux varied spatially and temporally, acting sometimes as a source and sometimes as a sink of thermal energy to the subsurface due to diurnal atmospheric input fluctuations. This allows for more temperature "mixing" between the surface and subsurface thermal energy regimes. Overall, the transient heat transport simulation demonstrated the importance of incorporating atmospheric conditions into thermal energy transport modelling framework, a component missing from many current subsurface thermal energy transport models. In addition, these simulations highlight the importance of collecting spatial and temporal atmospheric information that is representative of the field conditions. Ignoring these variations can significantly compromise the reliability of the predictions, and thus misrepresent the groundwater-surface water thermal interactions.

A suite of transient flow simulations involving discrete rainfall events also demonstrated that the entire surface and subsurface thermal energy regime is affected by the transient hydraulic response of the Pine River site. In the higher topographical regions, the applied rainfall mainly infiltrated into the subsurface and little overland flow was generated. As such, the surface temperatures were similar to the rainfall temperature, and the subsurface temperatures also increased as the event water infiltrated. An increase in rainfall rate increased the temperature of the subsurface and the depth to which the higher temperatures propagated. Along the stream banks, overland flow was the dominant hydraulic mechanism, with only slight spatially-sporadic infiltration occurring over the banks. Therefore, the temperatures of the overland flow waters of this region were influenced by both the air temperature and the dispersive temperature exchange to the subsurface regime. The effects of the air temperature and the thermal energy exchange to the subsurface regime counteracted each other, with neither being a dominant source or sink. This results in a slower thermal response to the rainfall event along the stream banks compared to the higher topographical regions. The subsurface temperatures below the stream banks were slightly elevated due to the dispersive transfer of thermal energy from the surface; however, they were not as high as in the regions furthest from the stream where both advective and dispersive thermal energy exchange flux into the subsurface occurs. Along the stream, the surface temperatures did not change because they are regulated by the inlet thermal boundary condition. The temperatures in the subsurface, below the stream, also did not change. Overall, the transient rainfall simulations demonstrated that the thermal energy responses varied with each event both temporally and spatially.

The simulation results from the discrete rainfall events applied to the Pine River domain indicate that the temperature signal from a rainfall event can be tracked through the surface and subsurface. As such, simulations of the Borden rainfall-runoff experiment were conducted in which a temperature tracer was used for hydrograph separation. A thermal energy mass-balance approach was found to give similar separation results compared to both the measured hydrograph separation results based on a bromide tracer as well as previously simulated dissolved tracer hydrograph separations. The sensitivity of the hydrograph separation to the pre-event temperature was also investigated, and it was shown that use of temperature is best suited when the difference between the event and pre-event temperatures is significant and measureable. Further field studies should be conducted to explore the practical and routine use of a temperature tracer for hydrograph separation. In addition, further simulations should be conducted on larger scale domains and under different hydrological conditions to determine the applicability of temperature as a tracer for hydrograph separation.

Atmospheric thermal inputs play an important role in the surface and subsurface temperature regime. As such, the impact of each atmospheric contribution was investigated to determine their relative importance. The net atmospheric contributions increased the surface and subsurface temperatures of the Pine River example; indicating that shortwave radiation and sensible heat flux are the dominant atmospheric contributions. However, the net atmospheric contributions decreased the surface and subsurface temperatures of the Borden rainfall-runoff example, indicating that longwave radiation was the dominant atmospheric contribution for this example. These results demonstrate that atmospheric thermal contributions are site-specific and that each atmospheric input can contribute differently to the temperature distributions. The collection of field data for thermal energy transport studies should include not only hydrological and geological parameters, but also atmospheric parameters that can characterize the shortwave and longwave radiation, and the latent and sensible heat fluxes. Ignoring any of these components may significantly reduce the reliability of the conceptual and/or computational model.

Overall, the integration of thermal energy transport into HydroGeoSphere provides a valuable tool that is capable of simulating field conditions, in addition to evaluating the effects of climatic change, on both the surface and subsurface thermal conditions. Future development of HydroGeoSphere should include the incorporation of winter/spring processes, such as soil freeze and thaw, and snow accumulation and melt. These processes are important for capturing the effects of seasonal changes with regard to the response of the hydrological cycle.

Future research involving HydroGeoSphere will include the sensitivity of thermal conditions, including surface and subsurface interactions, to land surface characteristics, the subsurface geology, and other pertinent parameters, as they might affect ecosystem health in natural and human-impacted water resource systems. In addition, large-scale examples will be simulated to demonstrate the robustness of the new capabilities of HydroGeoSphere, eventually leading to the evaluation of climate change on the entire hydrological system at the watershed scale.

References

Abdul, A.S. (1985). Experimental and numerical studies of the effect of the capillary fringe on streamflow generation. Ph.D. Thesis, University of Waterloo, Waterloo, Ontario, Canada.

Abdul, A.S. and Gillham, R.W. (1989). *Field studies of the effects of the capillary fringe on streamflow generation*. Journal of Hydrology, Vol. 112 pp 1-18.

Albert, M.R. and Krajeski, G.N. (1998). *A fast, physically-based point snow melt model for distributed applications*. Hydrological Processes, Vol. 12, pp 1809-1824.

Barlow, J.R.B. and Coupe, R.H. (2009). *Use of heat to estimate streambed fluxes during extreme hydrologic events*. Water Resources Research, Vol. 45 doi: 10.1029/2007WR006121.

Blume, T., Zehe, E. and Bronstert, A. (2008). *Investigation of runoff generation in a pristine, poorly gauged catchment in the Chilean Andes II: Qualitative and quantitative use of tracers at three spatial scales*. Hydrological Processes, Vol. 22, pp 3676-3688.

Burnett, R.D. and Frind, E.O. (1987). *Simulation of Contaminant Transport in Three Dimensions 2. Dimensionality Effects*. Water Resources Research, Vol. 22(4), pp 695 -705.

Caissie, D. (2006). *The thermal regime of rivers: a review*. Freshwater Biology, Vol. 51 pp 1389-1406.

Chaudhary, D.R. and Bhandari, C. (1968). *Heat transfer through a three-phase porous medium*. British Journal of Applied Phsyics, Series 2, Vol. 1, pp 815-817.

Chen, Y.D., Carsel, R.F., McCutcheon, S.C. and Nutter, W.L. (1998). *Stream Temperature Simulation of Forested Riparian Areas: I. Watershed-Scale Model Development*. Journal of Environmental Engineering, Vol. 124, No. 4, pp 304-315.

Clapp, R.B. and Hornberger, G.M. (1978). *Empirical equations for some soil hydraulic properties*. Water Resources Research, Vol. 14 pp. 601-604.

Conant Jr., B. (2001). A PCE plume discharging to a river: Investigations of flux, geochemistry and biodegradation in the streambed. Ph.D. thesis, University of Waterloo, Waterloo, ON, Canada.

Conant Jr., B. (2004). *Delineating and quantifying ground water discharge zones using streambed temperatures*. Ground Water, Vol. 42, pp. 243-257.

Conant Jr., B., Cherry, J.A. and Gillham, R.W. (2004). *A PCE groundwater plume discharging to a river: influence of the streambed and near-river zone on contaminant distributions*. Journal of Contaminant Hydrology, Vol. 73(1-4), pp 249-279.

Constantz, J. (2008). *Heat as a tracer to determine streambed water exchanges*. Water Resources Research, Vol. 44, doi: 10.1029/2008WR006996, 20 p.

Dickinson, R.E., Shaikh, M., Bryant, R. and Graumlich, L. (1998). *Interactive Canopies for a Climate Model*. Journal of Climate, Vol. 11, pp 2823-2836.

Dingman, S.L. (1994). Physical Hydrology. Published by Prentice Hall, New Jersey, USA.

Environment Canada (2008). http://www.climate.weatheroffice.ec.gc.ca/climate_normals/index_e.html

Fassnacht, S.R., Snelgrove, K.R. and Soulis, E.D. (2001). *Daytime long-wave radiation approximation for physical hydrological modelling of snowmelt: a case study of southwestern Ontario.* Soil-Vegetation-Atmosphere-Transfer Schemes and Large-Scale Hydrological Models; IAHS Publication No. 270, pp. 279-286.

Graf, T. (2005). Modeling coupled thermohaline flow and reactive solute transport in discretely-fractured porous media. Ph.D. Thesis, University of Laval, Ste-Foy, PG, Canada.

Graf, T., and Therrien, R. (2007). *Coupled thermohaline groundwater flow and single-species reactive solute transport in fractured porous media.* Advances in Water Resources, Vol. 30, pp 742-771.

Gusev, Y.M. and Nasanova, O.N. (2002). *The simulation of heat and water exchange at the land-atmosphere interface for the boreal grassland by the land-surface model SWAP.* Hydrological Processes, Vol. 16, pp 1893-1919.

Gutowski, W.J. Jr., Vorosmarty, C.J., Person, M., Otles, Z., Fekete, B. and York, J. (2002). *A Coupled Land-Atmosphere Simulation Program (CLASP): Calibration and validation.* Journal of Geophysical Research, Vol. 107, No. D16, pp 3-1 to 3-17.

Hidore, J.J., and Oliver, J.F. (1993). Climatology: An Atmospheric Science. Published by Macmillan Publishing Company, New York, USA.

Hokanson, K.E.F., McCormick, J.H., Jones, B.R. and Tucker, J.H. (1973). *Thermal requirements for maturation, spawning, and embryo survival of the brook trout, Salvelinus fontinalis.* J. Fish.Res. Board Can., Vol. 30, pp 975-984.

Hostetler, S.W. and Bartlein, P.J. (1990). *Simulation of Lake Evaporation with Application to Modeling Lake Level Variations of Harney-Malheur Lake, Oregon.* Water Resources Research, Vol. 26, No. 10, pp 2603-2612.

Hsieh, P.A., Wingle, W. and Healy, R.W. (2000). *VS2DI – A Graphical Software Package for Simulating Fluid Flow and Solute or Energy Transport in Variably Saturaetd Porous Media.* U.S. Geological Survey Water-Resources Investigations Report 99-4130, 16 p.

Idso, S.B., Jackson, R.D., Reginato, R.J., Kimball, B.A. and Nakayama, F.S. (1975). *The dependence of bare soil albedo on soil water content.* Journal of Applied Meteorology, Vol. 14, pp 109-113.

Jin, J., Gao, X., Sorooshian, S., Yang, Z.-L., Bales, R., Dickinson, R.E., Sun, S.-F. and Wu, G.-Z. (1999). *One-Dimensional Snow Water and Energy Balance Model for Vegetated Surfaces.* Hydrological Processes, Vol. 13, pp 2467-2482.

Jones, J.P., Sudicky, E.A., Brookfield, E.A. and Park, Y.-J. (2006). *As assessment of the tracer-based approach to quantifying groundwater contributions to streamflow.* Water Resources Research, Vol. 42, doi: 10.1029/2005WR004130.

Jordan, R. (1991). A One-Dimensional Temperature Model for a Snow Cover: Technical Documentation for SNTHERM.89. USA Cold Regions Research and Engineering Laboratory, Special Report 91-16.

Leavesley, G.H., Lichty, R.W., Troutman, B.M. and Saindon, L.G. (1983). Precipitation-runoff modelling system: User's manual. U.S. Geological Surface Water Resources Investigations Report 83-4238.

Lemieux, J.-M., Sudicky, E.A., Peltier, W.R. and Tarasov, L. (2008a). *Dynamicsof groundwater recharge and seepage over the Canadian landscape during the Wisconsinan glaciations*. Journal of Geophysical Research – Earth Surface, Vol. 113, doi: 10.1029/2007JF000838.

Lemieux, J.-M., Sudicky, E.A., Peltier, W.R. and Tarasov, L. (2008b). *Simulating the impact of glaciations on continental groundwater flow systems. 1. Relevant processes and model formulation*. Journal of Geophysical Research – Earth Surface, Vol. 113, doi: 10.1029/2007JF000928.

Lemieux, J.-M., Sudicky, E.A., Peltier, W.R. and Tarasov, L. (2008c). *Simulating the impact of glaciations on continental groundwater flow systems. 1. Model application to the Wisconsinian glaciations over the Canadian landscape*. Journal of Geophysical Research – Earth Surface, Vol. 113, doi: 10.1029/2007JF000929.

Lemieux, J.-M. (2006). Impact of Wisconsinian Glaciation on Canadian Continental Groundwater Flow. Ph.D. Thesis, University of Waterloo, Waterloo, ON, Canada.

Li, Q., Unger, A.J.A., Sudicky, E.A., Kassenaar, D., Wexler, E.J. and Shikaze, S. (2008). *Simulating the Multi-Seasonal Response of a Large-Scale Watershed with a 3D Physically-Based Hydrologic Model*. Journal of Hydrology, Vol. 357, pp. 317-336.

Lindsey, S.D. and Farnsworth, R.K. (1997). *Sources of Solar Radiation Estimates and their Effect on Daily Potential Evaporation for Use in Streamflow Modeling*. Journal of Hydrology, Vol. 201, pp 348-366.

MacFarlane, D.S., Cherry, J.A., Gillham, R.W. and Sudicky, E.A. (1983). *Migration of contamination in groundwater at a landfill: A case study: 1. Groundwater flow and plume delineation*. Journal of Hydrology, Vol. 63, no. 1-2, pp 1-29.

MacFarlane, N.A. and Laprise, R. (1985). *Parameterization of Sub-grid Scale Processes in the AES/CCC Spectral GCM*. Atmospheric Environment Service, Downsview, Ontario, No. 85-12 CCRN 17, 70 pp.

Markle, J.M., Schincariol, R.A., Sass, J.H. and Molson, J.W. (2006). *Characterizing the two-dimensional thermal conductivity distribution in a sand and gravel aquifer*. Soil Science of America Journal, Vol. 70, pp. 1281-1294.

Maxwell, R.M. and Kollet S.J. (2008). *Interdependence of groundwater dynamics and land-energy feedbacks under climate change*. Nature Geoscience, Vol. 1 pp 665-669.

Maxwell, R.M., Chow, F.K. and Kollet, S.J. (2007). *The groundwater-land-surface-atmosphere connection: Soil moisture effects on the atmospheric boundary layer in fully-coupled simulations*. Advances in Water Resources, Vol. 30, pp 2447-2466.

Maxwell, R.M. and Miller, N.L. (2005). *Development of a Coupled Land Surface and Groundwater Model*. Journal of Hydrometeorology, Vol. 6, pp 233-247.

Mengelkamp, H.-T., Warrach, K., and Raschke, E. (1999). *SEWAB – a parameterization of Surface Energy and Water Balance for atmospheric and hydrologic models*. Advances in Water Resources, Vol. 23, pp 165-175.

Molson, J.W., Frind, E.O. and Palmer, C.D. (1992). *Thermal energy storage in an unconfined aquifer 2. Model development, validation and application.* Water Resources Research, Vol. 28, No. 10, pp. 2857-2867.

Neff, B.P., Piggott, A.R. and Sheets, R.A. (2005). *Estimation of shallow ground-water recharge in the Great Lakes Basin*: U.S. Geological Survey Scientific Investigations Report 2005-5284, 20 p.

Palmer, C.D., Blowes, D.W., Frind, E.O. and Molson, J.W. (1992). *Thermal energy storage in an unconfined aquifer 1. Field injection experiment.* Water Resources Research, Vol. 28, pp. 2845-2856.

Renaud, J.–P., Cloke, H.L., and Weiler, M. (2007). *Comment on "An assessment of the tracer-based approach to quantifying groundwater contributions to streamflow" by J.P. Jonbes et al.*, Water Resources Research., Vol. 43.

Sass, J.H., Ziagos, J.P., Wollenberg, H.A., Munroe, R.J., di Somma, D.E. and Lachenbruch, A.H. (1977). *Application of Heat-Flow Techniques to Geothermal Energy Exploration, Leach Hot Springs Area, Grass Valley, Nevada.* U.S. Geological Survey Open File Report 77-762, 125 p.

Schmidt, C., Conant Jr., B., Bayer-Raich, M. and Schirmer, M. (2007). *Evaluation and field-scale application of an analytical method to quantify groundwater discharge using mapped streambed temperatures.* Journal of Hydrology, Vol. 347 pp 292-307.

Sellers, P.J., Mintz, Y., Sud, Y.C. and Dalcher, A. (1986). *A Simple Biosphere model (SiB) for use within general circulation models.* Journal of the Atmospheric Sciences, Vol. 43, No. 6, pp 505-531.

Snelgrove, K.R. (2002). *Implications of Lateral Flow Generation on Land-Surface Scheme Fluxes.* Ph.D. Thesis, University of Waterloo, Department of Civil Engineering.

Sudicky, E.A., Jones, J.P., Brookfield, A.E., and Park, Y.-J., (2007). *Reply to Comment by J.-P. Renaud, H.L. Cloke and M. Weiler on "An assessment of the tracer-based approach to quantifying groundwater contributions to streamflow".* Water Resources Research Vol 43.

Sudicky, E.A., Cherry, J.A. and Frind, E.O. (1983). *Migration of contamination in groundwater at a landfill: A case study: 4. A natural-gradient dispersion test.* Journal of Hydrology, Vol. 63, no. 1-2, pp 81-108.

Tarasov, L. and Peltier, W.R. (2007). *Coevolution of continental ice cover permafrost extent over the last glacial-interglacial cycle in North America.* Journal of Geophysical Research – Earth Surface, vol. 112, doi: 10.1029/2006JF000661.

Therrien, R., McLaren, R.G., Sudicky, E.A. and Panday, S.M. (2007). HydroSphere: a three-dimensional numerical model describing fully-integrated subsurface and surface flow and solute transport. Groundwater Simulations Group, Waterloo, Ontario, Canada.

United States Department of Agriculture (2008). http://www.ars.usda.gov/Services/docs.htm?docid=8955.

VanderKwaak, J. E. (1999). *Numerical Simulation of Flow and Chemical Transport in Integrated Surface-Subsurface Systems*, Ph.D. Thesis, University of Waterloo, Department of Earth Sciences.

Varis, O., Kajander, T. and Lemmela, R. (2004). *Climate and Water: From Climate Models to Water Resources Management and Vice Versa.* Climatic Change, Vol. 66, pp 321-344.

Verseghy, D.L. (1991). *A Canadian land surface scheme for GCMS. I. Soil Model.* Int. J. Climatol. Vol. 11, pp. 111-133.

Voss, C.I. (1984). *A Finite-Element Simulation Model for Saturated-Unsaturated, Fluid-Density-Dependent Ground-Water Flow with Energy Transport or Chemically Reactive Single-Species Solute Transport.* U.S. Geological Survey Water-Resources Investigations Report 84-4369, 409 p.

Wagener, T. and Franks, S. (2005). *Regional Hydrological Impacts of Climate Change – Impact Assessment and Decision Making.* Regional Hydrological Impacts of Climatic Change – Impact Assessment and Decision Making; IAHS Publication no. 295, pp. 1-88.

Weast, R.C. (Ed.) (1984). Handbook of Chemistry and Physics. CRC Press, Boca Raton, Fla.

Writt, R.J. (1996). The Angus PCE plume – Aquifer sedimentology and plume anatomy. Ph.D. thesis, University of Waterloo, Waterloo, ON, Canada.